Escola Universitària d'Enginyeria
Tècnica Industrial de Barcelona
Consorci Escola Industrial de Barcelona
UNIVERSITAT POLITÈCNICA DE CATALUNYA

Volum I
Memòria – Pressupost

TREBALL DE FI DE GRAU

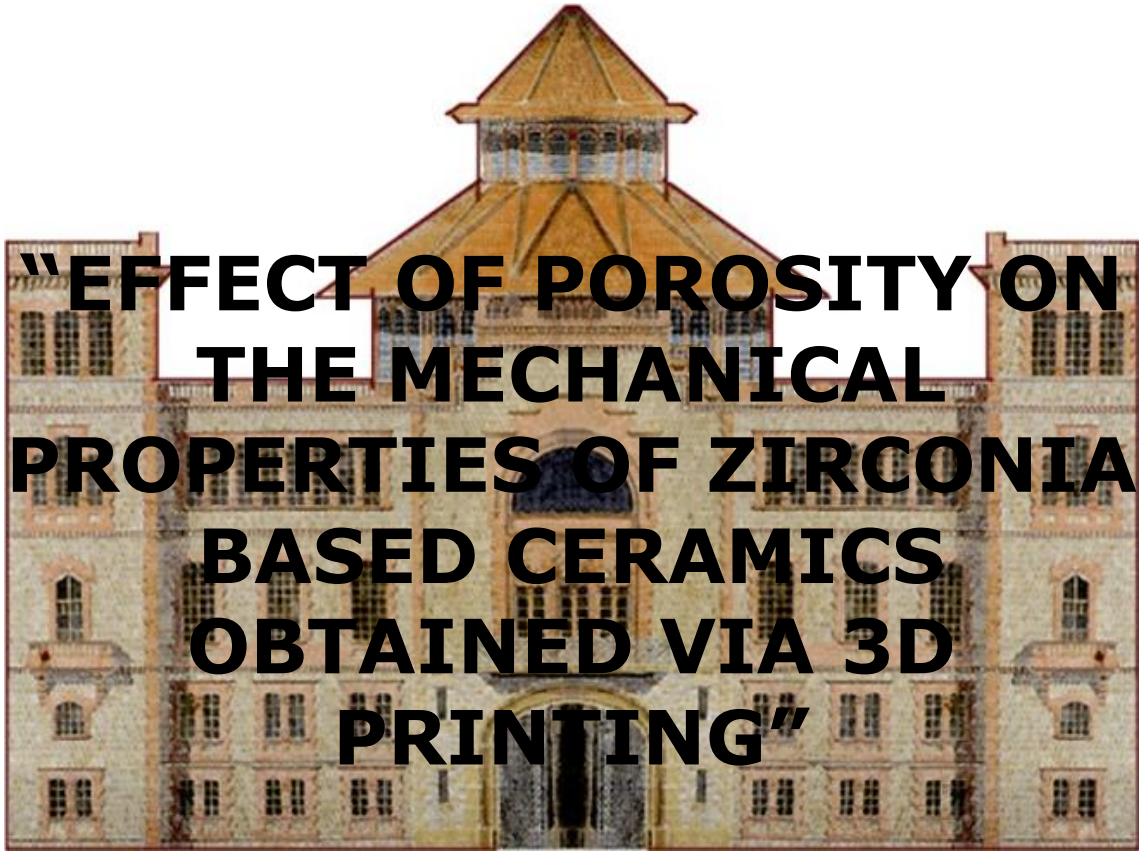

"EFFECT OF POROSITY ON THE MECHANICAL PROPERTIES OF ZIRCONIA BASED CERAMICS OBTAINED VIA 3D PRINTING"

TFG presentat per obtenir el títol de GRAU en
ENGINYERIA MECÀNICA
Per **Ferran Crespo Petit**

Barcelona, 26 de Juny de 2016

Directora: Gemma Fargas Ribas
Codirector: Joan Josep Roa Rovira
Departament de Ciència i Enginyeria dels Materials i Enginyeria Metal·lúrgica (CMEM)
Universitat Politècnica de Catalunya (UPC)

VOLUME I OUTLINE

Escola Universitària d'Enginyeria
Tècnica Industrial de Barcelona
Consorci Escola Industrial de Barcelona
UNIVERSITAT POLITÈCNICA DE CATALUNYA

Memòria

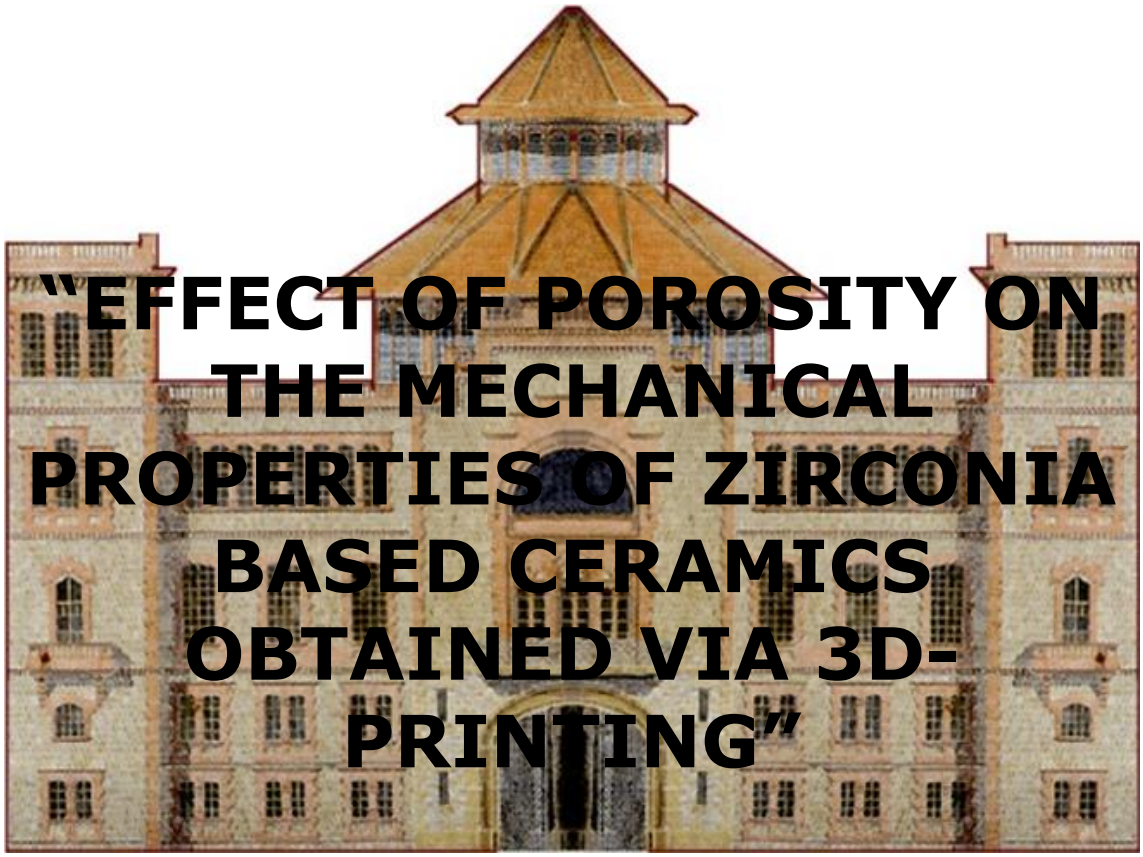

"EFFECT OF POROSITY ON THE MECHANICAL PROPERTIES OF ZIRCONIA BASED CERAMICS OBTAINED VIA 3D-PRINTING"

TFG presentat per optar al títol de GRAU en
ENGINYERIA MECÀNICA per

Ferran Crespo Petit

Barcelona, 26 de Juny de 2016

Directora: Gemma Fargas Ribas
Codirector: Joan Josep Roa Rovira
Departament de Ciència i Enginyeria dels Materials i Enginyeria Metal·lúrgica (CMEM)
Universitat Politècnica de Catalunya (UPC)

MEMORY OUTLINE

ABSTRACT

Engineering ceramics present a unique combination of mechanical, thermal and chemical properties becoming increasingly important in the nowadays-industrial landscape. Unlike other engineering ceramic materials, zirconia oxide displays very high resistance to crack propagation and thermal expansion which lead to be a candidate material for a wide range of applications such as biomedical, thermal barrier coatings and electrolytes for solid oxide fuel cell. However, manufacturing of ceramic components has still major limitation in production of highly complex 3D shapes, micro features or structures with tailored porosity.

Nowadays, new technologies enable adding up complex three-dimensional structures layer by layer. Powder based rapid prototyping technique is such a versatile method with unique flexibility in material and geometry. In this work, microstructural 3Y-ZrO2 based ceramic materials were design and produced by Rapid Prototyping with the main goal to study the influence of printing geometries on the microstructure and mechanical properties from macro-to microscopic length scale.

In this work, it has been working on three principal aspects:

- **The creation of printable materials based on ceramic powders**. This creation has been done using the Gel-casting technique, which has made possible the obtaining of viscous pastes using Zirconia, Alumina/Zirconia and Ceria/Zirconia ceramic powders.
- **The knowledge and applyment of the 3D-printing technologies**. In order to obtain the different printed samples, it has been required to know the existing 3d-printing techniques and get a formation on the working process of a Syringe extrusion 3D printer. Also, it has been necessary to configure the 3D printer to obtain a satisfactory printing process with the viscous pastes obtained.
- **The production of 3d-printed samples with different material compositions**. Different samples of 3Y-ZrO2 based ceramic composite materials have been designed and produced by Rapid Prototyping. The results were compared and discussed in terms of density, hardness and indentation fracture toughness response with 3Y-ZrO2 bulk ceramic materials produced under conventional production routes of gel-casting and Cold Isostatic Pressing. A detailed characterization of the microstructure was performed by X-ray diffraction, Field Emission Scanning Electron Microscopy (FESEM) and Focus Ion Beam (FIB).

Sintered samples of zirconia obtained using the syringe extrusion 3D printing technique have been successfully achieved. The results revealed that printed samples displayed lower density with similar properties compared with materials achieved using traditional technique.

On the other hand, although printable materials made by mixing alumina/zirconia and ceria/zirconia were succeeded, it was no possible to achieve a homogenous microstructure. Furthermore, higher sintererization temperatures were required, as a consequence; lower mechanical properties were achieved due to the formation of cubic zirconia phase.

AKNOWLEDGEMENTS

Firstly, I would like to express my sincere gratitude to Joan Josep Roa and Gemma Fargas, two professionals with an enormous work capacity and contagious passion.

Secondly, I would give a special acknowledgement to all the technicians and labmates that helped me on the realization of this bachelor's project, especially to Fernando Garcia, Lara de Luis and Albert Moreno.

Finally, I dedicate this work to my partner Anna Muñoz, for her patience and support.

CHAPTER 1: INTRODUCTION

In this chapter will be presented the main principles and characteristics (like microstructure, properties, among others) related to the base material investigated in this bachelor's project (Yttria-stabilized Zirconia, YSZ, as well as the different ceramics based on it).

This section will be divided in four main topics focused in the developing of porous advanced ceramic materials based Zirconia:

i) The chapter will start with a general introduction of the base ceramic material investigated along this research (YSZ) and other advanced ceramic materials, e.g. Alumina (Al_2O_3), Ceria (CeO_2), etc. Afterwards, in each section will be presented in detail the microstructure, the role of several doping agents to stabilize the material of interest, phase transformation and the main deformation. Finally, it will show a summary of the most important properties and applications of the Zirconia based ceramic materials,

ii) Afterwards, the main principles for porous ceramics materials,

iii) Then, some important reological aspects, and

iv) Finally, a section talking about the different rapid prototyping techniques will be summarized due to this is the technique used along this project.

1.1. Zirconia-based ceramics

Ceramic materials and concretely the advanced ceramic materials are those inorganic, non-metallic materials consisting of metallic and nonmetallic elements bonded primarily with ionic and covalent bonds. These materials present an extraordinary set of properties, like: high strength bonds give rise to the special characteristics of these materials as good electrical insulation, mechanical resistance, hardness, chemical stability and high melting temperature, as well as a fragile breaking [ref]. For those reasons, occupy a unique place in the spectrum of engineered materials offering many desirable alternatives to the conventional metals and polymers.

Concretly, one of those advanced ceramic materials is the Zirconium dioxide (ZrO_2) or also known as Zirconia. It is combined with other oxides, generating advanced ceramic materials with a wide range of industrial applications due to its good mechanical properties (high hardness and fracture toughness, low friction coefficient), chemical stability, corrosion resistance, biocompatibility or Ionic conduction, among others.

However, this material present an inconvenient due to it presents phase transformation (from tetragonal to monoclinic phase, t→m transformation or also well known as martensitic transformation). It is necessary to mention, the fact of combining pure Zirconia with other stabilizing oxides like Yttria (Y) lies in the ability of holding at room temperature its tetragonal phase, which appears at very high temperatures (around the range of 1000 -2370 ° C), and which this microstructure presents the most desirable mechanical properties [1].

This phenomenon can be created due to several factors:

i) During the cooling, which represents an increase of volume (of around 4%) and consequently, a generation of shear stress. This phenomenon in pure Zirconia has a worsen effect, generating cracks in the material and restringing it only to refractory applications.

ii) Stresses created during the grinding process or created during the mechanical resistance evaluation. The phase transformation originated due to the transformation under tension on points near a crack and holding it, generating compressing tensions due to the volume increase in the transformation, and

iii) When this material is in contact with humidity; and then a low thermal degradation process can be the main responsible to induce this phase transformation. In the other hand, the t-m transformation can also occurs due to the exposure on damp environments at low temperature. This phenomenon is known as aging or hydrothermal degradation of the material. The result is the undesired t-m transformation on the surface of the material, generating micro cracks that worsen the material. One solution to

reduce this worsen phenomenon is the introduction of Ceria (Cerium oxide (III), CeO_2) in the Zirconia [2], which increases its resistance to degradation, but also reduces its mechanical properties. To compensate this decrease of mechanical properties, it is also usual to introduce Alumina (Aluminum oxide, Al_2O_3).

1.1.1. Zirconia-based ceramics nomenclature

The Zirconia-based ceramic materials are designated according to the acronym **ZTC (*Toughened ZrO_2 Ceramics*).** Depending on the type of stabilization, the different ZTC based ceramics that can be obtained are grouped into three main families:

- **TZP: *Tetragonal Zirconia Policrystals*:** Zirconia based ceramics with almost 100% of tetragonal phase, stabilized with Yttria (Y_2O_3) or Ceria (CeO_2). The designation of these ceramics consists on a prefix of the letter of the stabilizing material (Y or Ce), with a number that represents the molar percent concentration of that material.

  The 3Y-TZP (material of study in this Bachelor's project), is one of the most widely industrially used ZTC, due to its high resistance to fracture (~ 1GPa), moderate fracture toughness (4-5 MPa√m) and the fact that it is considered a standard in ionic conductors and its biocompatibility [ref Chevalier].

- **PSZ: *Partially Stabilized Zirconia*:** Zirconia based ceramics with big grains (ranged between 0.2 and 1 μm) of tetragonal phase with lenticular precipitates of cubic phase. These ceramics are obtained by adding concentrations of 8-10% molar of Calcia or Magnesia, with a high temperature sintering (~ 1600 °C).

- **DZC: Dispersed Zirconia Ceramics:** Zirconia based ceramics with a ceramic matrix and a tetragonal Zirconia dispersion (5-30 wt%). The properties of these ceramics will strongly depend on the transformability of the dispersed Zirconia.

  An example of these materials is ZTA (*ZrO_2 Alumina toughened*), with a widely industrial applications.

1.1.2. Microstructure

The pure Zirconia presents three stable polymorphic (solid material's ability to exist in more than one form) crystal structures throughout its phases, depending on the temperature range which are the following:

- Cubic (*c*),
- Tetragonal (*t*), and
- Monoclinic (*m*).

Besides these stable structures, it has been experimentally demonstrated that there also exists a group of orthorhombic or rhomboedrical phases (*O* and/or *R*, respectively), which are stable at high pressures or under high stresses.

For a better comparison between these phases during its transformation, it is usual to simulate the cubic phase for the pure Zirconia with a fluorite-type crystal structure [3], which can be transformed from the tetragonal to monoclinic phases by slightly rotations, as it can be depicted in **Figure 1**

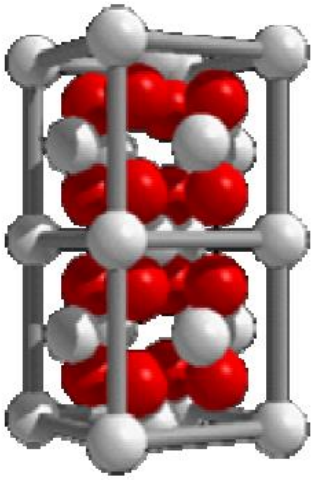

Figure 1. Fluorite type crystal structure of pure Zirconia. Where the white spheres symbolize Zirconia atoms and the red, Oxigen atoms [4].

Starting from a liquid Zirconia cooling, the first state change takes place around 2680 °C (which corresponds with the melting point of this material); the material solidifies into cubic phase (*c*) which presents a fluorite type crystal structure; a cubic face centered crystalline structure type (fcc), see **Figure 2**.

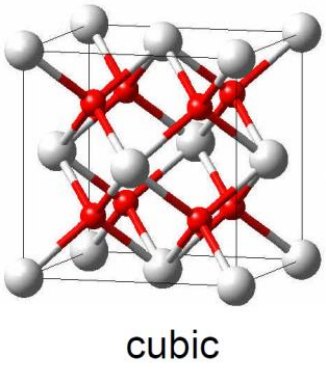

Figure 2. Crystallographic structure for the cubic phase of pure Zirconia [5].

Once solidified, if it continues cooling the Zirconia and at temperature around 2370 ° C, another crystallographic structure will appear, being thus the tetragonal phase (*t*). This structure presents a cubic body centered crystalline structure type (bcc), see **Figure 3**.

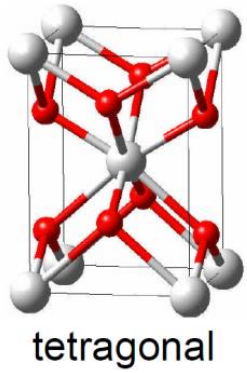

Figure 3. Crystallographic representation for the tetragonal phase of pure Zirconia [5].

Finally, at a temperature around 1170 °C, the monoclinic phase (m) appears and no longer transforms, see **Figure 4**.

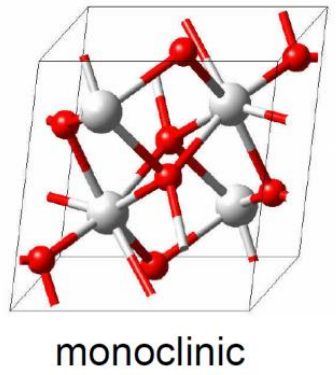

Figure 4. Crystallographic representation for the monoclinic phase of pure Zirconia [5].

The different microstructural parameters (stability range, density, reticular parameters and atomic positions) for each Zirconia phase are summarized in **Table 1**.

Table 1. Microstructural parameters of the pure Zirconia crystal phases [6].

Phase	Stabilty range (ºC)	Density (g/cm3)	Reticular parameters				Atomic positions			
			a (Å)	b (Å)	c (Å)	β (º)	Atom	x	y	z
Cubic	2680-2370	5.83	5.12	5.12	5.12	90	Zr	0	0	0
							O	0.25	0.25	0.25
Tetragonal	2370-1170	6.10	5.07	5.07	5.19	90	Zr	0	0	0
							O	0.25	0.25	0.20
Monoclinic	>1170	6.09	5.15	5.20	5.32	99.19	Zr	0.28	0.04	0.21
							O1	0.07	0.33	0.34
							O2	0.44	0.76	0.48

1.1.3. Stabilization

The stabilization of a material consists in the aggregation of another material (with small addition of secondary phases known as stabilization or dopping agent) into the base material or the application of a treatment, in order to modify its final properties. Mainly by adding secondary phases or by using thermal treatments you are able to improve their final properties and at the same time reduce some intrinsic defects created during the texture process (i.e. porosity, etc).

As we mention in **section 1.1.2.**, the microstructure of Zirconia which presents the most interesting engineering properties is the tetragonal phase. The main inconvenient of this phase is that is only stable at high temperature (see **Table 1**) due to a phase transformation (from tetragonal to monoclinic), which involves a positive volume increase accompanied by an extensive cracking in the material, producing an embritlement of their final mechanical properties during the ccoling process. As a consequence, these materials are not available for for any structural or mechanical application and reserving it only for refractory uses.

It was not until 1975 when it was discovered that the tetragonal phase of the Zirconia can be retained at room temperature with the addiction of stabilizing oxides like Yttria (Y_2O_3), Magnesia (MgO) or Calcium oxide (CaO).

The possibility to slow down or eliminate this crystal structure change from tetragonal to monoclinic phase allows its use for structural and mechanical applications apart from refractory uses [7]. Moreover, the control of this transformation has an improving behavior on the mechanical properties of the material, transforming under tension on the crack sides and introducing compensatory compressive stresses due to the volume increase.

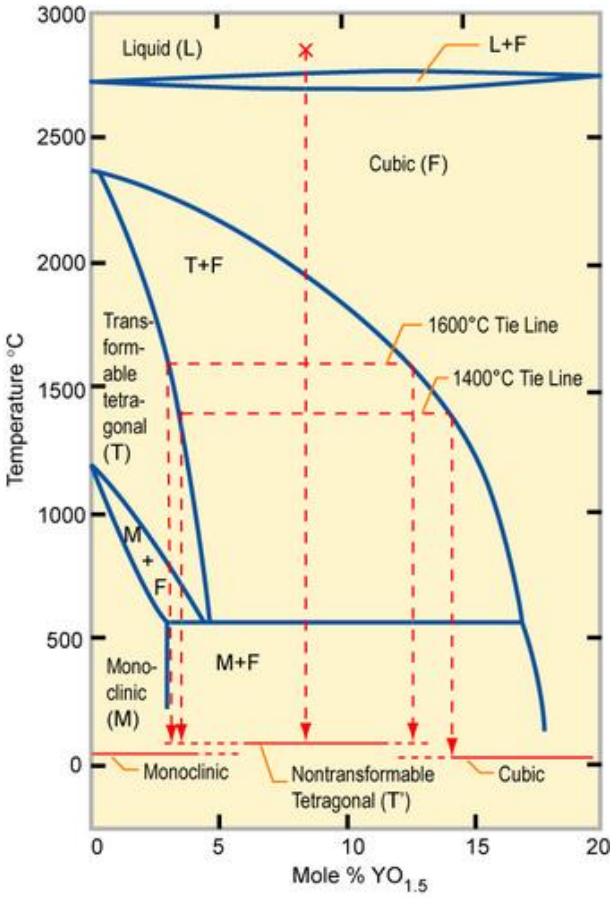

Figure 5. Phase diagram of Yttria stabilized Zirconia (% molar) [8].

The stabilization mechanism of these oxides is the creation of oxygen vacancies inside the crystalline structure for the Zirconia [9], maintaining the electric equilibrium between the positive and negative charges when the Zr^{4+} cations are substituted for these stabilizing oxides with a different valence number.

The monoclinic phase is stable at room temperature because his coordination number is around 7, the same as for the Zr^{4+} ions. At high temperatures, (above 1170ºC), the concentration of oxygen vacancies created during the thermal process is higher due to the pressure of the oxygen. To accommodate these thermal generated defects, the structure has to slightly change the coordination number to 8, being thus equivalent to the tetragonal and cubic phases.

These oxygen vacancies can be artificially generated at room temperature with the addiction of trivalent or pentavalent cations inside the Zirconia structure, obtaining the stabilization of the structures with coordination number 8 (tetragonal and cubic), see **Figure 6**.

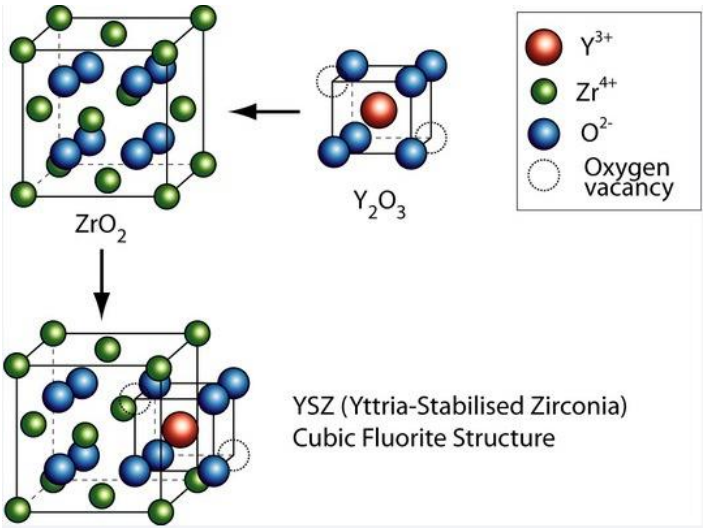

Figure 6. Stabilization of the cubic fluorite structure adding Yttrium Oxide [10].

1.1.4. Phase Transformation mechanisms

As we commented in **section 1.1.3.** Zirconia materials present a phase transformation from tetragonal to monoclinic structure, also known as martensitic transformation (without diffusion). This transformation takes place around 850ºC and involves a positive expansion in terms of unit cell volume change of around 4% and a shear stress of 16%. In pure Zirconia without stabilizing oxides, the impossibility to accommodate these phenomena involves the generation of high residual tensions and micro-cracks on the material, creating an embritlement of the resulting material and leaving it useless for structural applications.

For 3Y-ZrO_2, this transformation takes place for two different mechanisms: tension has enough energy to allow the transformation, and by hydrothermal degradation of the ceramic specimens also known as aging process, which transforms at low temperature (around 131-134ºC) and a pressure of around 2 bars. This transformation takes place in damp environments, causing micro cracks parallel to the surface of the material as presented [11]:

- **Transformation under tension:** This type of transformation happens when the energy accumulated by the concentration of tensions is enough to produce the change of phases in the structure of the Zirconia.

This transformation causes an increase of the volume and a consequent shear stress. This type of *t-m* transformation is a desirable phenomenon, due to it happens due to the stress present on the edges of the cracks [12], transforming and generating counteract tensions that prevent the propagation of the crack. This is an improving phenomenon that increases the resistance of the material, see **Figure 7**.

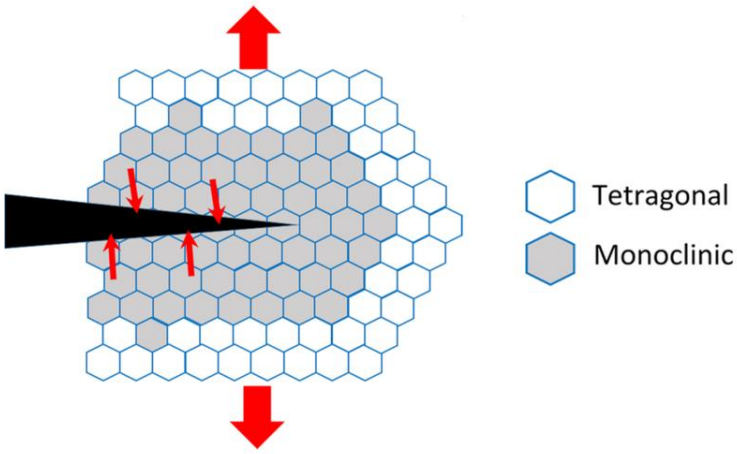

Figure 7. *t-m* phase transformation under tension [11].

- **Transformation by hydrothermal degradation:** This mechanism was reported first by Kobayashi et. al. [13] and has been widely investigated and characterized along the years.

The aging or hydrothermal degradation occurs at low temperatures (131-134ºC) in presence of wet environments (mainly water), and causes the change of tetragonal phase to monoclinic on the surface, accompanied by micro cracking which propagates from the exterior to the interior of the material, **Figure 8**. It also can be appreciated the effect of micro cracking propagation on the adjacent grains of a transformed grain, contributing on a superficial propagation of this phenomenon:

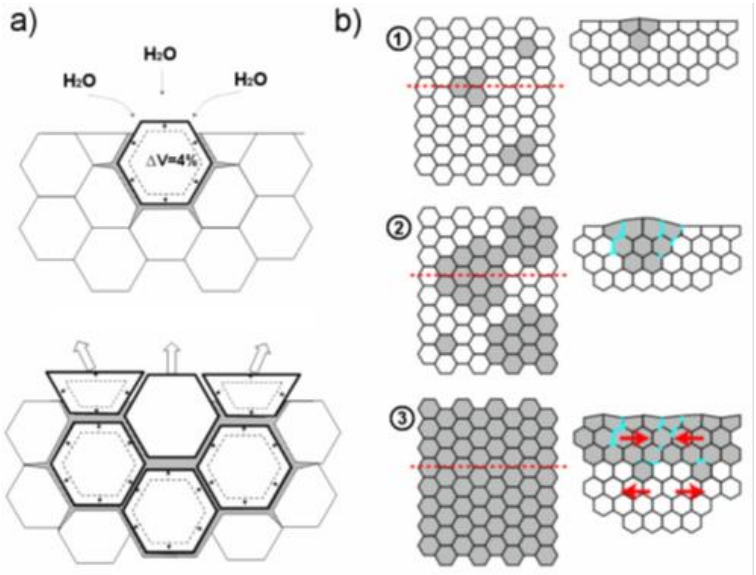

Figure 8. Mechanism of t-m phase transformation by Hydrothermal Degradation proposed by Chevalier [14].

The long term effect of this phenomenon results on a decrease on the mechanical resistance of the material. Table X shows the decrease of Hardness according to aged layer thickness [15]:

Table 2. Aged layer thickness and hardness depending on LTD time

LTD Time (hours)	Thikness (μm)	Hardness (GPa)
0	-	16
10	2	15
30	6.3	13
60	12	11

The hydrothermal degradation has been widely studied and an occasion of many articles as a result of the accelerated aging of the material when this phenomenon occurs [16].

There are some factors that beneficiates this phenomenon:

- **Temperature and environment**. The degradation occurs more quickly on a range of critical temperatures between 200 and 300° C, and it depends of exposition time. The water or water vapor enriched enviornments beneficiates to occur.
- **The size and shape of the grain**. Reducing the size of the particle increases the area/volume relation, facilitating the propagation of cracks.
- **Content and distribution of the stabilizing material**. An increase in the content of stabilizing material on Zirconia also increases the resistance against hydrothermal degradation, due to the greater number of oxygen vacancies. Another fact is that if there is heterogen distribution of the stabilizing content on the material, the zones with a poor content can work as nucleation zones due to the lower content of oxygen vacancies.
- **Contents of the cubic phase**. With the purpose of obtaining a completely dense material, and decreasing the time with the presence of the cubic phase in order to avoid the phase change, it is recommended to use the range of 1400-1450° C of sintering temperature for the 3Y-TZP).
- **Porosity**. A material with a lot of pores in his surface facilitates the infiltration of water, which facilities the propagation of the degradation).
- **Effect of residual stresses**. The residual shear and tensile stresses destabilizes the tetragonal phase and facilitates its transformation to monoclinic, while the compressing stresses make a stabilizing effect.

In order to avoid this transformation, there are different types of procedures that prevent the phase transformation:

- **Microstructural control**. The reduction of the grain size increases the free energy on the surface. This reduction is obtained sintering

the material at lower temperatures or using powders with a finer structure during the texture and sintering process. On the other hand, an excessive reduction on the grain size can be the main responsible to originate a decrease in the fracture toughness due to the reduction on the phase transformability of the material.

One option is adding some materials which improve the resistance against the hydrothermal degradation. One of the most common additives for the Zirconia to prevent the aging is the Cerium oxide (Ceria, CeO_2), which retards this phenomenon but also decreases the mechanical properties. Another option is the use of Alumina (Al_2O_3), which increases the mechanical properties but does not protect against aging as good as the Ceria.

- **Coating**. The creation of a coating allows the isolation of the Zirconia substrate against any aqueous medium, avoiding its interaction in order to protect against aging. The most widely used coatings are Ceria (CeO_2) or Alumina (Al_2O_3) based coatings.
- **Nitriding**: A thermal treatment for the infiltration of Nitrogen inside Zirconia increases the tetragonal phase stabilization introducing vacancies inside the structure.

1.1.5. Properties

The tetragonal zirconia policrystals based ceramic materials as the 3Y-TZP are extremely refractory materials which offer chemical and corrosion inertness to temperatures well above the melting point of alumina (aroud 2072°C)and present high density (around 6 g/cm^3) despite of being ceramics. Moreover, these advanced ceramic materials have high hardness and wear resistance, low thermal conductivity, electrical conduction above 600°C and exhibit biocompatibility as it is summarized in **Table 3**.

The stabilization and control of the *t-m* phase transformation reduces its intrinsic fragility, improving its fracture toughness due to the transformation under tension mechanism. It is common to introduce Alumina in Zirconia in order to improve its wear resistance, decreasing superficial roughness (0.01-0.03 μm), and increasing its hardness.These facts, combined with the prevention against hydrothermal degradation adding Cerium oxide make TZP as the 3Y-TZP, engineering advanced technical ceramics with very good mechanical, thermal and electrical properties.

Table 3. Summary of the main microstructural and mechanical properties for different advanced Zirconia based ceramics [17].

Mechanical properties	Units	Y-TZP	Ce-TZP	ZTA	Mg-PSZ
Density	g/cm^3	6.05	6.15	4.15	5.75
Porosity	%	0	0	0	0
Hardness	MPa	13.5	9	16	10.2
Bend strength	MPa	1000	350	500	800
Compressive strength	MPa	2000	—	—	2000
Young's Modulus	GPa	205	215	380	205
Poission's Ratio	—	0.3	—	—	0.23
Fracture Toughness	$MPa \cdot \sqrt{m}$	9.5	15-20	4-5	8-15
Thermal properties					
Thermal Conductivity	$W \cdot m^{-1} \cdot K^{-1}$	2	2	23	1.8
Coefficient of Thermal Expansion	10–6/°C	10	8	8	10

1.1.6. Applications

The good combination of properties (see **Table 3**) that Zirconia offers makes it an ideal material for a wide range of advanced engineering applications.

Some of the most common industrial applications for Zirconia-based ceramics are listed below:

- **Cutting sheets**. The high hardness and wear resistance makes Zirconia ideal for the creation of the most resistant cutting sheets, which hold a longtime sharping and don't get rusted. Companies such as Kyocera or Boker produce these type of cutting sheets for cooking and sport knives.
- **Ceramic bearings**. The superficial finish that can be obtained with Zirconia ceramics and the low friction resistance that gives, combined with its high hardness and wear resistance, makes it ideal for bearing applications. Furthermore, those components present lower density and higher resistance compared with the traditional bearings.
- **Ceramic brakes**. The good wear resistance makes this material a strong candidate for the fabrication of high performance ceramic brakes for automotive applications, due to their excellent wear resistance, high high work temperatures (900°C), corroding protection and low weight compared with other standard discs (50% less). All these skills give the brakes, apart from high performance specs, a guaranteed useful life of around 150000 km.
- **Thermal barrier coatings, TBC** (see **figure 9**). The material of study, presents a good refractory behavior, making their ideal for thermal isolation. The main application as TBC of this material is inside exhaust systems, in order to conserve a low temperature and force the exhaust gases to flow faster, increasing the performance of

the vehicle equipped as well as on the turbine blades of the aircraft engines.

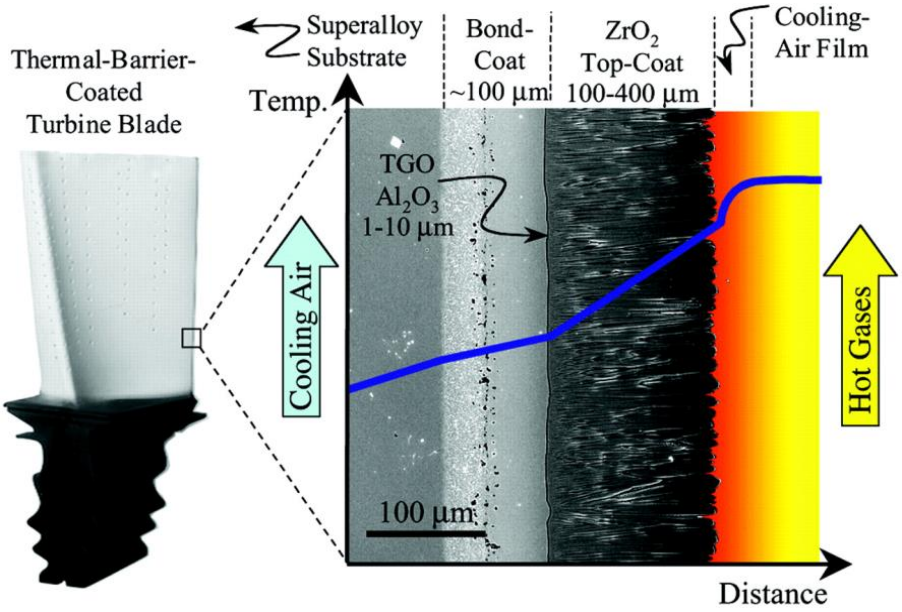

Figure 9. Example of Thermal barrier coating application for Zirconia [18].

- **Jewelry**. The cubic phase of pure Zirconia, also called Zirconita, is the most important diamond's competitor since 1976, due its low cost, durability and similar visual aspect. On the other hand, the tetragonal phase of Zirconia presents the visual aspect of pearls.
- **Electro-ceramic applications**. Due to the Ionic conduction properties that present some YSZ, can be used as a "filter" of oxygen ions for gas sensors applications to determine the oxygen content, or to measure the pH, among others.
- **Fuel cells**. Taking advantage of the Ionic conduction before mentioned, the YSZ can be used as electrolytes in solid oxide fuel cells (SOFC). Due to its isolating as ceramic, blocks the passage of electrons, allowing only the pas of oxygen ions through it. Complying with all of these specifications, the YSZ ceramics are considered a standard inside the ionic conductors for SOFC applications [4].
- **Medical Implants**. The biocompatibility of the ZTC, in addition to the surface finish that can present (bone colour) turns them into ideal materials for prostheses and dental implants. The wear resistance of Zirconia allows its use for friction surfaces as hip prostheses.

Even so, in the literature can be found several cases of medical implant fractures [19], mainly attributed to the low thermal degradation (LTD) or hydrothermal degradation of the material caused by the moist and warm conditions inside the human body.

Figure 10. Different examples of Zirconia applications [20].

1.2. Porous ceramics

The most important feature of the ceramic materials in comparison to other materials as metals is the presence of porosity in their internal structure, which modifies their mechanical, electrical and even ionic properties.

Along this section, it will be introduced porous ceramic materials, the concept of porosity as well as the change of their mechanical properties as a function of the porosity content. Finally, special attention will be paid into theneed to use specific characterization techniques.

1.2.1. Porosity

The porosity is a structural property of the ceramic materials, generally undesirable, that can be known as a measurement of the capacity of these materials to store fluids on their interior. A porous medium is most often characterised by its porosity, and many of its important properties can only be rationalized by this consiferation.

This parameter is defined as the fraction of the volume of voids (unoccupied material volume) over the total volume of the material (often called the "matrix" or "frame".):

$$\emptyset = \frac{V_{Voids}}{V_{Total}} \quad (1)$$

The value that porosity can take is ranged between 0 and 1, or 0 and 100 as a percentage, being 0 a non-porous material.

Once defined the concept of porosity, it has to be characterized its presence on the materials structure. Depending of which characteristic is considered to represent, there are different types of how the pores can be distributed on the materials, see **Figure 11**:

- ***Open or effective porosity***: It refers to the fraction of the total volume which is connected with the external part of the material, and for where a fluid flow can effectively fill the pore. This type of porosity includes all type of connected pores like catenary and dead-end pores (as these pores cannot be flushed, but they can cause fluid movement by release of pressure like gas expansion), and it excludes closed pores (or non-connected cavities).
- ***Closed or ineffective porosity***: It refers to the fraction of the total volume which is not connected with the exterior of the material, and where fluids or gases can be present but cannot take place an effective fluid flow. This type of porosity includes the closed pores.

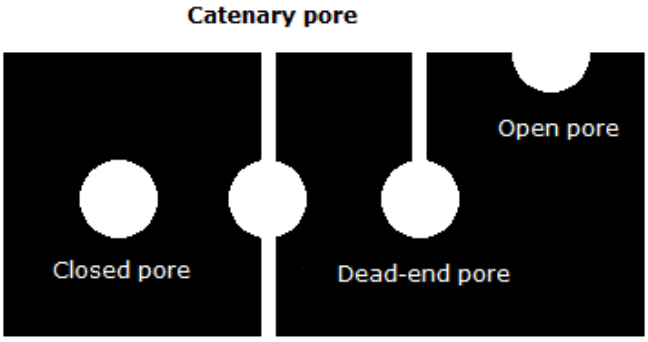

Figure 11. Different types of pores depending of their presence on the material's structure.

According to ISO rule 15901:2005 (Evaluation of pore size distribution and porosimetry of solid materials by mercury porosimetry and gas adsorption), depending on the size, there are three types of porosity:

- ***Macroporosity***: It refers to pores greater than 50 nm in diameter. Flow through macropores is described by bulk diffusion.
- ***Mesoporosity:*** It refers to pores greater than 2 nm and less than 50 nm in diameter. Flow through mesopores is described by Knudsen diffusion.
- ***Microporosity:*** It refers to pores smaller than 2 nm in diameter. Movement in micropores is activated by diffusion.

1.2.2. Porosity versus mechanical properties

The presence of porosity on the structure of materials has a decreasing effect on their mechanical properties, due to the introduction of the defects that pores represent. This introduction of defects, also modifies the characterization of these properties, being necessary to use a wide amount of samples and statistic methods as Weibull distribution, in order to determine the failure probability of the material.

A suitable simple empirical equation to describe the influence of these defects in the elastic modulus of porous ceramics proposed by L. Fuglsang [21] is given by:

$$E = E_o \frac{1-P}{1+\alpha P} \tag{2}$$

where Eo corresponds to the elastic modulus of 3Y-TZP free of pores and P is the porosity volume fraction. The parameter α has been related to the shape of the pores: 1 for spherical pores and increases as the spherical pores change to oblate spheroids.

Figure 12 represents the effect of pore shape and porosity content on elastic modulus for 3Y-TZP [22]:

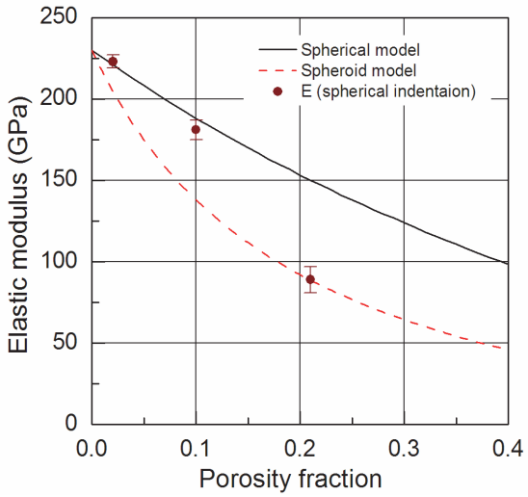

Figure 12. Effect of pore shape and porosity content on elastic modulus [22].

For porous materials, the reduction in their mechanical integrity in terms of hardness and yield strength follows a similar trend as presented on **Figure 13**:

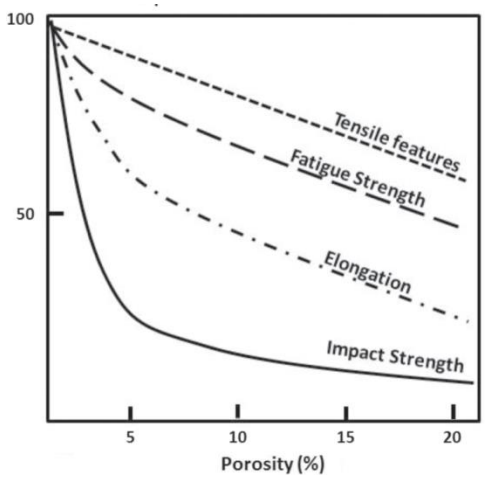

Figure 13. Decreasing of mechanical properties due to porosity content (%) in PM materials [23].

1.3. Material extrusion

In a lot of industrial conformation processes like stamping, extrusion or 3D-printing, the materials use should be fluid or semifluid state (melted or jellified) in order to offer a viscous/viscoelastic comportment to allow their pertinent extrusion.

The viscoelastic comportment is a combination of a fluid response and a solid response of the material of interest, which makes necessary to have in mind some characteristic parameters of these materials in order to have a good characterization and comprehension of their behavior for a satisfactory extrusion process in order to enhance a desirable industrial device.

Some of the main **rheological parameters** to take into account are presented below:

1.3.1. Viscosity and shear stress

The viscosity of a material is one of the most important parameters for this type of processes, due to it is an intrinsic property of the material, and it relations and affects the shear stress needed to obtain a certain shear rate.

Exist two different main classifications for the fluids: Newtonian and non-Newtonian materials:

a) The **Newtonian materials** present a constant linear proportionality between the shear stress and shear rate obtained called viscosity coefficient of the material (see **Figure**), which can be expressed as follows:.

$$\tau_{xy} = \mu \frac{\partial u}{\partial y} = \mu \dot{\gamma} \tag{3}$$

Where:

τ_{xy} is the shear stress

$\dot{\gamma}$ is the Shear rate

μ is the Viscosity of the fluid

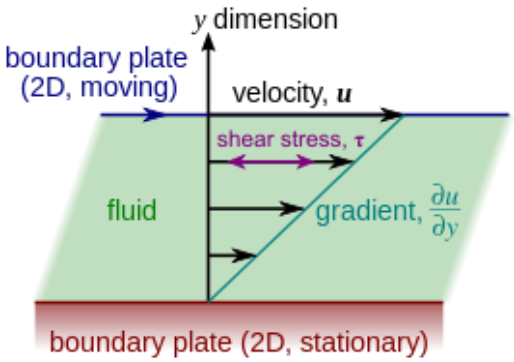

Figure 14. Representation of the linear relation between shear stress and shear rate for Newtonian materials [24].

b) **Non-Newtonian materials**, which do not present a constant coefficient of proportionality between shear stress and shear rate, depending on the way of application of the shear stress and shear rate or the temperature of the material, among other parameters.

Table 4 shows a comparision between the different types of materials depending on their fluid habilities:

Table 4. Material's clasification according to their viscous behaviour [24].

Viscoelastic	Kelvin material, Maxwell material	"Parallel" linearstic combination of elastic and viscous effects	Some lubricants, whipped cream, Silly Putty
Time Dependent Viscosity	Rheopecty	Apparent viscosity increases with duration of stress	printer ink, gypsum paste
	Thixotropic	Apparent viscosity decreases with duration of stress	Aqueous iron oxide gels, gelatin gels, pectin gels, many paints, many floc suspensions, many colloidal suspensions
Time-independent viscosity	Shear thickening (dilatant)	Apparent viscosity increases with increased stress	Suspensions of corn starch in water
	Shear thinning (pseudoplastic)	Apparent viscosity decreases with increased stress	Nail polish, whipped cream, ketchup, molasses, syrups, ice, blood, sand in water
	Generalized Newtonian fluids	Viscosity is constant.	Blood plasma, custard, water

Because of their characteristics presented in **table 4**, there is the needed to consider more rheological properties apart from viscosity on the characterization of the non-Newtonian materials, in order to understand their behaviour. Usually, this characterization includes some theoretical models based on constitutive equations of continuum mechanics field.

The necessity to know the relation between the shear stress and shear rate for the non-Newtonian materials defines new magnitudes, in order to obtain the higher adjust of their behavior with reality and avoid some mistakes during several industrial applications. These new parameters to take into considerationare:

- **Apparent viscosity**. The apparent viscosity is a ficticious value that gives a linear relation of proportionality for non-Newtonian materials, which is an approximation of the real viscosity. This relation consists on a straight line from the origin to the cross with the graph (see **Figure 15**), for a determined shear rate. This approximation is tipically used on industrial processes as an approximation of the Newtonian viscosity for low speeds, where the shear rate is lower and the approximation decreases its error due the similarity between the graphs of the Newtonian and non-Newtonian materials.

$$\mu_a = \frac{\tau}{\dot{\gamma}} \tag{4}$$

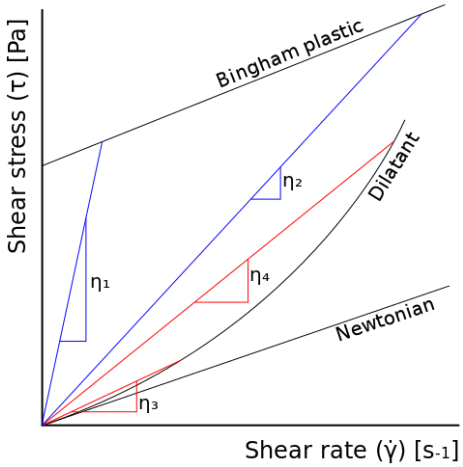

Figure 15. Examples of different apparent viscosity adjustments [24].

- **Power model**. For processes that demand more precise values, is usual to define a potencial model in order to have a better adjust on the experimental graph.This model consists on the introduction of two parameters; *k* and *n* being the viscosity coefficient and flux index, respectively. With these parameters is possible to obtain a new relation, which represented logaritmichally based, shows a linear relation between the sehar stress and shear rate for a non-Newtonian materials. Below are presented the equations for this model:

$$\tau = K * \gamma^n \rightarrow \ln(\tau) = n ln(\gamma) + \ln(K) \quad (5)$$

Where K is the viscosity coefficient and n is the flux index.

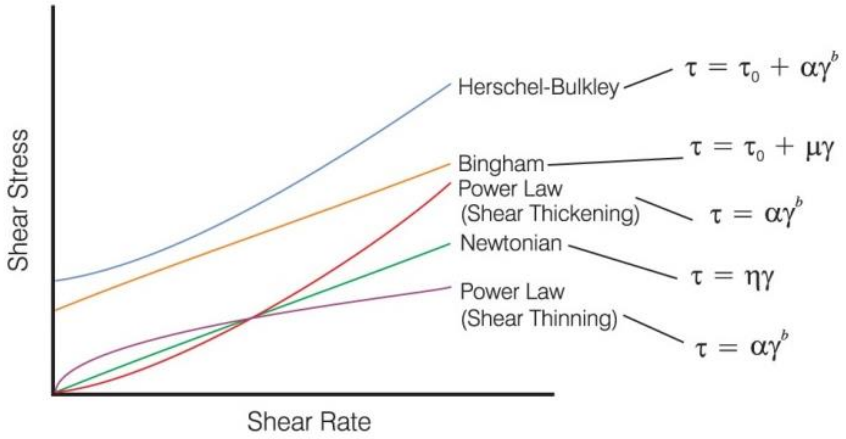

Figure 16. Examples of different viscosity adjustment models [24].

It has to be mention that all of these models are also approximations of the real viscosity value of the material, increasing its error with the increase of the process speed.

1.3.2. Conformation technique: 3D-printing

The Syringe Extrusión 3D-Printing technique is basically an extrusión of viscous materials, normally non-Newtonian material, throughout a nozzle, which creates a filament in order to build a desired 3D geometry, see **Figure 17**:

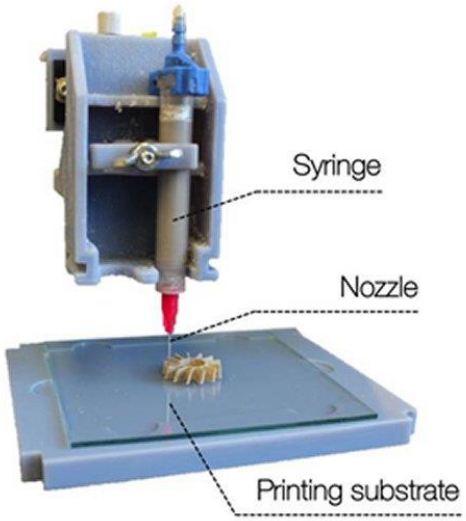

Figure 17. Syringe Extrusion 3D-Printing technique diagram [25].

The characterization of this process is based on the rheometric analysis of the material's flux, which needs to present a viscous behavior in order to pass troughout the nozzle. In order to do an appropriate characterization it is necessary to have in mind the following considerations:

- The flux is zero on the walls of the nozzle,
- the flux remains constant on time (during the entire extrusion process),
- the flux profile remains constant over the nozzle,
- the material is uncompressible,
- the flux is isothermic (the temperature remains constant during the entire process as well as the temperature does not increase when exist friction forces through the nozzle),and
- the gravity force is negligible.

The application of a force (*F*) over the piston's area (*A*) is nedded to push the material throughout the nozzle, creating a pressure diferential (ΔP):

$$\Delta P = \frac{F}{A} \tag{6}$$

The pressure decreasion throughout the nozzle is the opposition that feels the material due the shear stress (τ) needed to deform it:

$$\tau = \frac{F}{A} = \frac{\Delta P * S}{2\pi RL} \quad \text{(Cilindric nozzle)} \tag{7}$$

$$\tau = \frac{F}{A} = \frac{\Delta P * S}{\pi (R+r) g} \quad \text{(Conic nozzle)} \tag{8}$$

Where S is the pressure application surface, R and r the big and small nozzle's radiums, L the nozzle height ang g the slant height.

This shear stress generates a shear rate ($\dot{\gamma}$) on the material, which can be calculated using the Newton's viscosity equation explained in **section 1.3.1.** and using the following expression:

$$\dot{\gamma} = \frac{4Q_V}{\pi R^3} \tag{9}$$

Where Q_V is the volumetric flow of the extruded material, and R is the nozzle's radium.

Finally, the volumentric flow can be defined as the ratio between the material mass (m) and time (t) being the final units m3/s:

$$Q_V = \frac{m}{t} \tag{10}$$

Once characterized the flux properties, is necessary to know the most important parameters of the extrusion process [26], in order understand its behavior and realize a satisfactory industrial application or optimization. There are a lot of variable and relationed parameters on the 3D-printing process, and only the correct adjustment and combination of all of them allows the obtaining of a satisfactory result.

The most important and controllable process parameters are listed below:

- **Nozzle diameter**. Diameter of the nozzle opening in μm. It affects the flow rate of the viscous material and the diameter of the extruded track. The choose of the diameter size is delimited for the minimum particle size of the material desired to extrude, in order to avoid material obstructions on the nozzle. The geometry of the nozzle determines an intrinsec shear stress (see **equations 7** and **8**), and consequently a certain shear rate, forcing to modify parameters as the material's viscosity or the volumetric flux in order to obtain a good extrusion
- **Viscosity.** This property of the viscous material affects the flow of the viscous material throughout the entire print cycle. A combination between the noozle diameter and shape, and a determined viscosity is needed in order to avoid the undeseared pouring of the viscous material and the correct flux throughout the nozzle beating the shear stress.
- **Extruder pressure**. Applied at the back end of the syringe that contains the paste that the system needs to extrude. The pressure applied on the extruder influences the flow rate of the viscous material, affecting on the quantity of the deposited material and generating a wider or thiner printed filament. This fact can be traduced, in combination with the travel speed of the extruder, on the piling or dragging on the printed filaments if the combination of parameters is not the addecuate**.**
- **Feed rate**. Travel speed, in mm/s, of the nozzle during printing controls the amount of viscous material deposited per unit length, and affects the width and continuity of the bead. It also affects the motion delay deeded to allow initial flow of material and to obtain a uniform bead width over the entire bead. It is measured in seconds and it is widely affected by the viscosity of the material.
- **Standoff distance**. The distance between the nozzle tip and the printing substrate, measured in 'mm'. This fact, combined with the extruder pressure and the feed rate, influences the shape of the track.

Table 5 summarizes the different types of the filament extrusion (or main problems observed in the filament extrsusion) for this technique and their possible causes:

Table 5. Different types of the 3D printing filament extrusion.

Type	Description	Possible causes
	Narrow filament	Standof distance too large Extruder pressure too high Inadecuate viscosity of the material
	Dragged filament	Feed rate too fast Extruder pressure too low Inadecuate viscosity of the material
	Squashed filament	Standoff distance to short Extruder pressure too high Feed rate too slow
	Crowded filament	Feed rate too slow Extruder pressure too high
	Discontinuous filament	Standof distance too large Feed rate to fast Inadecuate viscosity of the material
	Right filament	All parameters correct

1.4. Conformation

This section will talk about the different techniques employed to develop advance ceramic materials, giving special attention to the 3D-printing technique. Concretly, in this section several techniques will be presented and described in detail; being the most importants: Cold Isostatic Pressing technique, Sol-Gel technique and 3D-printing process, presenting completely different manufacturing possibilities and final material properties among them.

1.4.1. Cold Isostatic Pressing, CIP

Cold Isostatic Pressing (CIP) technique is a powder pressing process inside the pulvimetallurgical techniques, which allows the obtaining of solid ceramic powder materials for their posterior sintering. This technique allows the shaping of complex geometries in final products with mass-conserving (no machining is needed), and pretends to obtain the minimum quantity of defects and maximum homogeneity for materials which would be impossible to melt or form in other ways.

This conformation technique was used for the first time in 1913 by H. D. Madden [27], to compact metals, and developed afterwards by Turner and Ashby, which helped to understand in depth the effects that produced on the materials. Currently this technique is still the most used powder compression technique for ceramic and metallic materials, due to its high efficient type of powder compacting [28]. The density of isostatic compacted products is around 5-10% higher than with other powder metallurgy (PM) processes, and the tolerances that this process can achieve are very precise, ranging from +/- 0.2 mm and 0.5 mm for axial and radial dimensions, respectively. One the other hand, one of the most significant problems that this technique presents is the volume reduction, which ranges between 40 - 50% after the powder pressing, for ceramic materials with a grain size ranged between 44-440 μm. To sum up, the efficiency of this process will depend on the PM used during the pressing process.

This technique is based on the application of a uniformed high pressure over all the surfaces (isostatic) of the pressed body. This body is usually placed inside a mold in order to protect it against the pressing fluid, which could modify and decrease its properties after the pressing. The mold employed is fabricated of an elastomer with a specific geometry, according to the desired design of the final product, and can be fixed inside the compression shirt or removable (mold free). The thickness of this mold varies between 1.5 and 3 mm, but it has been demonstrated that the thickness of their walls does not influence on the final product, and only makes a protection function against the fluid mentioned before. An schematic representation of this process is depicted in **figure 18**.

The most commonly pressing fluid employed to transmit the isostatic pressure, is oil or water with any anti corrosive additive. Compaction pressures can vary between 200 and 760 MPa, always at room temperature (cold pressing).

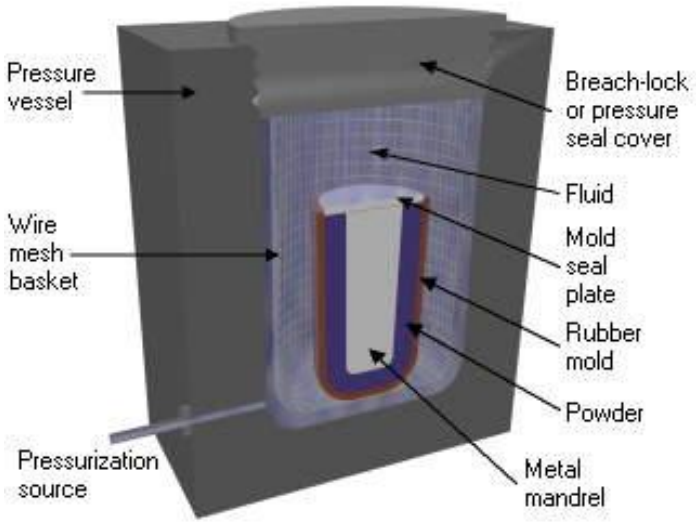

Figure 18. Cold Isostatic Pressing diagram [29].

There are no specified limitations for the geometry of the pressed body, as height to diameter ratio, wall thickness variations, undercuts, reliefs, threads, and cross holes. Pressed body operational sizes range between 1.27 and 127 mm thick and 1.59 mm to 1,016 mm long, with a weight ranged between 18 and 136 kg.

Finally, the result of this compaction is a product called "body in green" (without sintering), sufficiently resistant to allow its transport until the furnace for its posterior sintering process. This sintering process consists on a thermal treatment until the sintering temperature of the material (which is around 0.75 lower the melting point) for a certain period of time, in order to obtain a solid material after the cooling. This sintering process can be separated in three steps:

- compacting of powder particles starts rapidly, but they still remain discrete,
- densification occurs, the structure recrystallizes and particles diffuse into each other, and
- finally, the pores tend to isolate and becomes spheroidal. Along the entire sintering process, the densification continues at a much lower rate.

In order to prevent contamination, surface damage or sticking on the pressed body during the sintering inside the furnace, it is usual to use ceramic powder separating sheets made with materials such as Zirconia, Alumina or Magnesia.

1.4.2. Gel-casting Technique

Gel-casting is a conformation technique developed by Oak Ridge National Laboratory (ORNL) at the rounds of 1990, which allows the obtaining of ceramic material powder based slurries and viscus pastes [30].

Advanced ceramics display some superior properties compared to other materials, **see section 1.1.5.**, nevertheless the obtaining of these excellent properties was reserved for large production conforming techniques vinculated with simple shape restrictions or extensive and expensive machining processes. The creation of Gel-casting technique was the response to the necessity for obtaining complex-shaped ceramic metarials with a low cost method, combining the advantadges of each traditional conforming technique.

Gel-casting process consists on creating a colloidal solution between the ceramic powder material, present as small particles (dust) and a polymeric material (usually a monomer) which works as a gellying agent, creating a network between the ceramic powder and the solvent (usually water particles) on the solution and obtaining a new viscous material (gel). A detailed description of the basic steps present on this process is listed below:

1. **Ingredients mixture.** The first step consisting on mixing the ceramic powder with the solvent (usually water) and the gellying agent (usually monomer) creating a colloidal solution.This step is also the most critical due to the component proportions adopted, which will be determinating on the obtaining of the final product. The addition of more ceramic powder on the solution will provide higher viscosity on the ceramic slurry, and higher density on the final product. Furthermore, the reduction on solvent proportion will reduce the drying time and consequently, the possibility to suffer volume decrease and crack generation on the ceramic green body during it. Usually the ceramic powder proportion on the solution is around 50vol% in order to reduce as much as possible the solvent and gellying agent proportions maintaining the fluidity hability of the slurry.

   This step can be improved with the addiction of a milling process step on the ceramic powders before the mixture, in order to decrease their particles size and thus improve their mixture.

2. **Molding.** Once obtained the ceramic powder solution, the next step consists on pour it inside a mold in order to obtain the desired product shape during gellying reaction. This step can also be improved applying the vacuum on the casting in order to avoid the formation of undesired air bubbles on it.

   One of the most important advantages of the Gel-casting technique is that the mold employed only has a geometrical function, thus it can be made of almost any material such plastics, in opposition to other molding techniques as Cold Isostatic pressing where the mold has structural requirements (pressure application on it).

3. **Gellying reaction.** During the molding, it takes place a gellying reaction on the ceramic powder solution, curing it and increasing its slurried texture until becoming a viscous material (gel). This curing reaction consists on the formation of cross-linked polymer molecules of the gellying agent, which work as a unifying web structure between the ceramic powder and the solvent, immovilizing them permanently and obtaining the gel.

   If a catalyzing agent is needed to start and accelerate the cross-linked polymer molecules in order to cure the powder solution, it is applied on this step. In some process variations with no need of catalyzing agent, the curing process consists on the cooling of the gellying agent, previously melted and blended on the ingredients mixture step.

4. **Drying.** After the solution's gellying, it is needed to remove the conformed product from the mold in order to allow the solvent drying, thus eliminating its excees and letting the conformed product solidify completely.

   During the drying step, the conformed product suffers a volume decreasing relationed with the solvent proportion on the solution. This constriction can generate wraping and cracking. In order to avoid this problem, is recommended to effectuate the drying step on a humidity controlled chamber with high relativy humidity of around 90%, thus generating a progressive disminution on solvent drying.

   Once completely dried, the green body conformated material is stronger than a green body ceramic made by any conventional technique before sintering, but it is soft enough to be "green-machined" by carbide steel tools.

5. **Sintering.** Finally, the last step consists on the gellyfing agent elimination and material sintering. These two parts can be englobed on a single thermal threatment with a furnace, burning the gellying agent in order to eliminate it, and increasing the temperature until the ceramic sintering temperature. After the sintering process, a dense and strength ceramic material is obtained.

The **figure 18** shows a flow chart of the Gel-casting process in order to resume all the steps explained before:

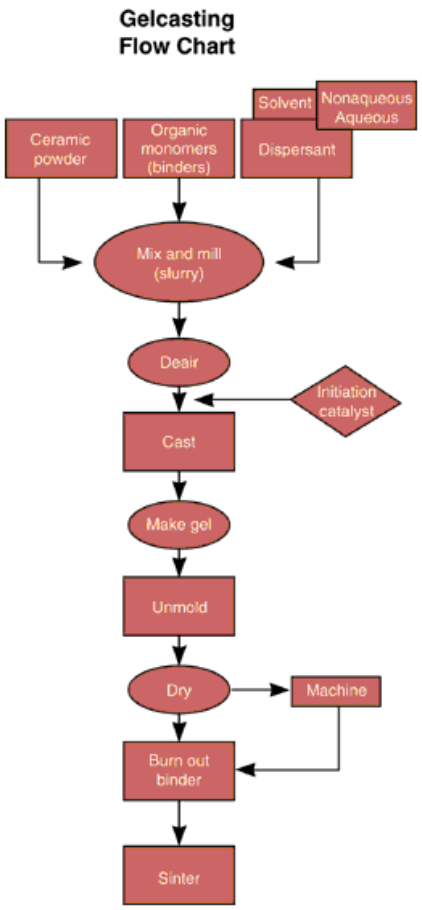

Figure 19. Gel-casting process flow chart [30].

1.4.3. Rapid Protothyping: 3D-printing

Rapid Protothyping is a group of Additive manufacturing technologies, which include, among others, all 3D-printing technologies [31]. These technologies are based on the addition of material as a superposition of different layers upon one another, in order to create a tridimensional solid product directly from a digital 3D model created through Computer Aided Design (CAD) software. In the beginning, rapid protothyping techniques (mainly 3D-printing) where employed to achieve models and prototype parts on a faster way, but with the constant developing and improving of these techniques, nowadays it is possible to obtain functional products made of a wide range of materials.

The 3D-printing technologies englobe Fused Deposition Modeling (FDM), Fused Filament Fabrication, Stereolithography (SLA) and Selective Laser Sintering (SLS) techniques, among others. These group of manufacturing technologies are nowadays one of the biggest tendencies in the technological camp, giving signals to think that we are actually in front of a third industrial revolution, changing the nature of commerce with the open fabrication idea and succeeding the production line assembly that has dominated manufacturing technologies since the 19th century. These

predictions are due to the good characteristics of their manufacturing process [32], that compared to other actual technologies are faster and easier, cheaper and have an open sourced character:

- **Fast and easy processes**. All additive manufacturing processes have in common that they can generate products with very complex geometries and internal features in very building times, compared to traditional technologies. These technologies do not require fixtures, custom tooling and planed tool movements as machining, or spend several weeks on a mold creation with expensive equipment as molding. Furthermore, additive fabrication includes the advantage to use multiple materials in a same product.

  All these advantages represent a breakup between process complexity and build time, and added to the reduction of the process requirements make these technologies more easier to use and faster to produce final products compared with conventional technologies, reserving them for production features of high accuracy and surface finishes, high fabrication production or a need of material properties.

- **Cheap production**. In traditional subtractive manufacturing processes such as milling, turning or drilling, the fabrication of the product starts with a block of the base material which is conformed removing volume, using different operation movements, equipment and tools to leave the piece with the desired shape. On the other hand, additive manufacturing starts from zero, adding only the material needed to create the final product just with the use of the 3D-printing equipment, optimizing the fabrication process, the use of the material, and consequently, a cost and build time reduction on the fabrication.

  These skills make 3D-printing technologies very cost effective for low volume productions compared to conventional processes, due to the suppression of the high initial costs of custom tooling and lengthy setup times

- **Open-sourced character**. The growing popularity and good future perspectives of these technologies is due to their open sourced character. The expiration of certain patents related to FDM Technology has made possible the birth of the RepRap Project in 2005. All Companies that are currently in the market for 3D-printing are driven due to the success of the RepRap Project. Another fact that beneficiates this growing is the possibility to interchange CAD designs of 3D products via internet or improve the 3D-printing programs due to its open source language.

  This creates a worldwide interconnected user society that improves the technology day-to-day, converting the consumers of the 3D printing technology also in the same product producers, creating a new technological term in the industrial world known as a "*pro-sumer*" (producer & consumer user).

There are three different technologies when talking about 3D printers and the products and finishes that can be obtain with one or other are delimitated:

- Fused material deposition technologies
- Laser 3D printing technologies
- Other 3D printing technologies

Fused material deposition technologies

The 3D printing technology that has popularized the manufacturing method and the first when someone thinks about a 3D home printer is the **Fused Deposition Modeling (FDM)** [33]. This technology was invented and patented to 80's for Scott Crump, who started to commercialize it through the business that he and his wife Stratasys founded together.

This technology allows obtaining products using ABS plastic (a similar material used in LEGO toys) or PLA (a biodegradable polymer produced using an organic material). The FDM technology was protected for a patent and was invented a similar technology called **Fused Filament Fabrication (FFF)**, which is widely used nowadays by the RepRap project printers as an example.

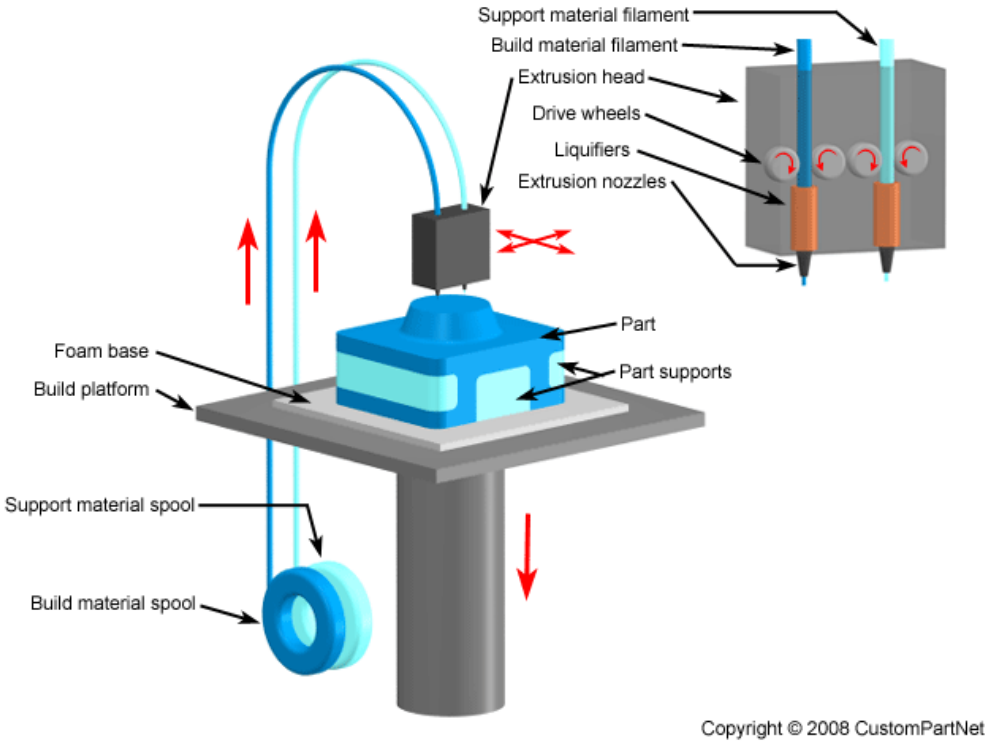

Figure 20. Example of Fused Filament Fabrication (FFF) 3D printing technology [34].

The printing process of this technology uses a fine filament of the printing plastic, which passes through the extruder in order to be heated until it arrives at its vitreous transition temperature and presents a viscoelastic

state to be extruded. In this moment, the plastic is deposited in the right position of the layer that is printing.

Once the plastic has been deposited, it cools and solidifies, allowing the deposition of the next layer over it with the vertical movement of a determined distance by the extruder. This distance will decide the final finish and precision, having a direct influence on the quality of the product. Increasing the number of layers and making them more fine, will improve the quality of the final 3D printed product but also the printing process will keep more time.

Laser 3D printing technologies

The 3D printing technologies that use laser allow obtaining final products with higher precision in a lower printing time. The most popular 3D printing technologies that use laser are Stereolithography (SLA) and Selective Laser Sintering (SLS).

The **Stereolitography (SLA)** technology [35], abbreviated as SLA, was invented for Charles Hull in 1984, before invention of the FDM and FFF technologies. Charles Hull also founded 3D Systems Company, the first business to keep a commercial 3D printer at the market.

The printing process of a SLA printer is also layer-to-layer, but the principal difference between the previous method and SLA is that it creates the product using a mobile base submerged into a swim of liquid resin which reacts in contact with a laser and solidifies afterwards.

The process of this method consists in the submersion of the mobile base inside the liquid resin in order to create the first layer using the laser beam. Once the laser has created the first layer using the curing reaction of the liquid resin and its posterior solidification on the surface of the mobile base, this base moves a determined distance to allow the creation of the next layer with the same process.

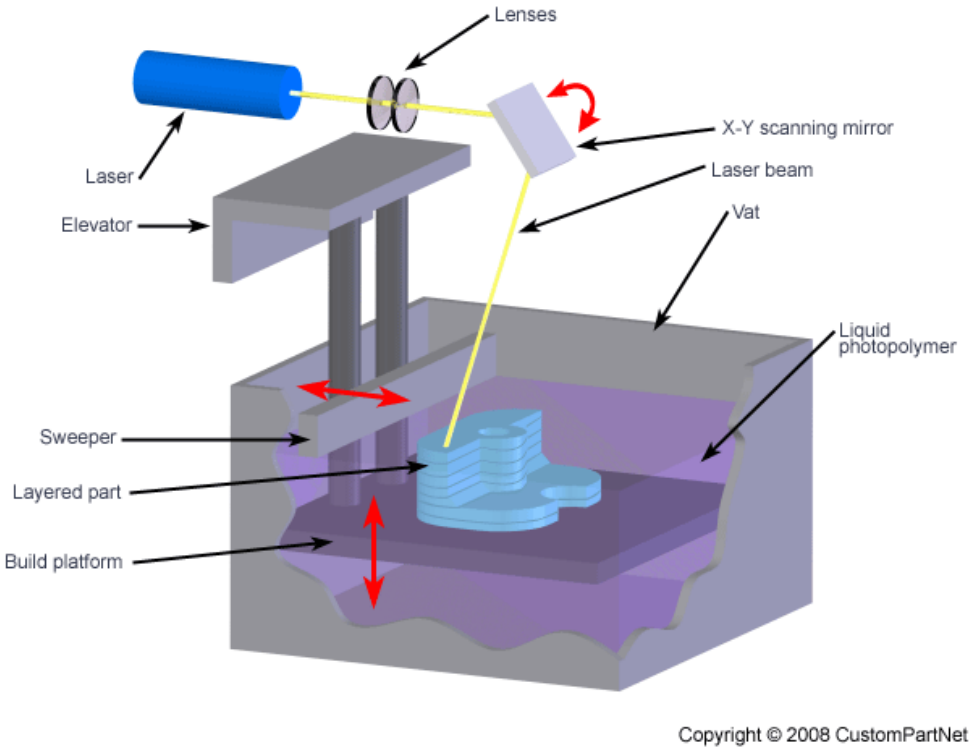

Figure 21. Example of Stereolitography (SLA) 3D printing technology [34].

With this technology is possible to obtain final products with a big grade of detail, but like the same as the fused material deposition technologies, it wastes a certain amount of material according to the necessity of adding supports to the product for its creation, which will be eliminated at the end of the process.

Another 3D-printing technology that used laser is the **Selective Laser Sintering (SLS)**. This technology was invented around 80's just as SLA technology, and in spite of having certain similitudes one another, the SLS technology has a differentiated process method that allows the use of a wide range of materials.

The principal difference between both methods is that SLS uses a mobile base submerged into a swim which the material is in powder state, in opposition to the liquid state of the SLA technology material. The laser beam only impact and reacts on the desired points of the material in order to create the layer, leaving the rest at the same initial position in powder state, and moving the mobile base surface to add more material powder for the next layer.

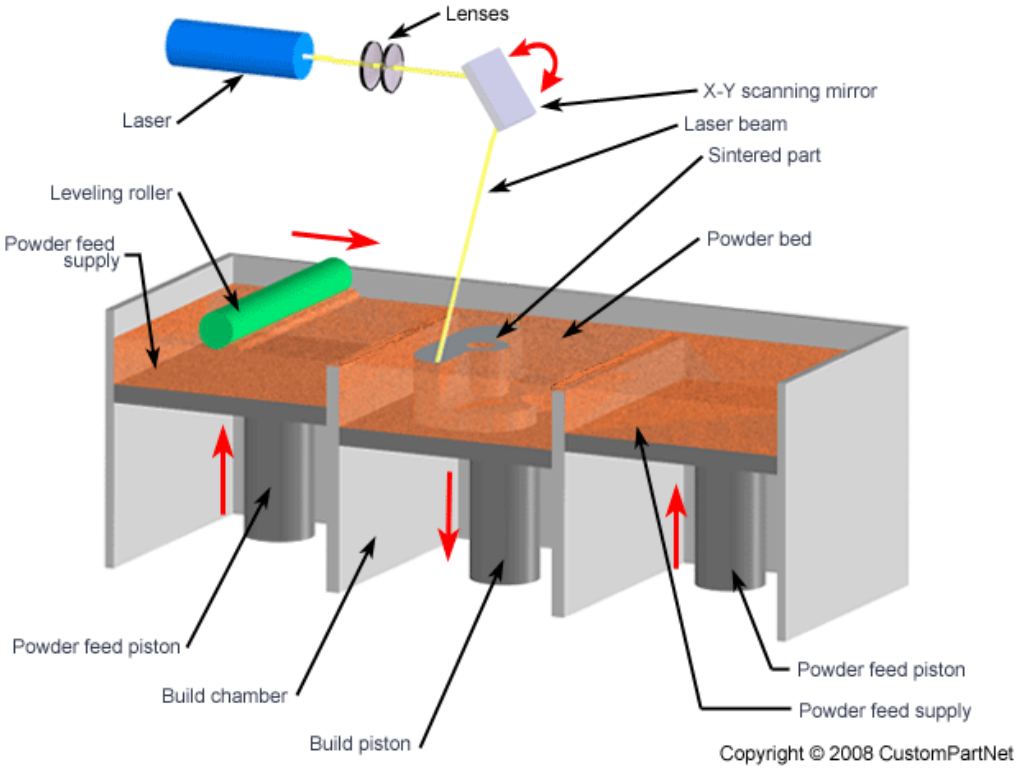

Figure 22. Example of Selective Laser Sintering (SLS) 3D printing technology [34].

The first advantage of this technique is that the not sintered material by the laser beam remains at the same initial position and it is used as support for the creating product, preventing to use and waste extra material for the creation of supports. Another big advantage is that due to the characteristics of the process it is possible to use a wide range of materials like Polystyrene, ceramic materials, crystal, Nylon and metallic materials.

Other 3D printing technologies

These technologies explained before are the most popular and common 3D printing methods, but there are also other methods or modifications of the previous that are less used nowadays but they could be popularized in the future.

The first method is the **Jetted Photopolymer** or Photopolymer Inkjet Printing, introduced and developed by Objet Company in 2000 as Polyjet Photopolimer (acquired by Stratasys) and 3D Systems as InVision, in 2003. Actually, this technique could be englobed with the laser 3D printing technologies, but for its type of process, has enough differences between SLA and SLS processes to be considered another different technology.

This method combines the processes of Inkjet printing and Stereolitography techniques; a liquid photosensitive polymer is deposited layer over layer and solidified with an UV curing laser to sinter the material, with every pass of the printing heads. This technology allows the use of different materials on a same layer simultaneously.

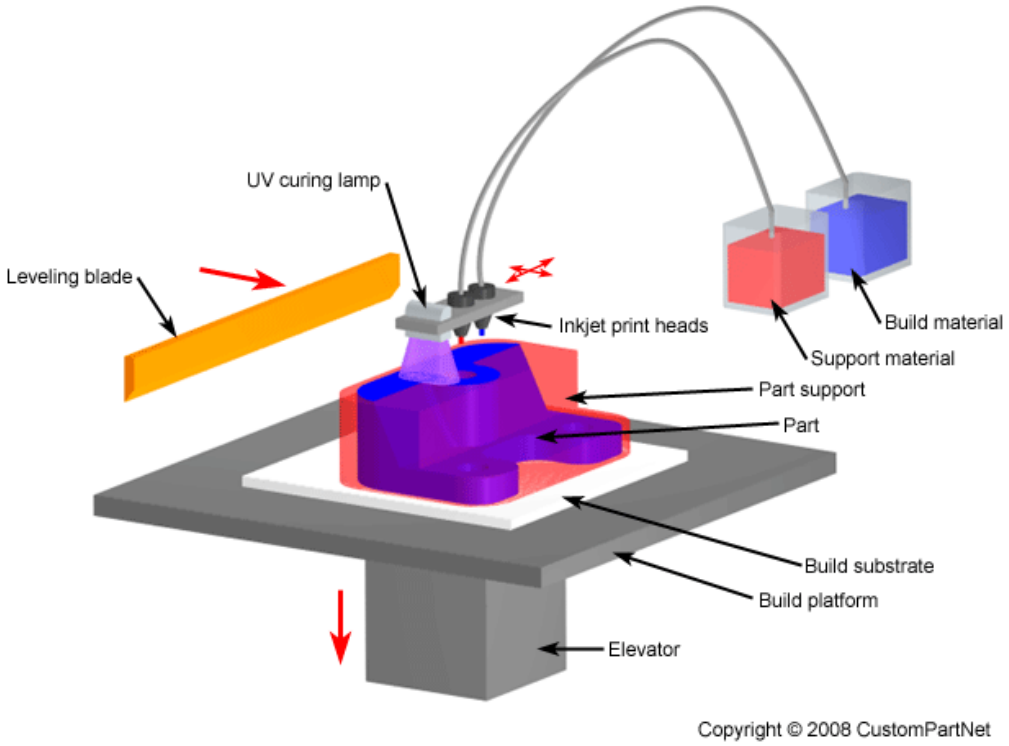

Figure 23. Example of Photopolymer Inkjet 3D printing technology [34].

A 3D printing technique that has not to be confused with Jetted Photopolymer is the **Inkjet Printing technique**, which is a combination between Inkjet printing and the fused 3D printing processes.

In a half way between fused and laser 3D printing technologies, there are some techniques as **Selective Laser Melting (SLM)**, which is similar to the Selective Laser Sintering (SLS) explained before, with the difference between both on the material state; in SLM, as its name shows, the powder material is melted, as opposed to SLS, where its sintered at low temperature. This SLM process is equivalent to another process called **Electron Beam Melting (EBM)**, which uses an electron beam instead of an UV laser to melt the material powder. The **Direct Metal Laser Sintering (DMLS)** is also another variation of this type of fused/laser combined techniques, with the same concept as the SLM, but changing the polymeric powder material for a metallic powder. DMLS was developed jointly by Rapid Product Innovations (RPI) and EOS GmbH in 1994, and was the first commercial rapid prototyping method to produce metal parts in a single process.

Another Rapid Prototyping technology that reminds to traditional machining manufacturing technologies, but for its addition of material characteristic and the layer-to-layer fabrication, is considered a 3D printing technology is the **Laminated Object Manufacturing (LOM)**. This process was invented and developed by Helisys of Torrance, CAIn, in 1991.

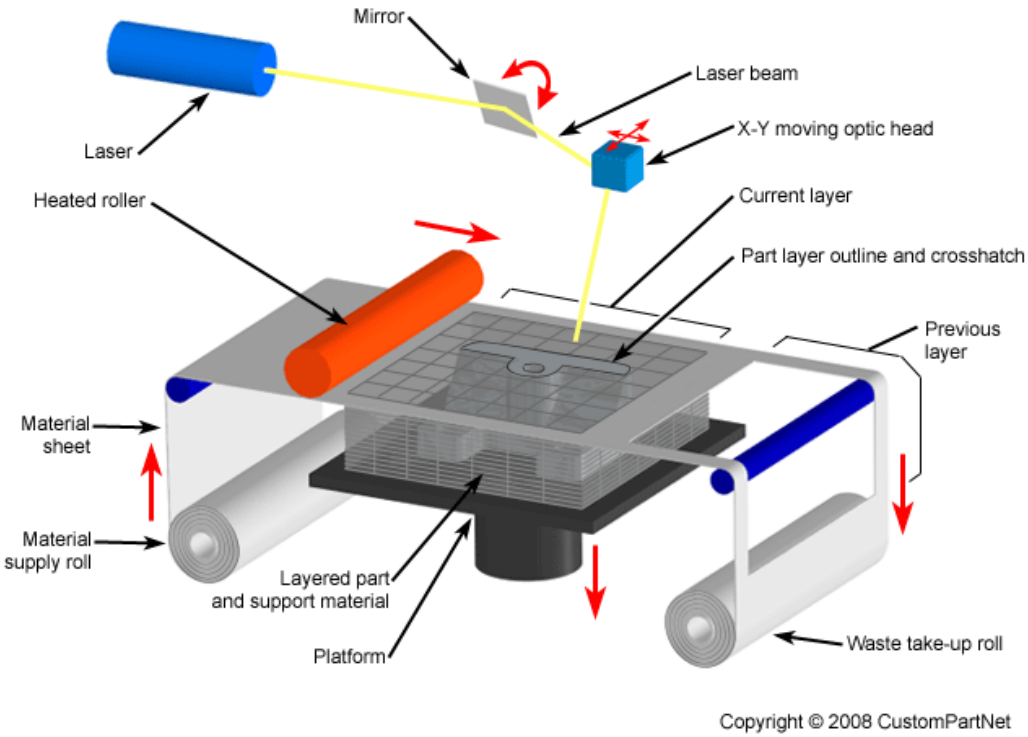

Figure 24. Example of Laminated Object Manufacturing (LOM) 3D printing technology [34].

The material is added entirely as a layer, and joined with the other layers using adhesive resin. After the joining, the added layer is cut with the correct shape using a laser, allowing the addition of the next layer. This technique allows the use of any material that could be joined using layers and machined afterwards, like wood, plastics or metals.

Finally, the last 3D printing technology and, for the porpoise of this project, the most important, is the method known as **Syringe Extrusion**. This method consists of an extruder that is a combination of an infilled syringe with the printable material and a nozzle with a determined section shape. Applying pressure on the top of the syringe it is possible to extrude the printable material in the form of filaments, with a section determined by the nozzle shape. The printing process to conform the layers using these extruded filaments is the same as the utilized for the fused 3D printing technologies explained before.

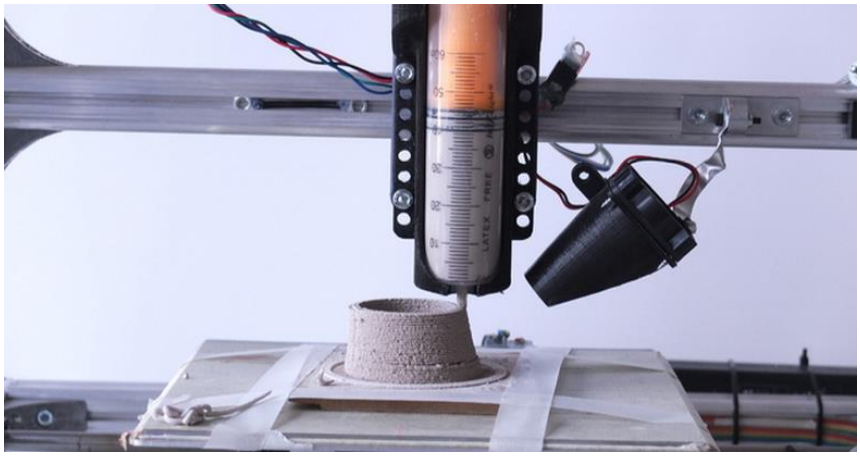

Figure 25. Example of Syringe Extrusion 3D printing technology [36].

This technique allows the 3D printing of any viscous material that presents the appropriated viscosity to flow through a nozzle. Also, it is possible to print some materials, which do not have a viscous comportment, like ceramic powder materials, using jellification techniques to provide them to this viscos state. Depending on the printing material, the extruder could need to be heated, in order to melt of obtain a desired viscosity for a non-Newtonian material.

To conclude, it will be presented two resuming tables; the first table presented below shows some of the usual characteristics of all the techniques explained before, with information as the materials that can be used, tolerances, finishes and build speed that offers each one of them:

Table 6. Information of 3D printing techniques [34]

Technique	Material Type	Materials	Min layer thickness (inches)	Tolerance (inches)	Surface finish (inches)	Build speed
FDM/FFF	Solid (Filaments)	Thermoplastics (ABS, Polycarbonate, Polyphenylsulfone), Elastomers	0.005	0.005	Rough	Slow
SLA	Liquid (Photopolymer)	Thermoplastics (Elastomers)	0.001	0.005	Smooth	Average
SLS	Powder (Polymer)	Thermoplastics (Nylon, Polyamide, Polystyrene), Elastomers,	0.004	0.01	Average	Fast

		Composites				
Jetted Photopolymer	Liquid (Photopolymer)	Thermoplastics (Acrylic), Elastomers	0.0006	0.0010	Smooth	Fast
DMLS	Powder (Metal)	Ferrous and non-ferrous metals (Steel, Aluminum, Bronze, Cobalt-chrome, Titanium), ceramics	0.001	0.0100	Average	Fast
LOM	Solid (Sheets)	Thermoplastic(PVC), paper, composites, ferrous and non-ferrous metals, ceramics	0.002	0.004	Rough	Fast
Syringe Extrusion	Viscous materials	Any material which has a viscous texture and a good viscosity	0,005	0,005	Rough	Fast

And the next table shows a comparison between Cold Isostatic Pressing and 3D Printing techniques, showing the advantages and disadvantages that presents each one:

Table 7. Comparison between Cold Isostatic Pressing and 3D Printing techniques

Cold Isostatic Pressing		**3D Printing**	
Advantages	**Disadvantages**	**Advantages**	**Disadvantages**
Good mechanical properties	Slow process	Fast process	Lower mechanical properties
Excellent surface finish	Fixed product geometry	Product variability	worse Surface finish
Excellent geometric tolerances	Use of matrixes	Does not needs matrix	worse geometric tolerances
Large quantity production	Expensive process	Cheap process	

1.5. State of the art

The 3D printing technologies as it has been shown, present a large number of variations that make them very innovative, adaptive and full of potential to develop complex materials with particular microstructures and chemical compositions. The field of 3D Printing is still too young but, owing to its

current expansion and wide amount of investigation researches, is possible to have an approximated future idea of which way these techniques will take.

Making a general view on the current applications of the 3D printing, it is easy to justify the skills mentioned before:

The innovation that these techniques present can be appreciated on the manufacturing revolution that ther are generating, offering a new concept of open fabrication and a constant updating inside the technological field. As an example, the OLO 3D Inc. offers the possibility to use a mobilephone as a stereolithographic 3D printer with its Smartphone 3D printer [37], which uses the mobile's screen light and a specific photocurable resin to obtain the CAD design.

Due to their adaptive manufacturing process, the 3D printing allows the fabrication of some products that otherwise could not be possible. Made in Space Inc. in collaboration with NASA group has developed the concept of lauching a 3D printer on space voyages, in order to develop and satisfy the requeriments during the expedition in the space [38].

This adaptation is also present on the application of other materials apart from polymers, such as metals, wood, ceramic or even biological materials [39]. This skill lends to these technologies a lot of potential for future applications on fields like arts, arquitecture, engineering or medicine, among other fields.

During the last years, the 3D printing with ceramic materials and particularly using ceramic Zirconia based materials has taken importance inside the medical field, in order to create implants and prostheses. The researches realized are based on two aspects; the 3D printing process itself, and the materials used on the process.

Regarding to the 3D printing process, it is possible to mention:

A first introduction and organization on the use of 3D printing with ceramics can be found on the aticle "A review of process development steps for new material Systems in three dimensional Printing (3DP)" by Ben Utela et al. [40], which focuses on five steps; powder formulation, binder method selection, binder formulation and testing, printing process specification, and post-processing specification.

On the hand, a manuscript published by J.Ebert et al. [41] and entitled"Direct inkjet Printing of dental prostheses made of zircònia" comments the advantages of 3D printing on the obtaining of dental prostheses, compared with other traditional manufacturing technologies. The principal advantage of 3DP techniques is their higher precision, but on the other hand, their also present post-processing problems, like the cracking during the drying process.

Related to the type of 3D design made, the article "High-strength cellular ceramic composites with 3D microarchitecture", by Jens Bauera and co-workers [42], shows the mechanical and structural properties of different types of 3D printed ceramic microarchitectures.

Another research related with the properties of the 3D printed structure is the article "Analysis of the mechanical response of biomimètic materials with highly oriented microestructures through 3D Printing, mechanical testing and modeling" by Enrique Escobar de Obaldia et al. [43]. On this article is investigated the effect of microstructure orientation on the structural properties of 3D printings using a biological material extracted of the Chiton tooth molusc, which presents a honeycomb type structure.

Focusing our attention to the material used on the 3D printing process, in the literature it can be found:

A first introduction on the use of the Gel-casting technique in order to obtain a viscous material from ceramic powders, is valorated on the article "Gelcasting: From laboratory Development Toward Industrial Production" by Ogbemi O. Omatete et al. [44]. On this article is exposed the industrial procedure for obtaining advanced ceramic parts using the Gel-casting technique.

The application of the previous technique for the obtaining of 3D printing materials using Zirconia based ceramic powders, is shown on the articles "Gelcasting of Zirconia Using Agarose" by E. Adolfsson [45], and "Extrusion-based 3D Printing of ceràmic components" by M. Faes et al. [46]. On these articles is shown the particular characteristics of Gel-casting process for Zirconia based ceramic powders, and the characterization of the viscous material obtained.

Due to the future tendence of using Zirconia/Alumina composites to obtain better properties, it is good to have presented the article "Influence of 3Y-TZP on Microstructure and Mechanical Properties of Al2O3-based Composites" by M.-T. Weng et al. [47].

Finally, due to the particular 3D printing properties that Alumina presents, articles like "Property enhancement of 3D-printed alumina ceramics using vacuum infiltration" by S. Maleksaeedi et al. [48], or "Near zero shrinkage porous Al2O3 prepared via 3D-printing and reaction bonding" by D. Yao et al. [49], pretend to improve the structural and mechanical properties of 3D printed Alumina ceramics using vacuum infiltration of controlling the particle size and shape on the printing process.

CHAPTER 2: OBJECTIVES

The rapid prototyping techniques (mainly the 3D printing technique) are nowadays the group of manufacturing tools with the biggest evolutive tendencies, due to their faster, cheaper, open-sourced, and adaptable processes that allow the use of a wide range of diffrent materials; from polymeric up to metallic materials. The excellent qualities of these techniques result on their application on a lot of fields as arts, arquitecture, automotion or even medicine. Inside the medical field, the most popular application is the 3D printing of Zirconia based ceramic powders for the building of dentistry prostheses, due to its excellent mechanical properties and the presence of biocompatibility with the human body. The future tendence on the material employed for the 3D printing is the introduction of Alumina and Ceria on Zirconia in order to create Zirconia based ceramics with better mechanical properties and aging resistance.

The principal objective in this work is the obtaining of printable Zirconia powder based ceramic materials using the Gel-casting technique, for their posterior conformation using the Syringe extrusion 3D-printing technique.

Due the future tendence on the use of Zirconia-based ceramics mentioned before, the Zirconia powder based ceramic materials choosed are three: 3Y-TZP, 3Y-TZP with different Alumina proportions, and 3Y-TZP with 15% wt of

Ceria, as an alternative to 12Ce-TZP (optimal Ceria on TZP's proportion in order to prevent hydrothermal degradation [50]).

Once obtained viscous printable materials with the gel-casting technique, it is needed to obtain the knowledge and working formation on Syringe extrusion 3D-printing technique, in order to make the correct configuration of all the 3D-printer working parameters. Every ceramic material obtained via 3D printing is compared with other conforming techniques using the same material. The conforming techniques used to build samples in order to compare 3D-printing technique are Gel-casting technique and Cold Isostatic Pressing (CIP) technique.

Finally, the comparative between conforming techniques is realized making a detailed microstructural and mechanical characterization as a function of their chemical composition in terms of roughness, density and rheological properties (mainly viscosity) to take into account by using this technique; afterwards, the hardness and fracture toughness should be evaluated to compare their properties with the mechanical properties of bulk materials.

The study is mainly focused from a mechanical and materials science point of view, without focusing on the chemical, electrical or biologic concepts that may be related to it. At the same time, this work also has the goal to get the knowledge and training with the largest range of advanced characterization techniques, procedures and/or protocols, experimental methodology, acquiring the scientific rigour and seriousness required for the investigation of an industrial engineer.

CHAPTER 3: EXPERIMENTAL PROCEDURE

3.1. Sample nomenclature

In order to present and facilitate the result's analysis on this work, it has been adopted the following nomenclature for each sample:

MP_C_T

where *M* is the sample's material of study, *P* is the proportion of this material on the sample, *C* is the conformation technique used to built the sample, and *T* is the sintering temperature of the sample's material. All the possible terms used to designate the samples are listed on **table 8**. Obviously the rest of the sample's proportion regarding to the indicated is the 3Y-TZP Zirconia proportion, due to all the sample's materials on this bachelor's degree are 3Y-TZP Zirconia based ceramics.

Table 8. Nomenclature of the samples of study.

Material		Proportion	Conformation technique		Thermal threatment temperature
Z	Zirconia	**5%, 10%, 15% 20% or 25%**	**IMP**	3D printing	**1450ºC**
A	Alumina		**SG**	Gel-casting	**1550ºC**
C	Ceria		**CIP**	Cold Isostatic Pressing	**1660ºC**

Examples of sample designation using the nomenclature proposed above:

- **A25 IMP 1550**: 3Y-tzp Zirconia sample with 25% Alumina obtained via 3D-printing and sintered at a temperature of 1550ºC.
- **Z100 SG 1450**: 3Y-TZP Zirconia sample obtained via Gel-casting and sintered at a temperature of 1450ºC.
- **C15 CIP 1650**: 3Y-TZP Zirconia sample with 15% of Ceria obtained via Cold Isostatic Pressing and sintered at a temperature of 1650ºC.

3.2. Materials

3.2.1. 3Y-TZP

The base ceramic material used in this experimental work is Zirconia, which presents a tetragonal strutcute due to it is stabilized with 3% molar of Yttria. Then, the material used is a polycrystalline zirconia powder stabilized with 3 % molar of Yttria, also known as 3Y-TZP. The raw material has been provided by *TOSOH* manufacturer (type *TZ-3Y-E*). **Table 9** summarizes the main chemical elements for the material studied here [51].

Table 9. Chemical composition analysis for the Tosoh's 3Y-TZP Zirconia [51]

Y_2O_3 (wt%)	HfO_2 (wt%)	Al_2O_3 (wt%)	SiO_2 (wt%)	Fe_2O_3 (wt%)	Na_2O (wt%)	Pigment (wt%)
5.2±0.5	>5.0	0.1~0.4	≤0.02	≤0.01	≤0.04	-

3.2.2. Alumina

Aluminum oxide, commonly referred to as Alumina (Al_2O_3), is a widely used advanced ceramic inside engineering aplications, due to its good mechanical properties (**see section 1.1.5.**) and reasonable price. It can exist in several crystalline phases, but the most stable is the hexagonal alpha phase, which appears at high temperatures. Alpha phase alumina is the strongest and

stiffest of the oxide ceramics, being the most interesting structure for structural applications.

The Alumina emploied in this work is a 99.99% alpha phase Alumina powder provided by *Alfa Aesar* manufacturer. The reason to use Alumina as a compound for the creation of the Zirconia based caramics studied on this bachelor's degree is to take benefit of its improving character on the mechanical properties of the Zirconia, following the evolutive tendence of the zirconia-based ceramics.

3.2.3. Ceria

Cerium Oxide, commonly referred as Ceria (CeO_2), is an advanced ceramic with engineering applications as fuel cell components due to its ionic conductivity, as a catalyst in automotive applications of catalyst converters, and as a water splitting or antioxidant.

The Ceria used in this work is Cerium Oxide (III) provided by *Alfa Aesar* manufacturer. The reason to use Ceria as a compound for the creation of the Zirconia based caramics studied on this bachelor's degree is to take benefit of its improving character on the resistance of Zirconia against Hydrothermal Degradation.

3.2.4. Agar-Agar

Agar-Agar or only Agar is a substance obtained from algae, which contains a gelling agent that can be released on boiling and used as a binder or as a matrix component to embed the ceramic particles in order to obtain jelly products. The gelling agent in agar is an unbranched polysaccharide agarose obtained from the cell walls of some species of red algae, primarily from the genera Gelidium and Gracilaria. In chemical terms, agar is a polymer made up of subunits of the sugar galactose. Agar-Agar is principally used on Asia, where it was discovered at rounds of 1960, and the most common applications are as an ingredient in the Asian cuisine and as a gellying agent on solutions, creating a polymeric web that works as a binder between the particles.

The gelling agent used as binder on the gel-casting solution is Agar-Agar seaweed *organic/biological Atlantic* from *NATUURLIJK* (Germany) manufacturer. The reason to use Agar as the gellying agent of the ceramic powder based viscous pastes obtained by Gel-casting technique is its reduced price and extended use as a binder on solutions.

3.3. Conformation techniques

3.3.1. Gel-casting Technique

In order to obtain a ceramic powder-based viscous paste which offers all the rheological properties to be extruded by using the Syringe Extrusion 3D-printing process, it has been used the gel-casting technique, see **section 1.4.3.** for more details.

During the process, there are a number of very important features depending on the textures and properties that is desired to obtain. Below, the different steps employed to obtain a viscous ceramic material from a colloidal solution are briefly presented:

1. The first step consists on pour the powder of the material that is desired to jellify on a specific quantity of distilled water and the jellifying agent, that it is normally a polymeric material.
2. Once poured, depending on the powder material type is recommended to pre-mix the dissolution using the sonicator *OMNI International Inc.* model *Omni-ruptor 4000* with a power output of 40, which helps the correct mixing between the powder, the water and the jellifying agent. There are some types of ceramic powders that once sonicated, present an emulsified state, but some others do not and precipitate during the mixing.

Figure 26. Aspect of an emulsified 3Y-TZP Gel-casting colloidal solution after sonifying process.

3. Heat the mixture until 100 °C at bain-marie and mixed using an *AREC X* heating magnetic stirrer and an iman to get an homogeneous solution (see **Figure 27**). The critical parameter in this step is the temperature, which has to be kept constant and around 100ºC during 20 minutes due to favorices the gelidifcation process. Furthermore, during this process, the iman has to spin at 200 rpm in order to guarantee the homogenization of the gellying agent and avoid the precipitation of the ceramic powder. This step blends the gelling agent with the ceramic powder, creating a unique solution, where the powder particles will be suspended and will not precipitate.

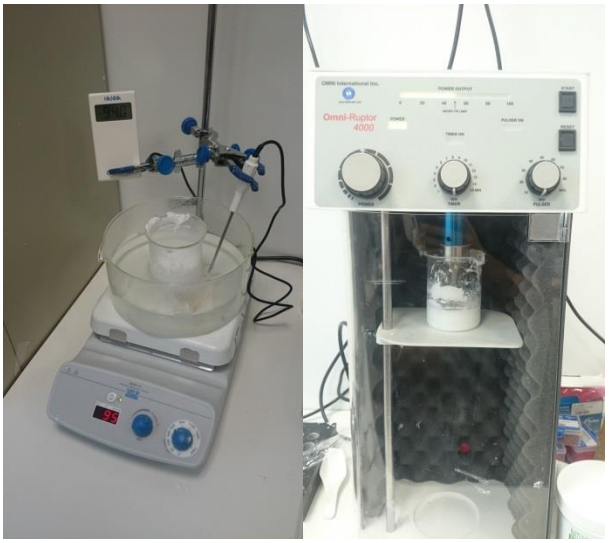

Figure 27. General view of the heating megnetic stirrer (left) and the sonicator (right).

Consideration: It is recommended to apply a sonication at the middle and the end of this step to improve and guarantee the correct blending of the components in the solution.

4. Cooling process of this mixture until room temperature, where the resulting material presents a viscous texture. Depending on the quantity of the jellifying agent used, it will be obtained a more or less viscous paste.

   If the sample desired to obtain is conformed using the Gel-casting technique, is necessary to pour the dissolution on the matrix during the cooling process, in order to obtain the final product, see **Figure 28**.

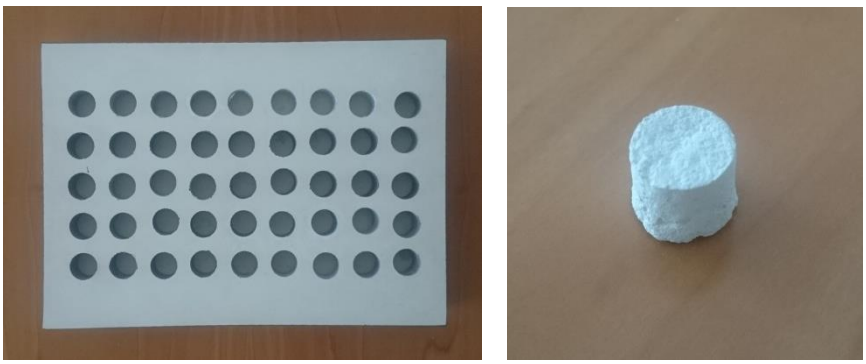

Figure 28. Gel-casting sample's matrix and conformed Gel-casting sample.

5. On the other hand, if the desired final product is a viscous paste for 3D-printing use, the gellyfied solution deeds a grinding and drying step. The obtained product fills a metallic container when the mixture is cooled until reach the room temperature (where a deshidratation process takes place, see **Figure 29** (right)). Before fill the extrusor from the 3D printer, it is required to mixt the ceramic paste in order to reduce the preexisting porosity, see **Figure 29** (left).

Figure 29. Gellyfied and grinded ceramic powder based viscous paste ready to be 3D-printed.

> **Consideration:** This water-loss, which can be desirable or not, has to be kept in mind and doing carefully, because the modification on the water content of the paste will widely modify its properties of texture and viscosity. Another fact to keep in mind is the water evaporation that this paste suffers, in order to conserve it and calculate the volume reduction on its utilization.

The product conformation with the paste obtained from the powder material, can be realized with Syringe extrusion 3D-printing technique if their present the appropriate viscosity. High water content pastes are worse due to the water separation and loss during the extrusion process. Furthermore, viscous pastes with high water content need longer drying times being thus higher than a week and suffer higher volume decreasing, which can generate cracks on the samples.

The determination for the proportions of ceramic powder, water and gelling agent on Gel-casting solution in order to obtain the viscous paste with the optimal 3D-printing comportment has been found fixing a specific amount of ceramic powder and leaving as unknown variables water and gelling agent. From my experience, the proportion of gelling agent results more critical than water on the texture and viscous behavior of the obtained paste, showing a plastic texture if it is excessive or a liquid behavior if it is not enough. Once found the gelling agent's proportion, it has modified the water proportion, which affects on the the extrusion quality during 3D-printing process, improving the viscous paste obtained. All the viscous paste tests with Gel-casting technique investigated along this Bacheloor's degree are summarized in **Table 10**.

Table 10. Proportions of different components for the Sol-Gel solution.

Test	Water (g)	3Y-TZP (g)	Agar-Agar (g)	3Y-TZP (%)	Agar-Agar (%)
1	43	15	1	25.4	1.7
2	43	15	2.5	24.8	4.1
3	43	15	1.75	25.1	2.9
4	43	15	1	25.4	1.7
5	43	15	1	25.4	1.7
6	43	15	0.5	25.6	0.9
7	43	15	0.5	25.6	0.9
8	43	15	0.5	25.6	0.9
9	43	15	0.5	25.6	0.9
10	43	15	0.5	21.6	0.9
11	43	15	0.5	25.2	0.9
12	53	15	1.3	23.1	1.9
13	43	15	1.625	18.9	2.7
14	48	15	1.95	18.8	3.0
15	63	15	1.3	19.0	1.6
16	63	15	1.7	18.6	2.1
17	63	15	0.85	19.0	1.1
18	63	15	2.55	21.8	3.2
19	63	15	1	21.8	1.3
20	53	15	0.8	33.3	1.2
21	53	15	0.9	18.6	1.3
22	43	15	1	22.9	1.5
23	65	15	0.82	18.6	1.0
24	50	15	0.6	22.9	0.9
25	67.5	15	0.825	18.0	1.0
26	55	15	0.71	21.2	1.0
27	57	15	0.73	20.6	1.0
28	55	15	0.71	21.2	1.0
29	53	15	0.69	21.8	1.0
30	50	15	0.7	22.8	1.1

Finally, after the conformation and drying process, the grren bodies are sintered, in order to eliminate the gellying agent and obtain structural and mechanical properties desired. The specimens have been introduced in a Nabertherm furnace until 1450ºC -1650ºC (depending of the sample, see **section 3.3.4.**) for 2 hours. The heating and cooling temperature rates has been keep constant and equals to 3 ºC/min.

3.3.2. 3D printing

The 3D printer used to build all the samples using viscous ceramic powder based pastes obtained for the Gel-casting technique is a *BCN 3D Technologies*, model *BCN3D+ Dual Paste*, constructed and customized for the *CIM foundation* in collaboration with the *Universitat Politècnica de Catalunya*. The syringes, pistons and nozzles used to extrude the viscous pastes have been *Nordson EFD Optimum Systems* syringe & piston *model 3cm^3* with 9.5 mm of internal diameter and 8cm of length, and *Engineering fluid dispersing Precision tips* models *15GA GP Amber 50PC, 18GA GP Green 50PC, 20GA GP Pink 50PC, 20GA TT Pink 50PC and 25GA TT Red 50PC*, being the selected to build the samples the Amber model for presenting the best printing results. **Figure 30** shows a general view of the 3D printer (left side) and the syringes, pistons and nozzles employed (right side).

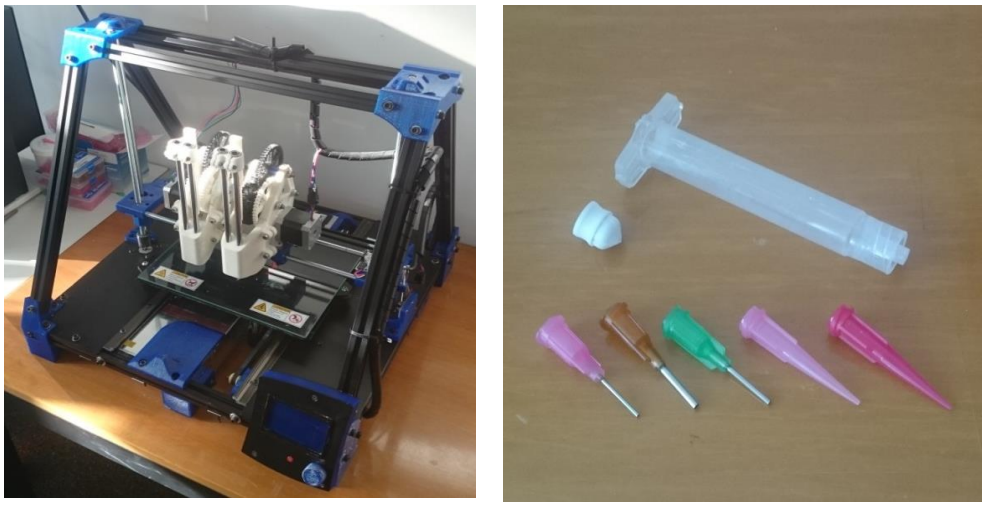

Figure 30. General view of the 3D printer, syringes, pistons and nozzles employed.

3.3.2.1. 3D-printer working

This 3D-printer is an adaptation of a commercial *BCN3D+* FDM 3D-printer to be used as a Syringe extrusion 3D-printer, with the replacing of the polymeric extruder for two syringe extruder type units. The syringe extruder unit consists on a toothed shaft which allows the application of a constant pressure on the syringe's piston in order to extrude the viscous material inside it. The linear movement of the extruder shaft is subministred by the electric motor rotation. The **figure 31** shows a general view of the Syringe extrusion system of the 3D-printer.

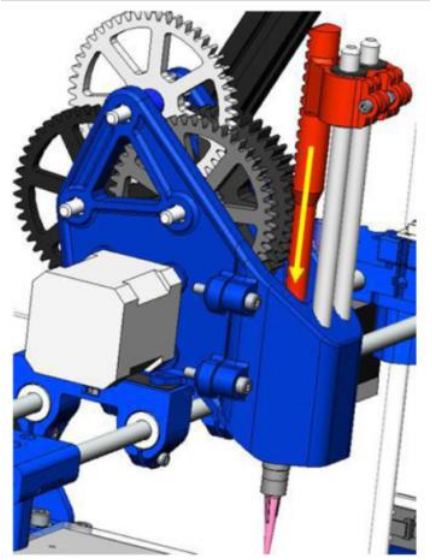

Figure 31. General view of the Syringe extrusion system of the 3D printer [52].

The mechanical transmission between the extruder shaft and the electric motor is realized employing a gear transmission, which has a reduction rate of 256. This reduction is needed to supply the necessary pressure on the extruder shaft to allow the extrusion of the viscous material, which makes an opposing resistance due to shear stresses generated on the nozzle, **see section 2.3.2** to get more details. **Figure 32** shows a general view of the gear transmission employed to transmit and convert the rotational movement of the electric motor on the longitudinal movement of the extruder shaft (*z1=z3=z5=12 teeth, z2=z4=z6=z8=48 teeth*).

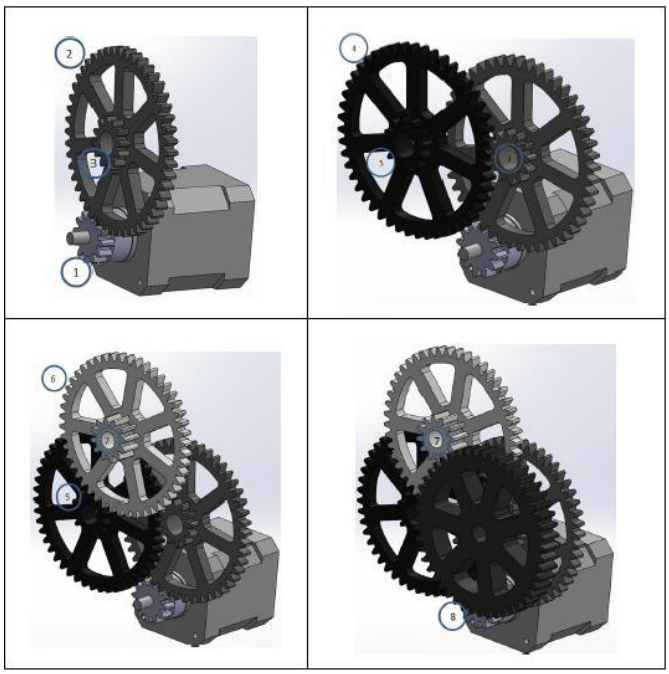

Figure 32. Gear transmission diagram [52].

The plate's printing movement in order to build the 3D model is obtained by a simultaneous longitudinal, transversal and vertical movements; the movements on the *x*- and *y*- axis are obtained with the gear assembly with two different plastic toothed belts and electric motor gears, and the movement on the *z*-axis is obtained with the rotation of a threaded shaft accopled on another electric motor. In order to maintain the belts stretched there is a belt tensor for every belt. The resulting plate's movement is controled and delimited by different limit switches, being only modificable the vertical limit switch as it is depicted in **Figure 33**.

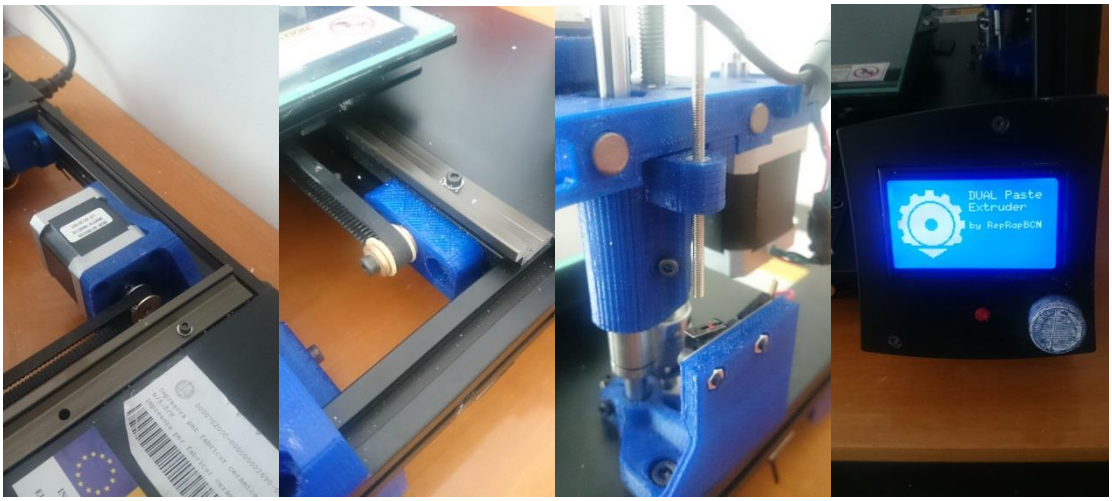

Figure 33. General view of the electrric motor, toothed belt, vertical limit switch and LED display of the 3D printer (from left to right).

Finally the printing process is governed by a Control Process Unit under the 3D-printer, which has a controller with a LED display that allows the entire configuration of all its parameters (see the right image in **Figure 33**). The 3D-printing archive's inserting can be realized using an SD card or directly pluging in a computer with the 3D-printer/computer slot. **Figure 34** shows all the options available in the 3D-printer programme and present in the 3D-printer LED display:

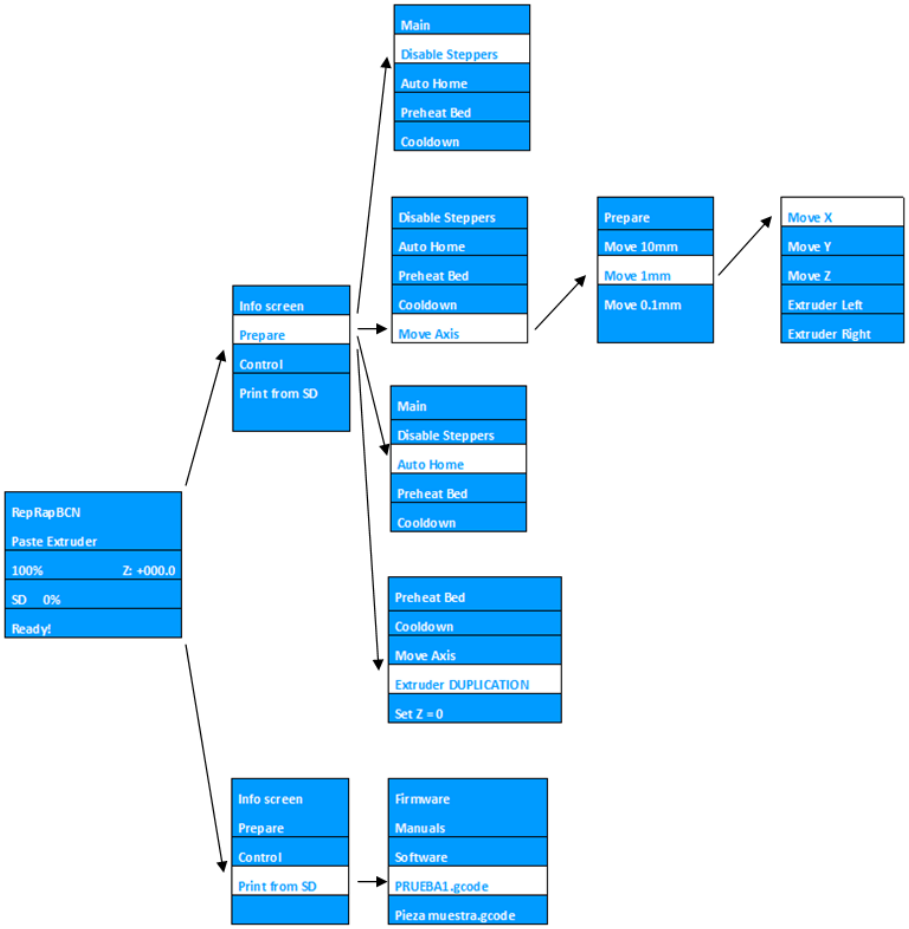

Figure 34. 3D-printer's programme comanders diagram [52].

3.3.2.2. 3D-printing process

Once explained the 3D-printer operation above, it will proceed to mention and briefly explain the different 3D-printing steps.

Mainly, the 3D-printing process consists on four differentiated steps:

- **Creation of a CAD design**. In order to obtain a 3D geometry of the design desired to print, is generated a CAD design with any computer aided design program as Solidworks, Catia or Rhynoceros.
- **Obtaining of a 3D printer understandable archive**. To obtain an archive of the CAD design which could be on an understandable language for the 3D-printer, it is necessary to convert the STL. Archive into a G-CODE archive.
- **Configuration of the 3D printing parameters**. The correct printing of a 3D design using the G-CODE archive it is only possible with the correct configuration of all the 3D printing parameters and the 3D-printer adjusting.
- **Printing of the CAD design**. Before starting the printing process, there are some steps that have to be realized as the syringe filling or the 3D-printer's height adjustment, among others.

Each process commented and briefly described above will be explain in more detail below:

i) CAD design creation

The 3D design of the samples has been done using the SolidWorks programme in order to obtain a CAD archive. All the parameters on the sample's design have been choosed considering the restriction of the material mass available to print inside the syringe. The parameters adopted to build the samples are:

- **Geometry of the designed samples**, which has been kept constant and equals to 20x20x6 mm (square shape).
- **Number of printed layers** and **printing diameter**, which has been four layers with a maximum height of 1.5, which corresponds to the diameter of the nozzle emploied.
- **Printing geometry** of the layers has been rectilinear type geometry, being the faster and easier option in comparison to concentric type, honeycomb type and others.

Once created the CAD archive with Solidworks, this archive has to be saved as an STL. File format (STereoLithograpy), which is a standard surface geometry description file inside the CAD modelization, describing the 3D design as triangulated surfaces. This step is necessary in order to allow the posterior transformation into an understandable 3D-printer language archive. **Figure 35** shows the creation of the CAD file of the samples.

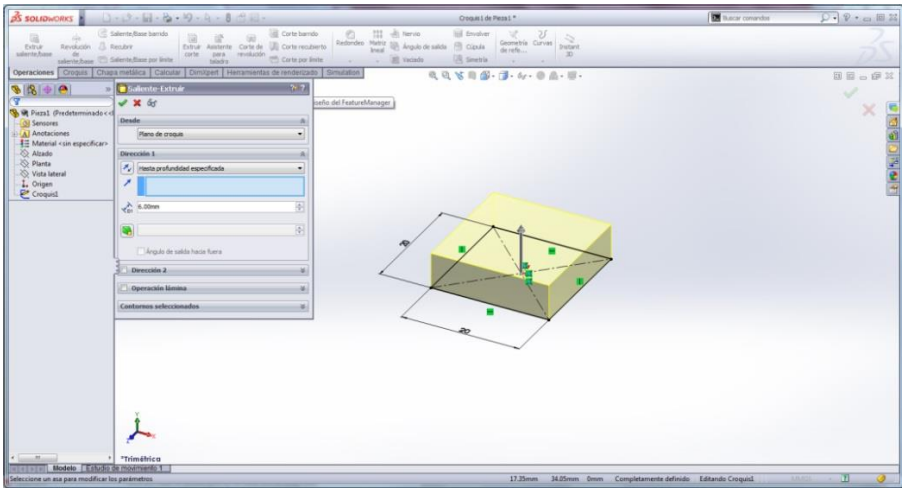

Figure 35. 3D design using the SolidWorks CAD programme.

ii) Obtaining of a 3D printer understandable archive

The final 3D printer geometry has ben possible with the use of two programmes: Netfab basic and Slic3er.

Netfab basic programme is used to establish a new coordinate system for the 3D-printer, and positionate the CAD design according to the desired specifications using rotations and traslations, among other options, due to

the coordinate system of the CAD design and the 3D-printer could not be the same. **Figure 36** shows the coordinate system difference between Solidworks and Netfab basic programmes using the same CAD file. It also shows the most important positionating commands of part alignment, moving, rotating and scaling respectively.

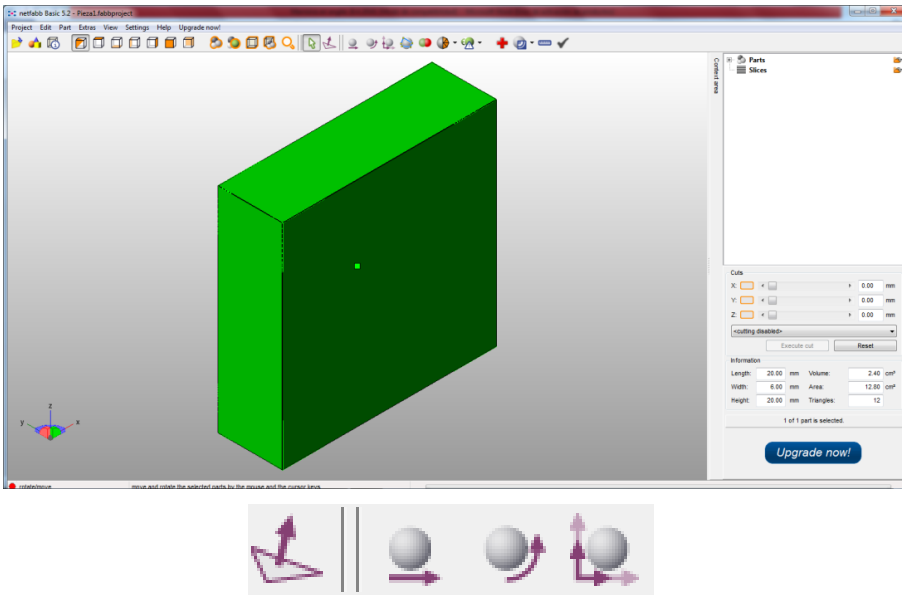

Figure 36. Most important Netfab basic positioning commands

Once configurated, the saved archive of the 3D design continues being a STL. File format, needing the second programme Slic3r in order to transform it into G-CODE.

iii) Configuration of the 3D printing parameters

The Slic3r programme changes the STL. Archive file format into G-CODE format cutting the CAD design into different layers and transforming it on a sliced geometry. This program allows the configuration of all the printing parameters, being grouped intro Plater, Printing settings, Filament settings and Printer settings, see **Figure 37.**

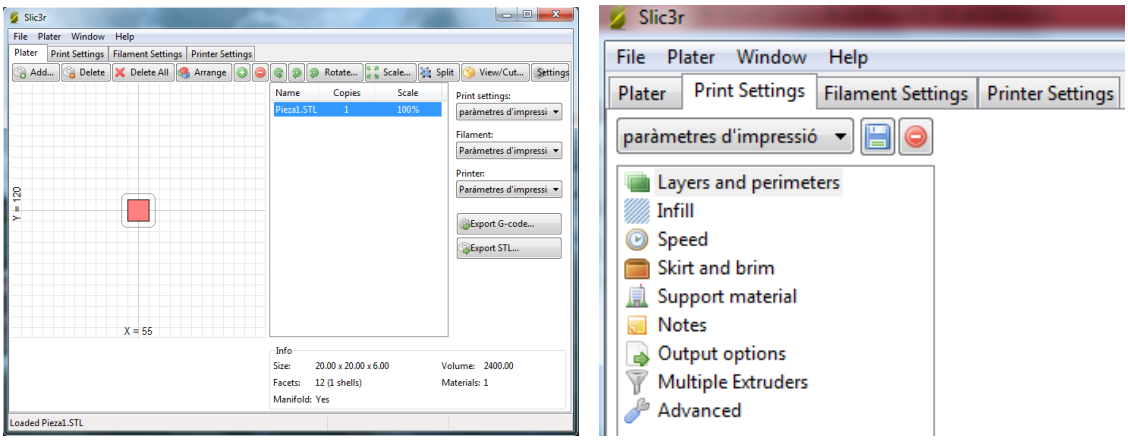

Figure 37. General view of Slic3r programme sections.

Inside **Printer settings** there are nine items: *Layers and perimeters, Infill, Speed, Skirt and Brim, Support material, Notes, Output options, Multiple Extruders* and *Advanced*. The only sections available to be modified to print ceramic materials are the first four, leaving the next five with the default configurations due to these insets do not modify the printing process of ceramic materials. In other words, these sections may take into account when the printing process is desired to be done with polymeric materials. Below are described and briefly explained the main items to take into account to print ceramic materials:

- **Layers and Perimeters**: In this section there are all the layer size's configurations. The size of the sample's height has been modified to 1.5 mm, the rest of the values have been configures to zero in order to desactivate them.
- **Infill:** This section configures all the printing geometry and density. The different printing geometries available are the following: Rectilinear, Line, Concentric, Honeycomb, Hilbertcurve, Archimedeanchords and Octagramspiral. It also can be configurated the filament's angle on the printing geometry, having a range of 180 degrees. The density of the printed body can also be configured changing the separation between filaments.

  It has to be kept in mind that some geometries employ easier printing movements in order to draw the printing route of the geometry. The printing geometry that has achieved less time and printing imperfections as paste spiting, maintaining a good density and structural integrity for the sample building has been the rectilinear geometry with a 100% of density. **Figure 38** show an example of all the printing geometries that can be selected at different densities:

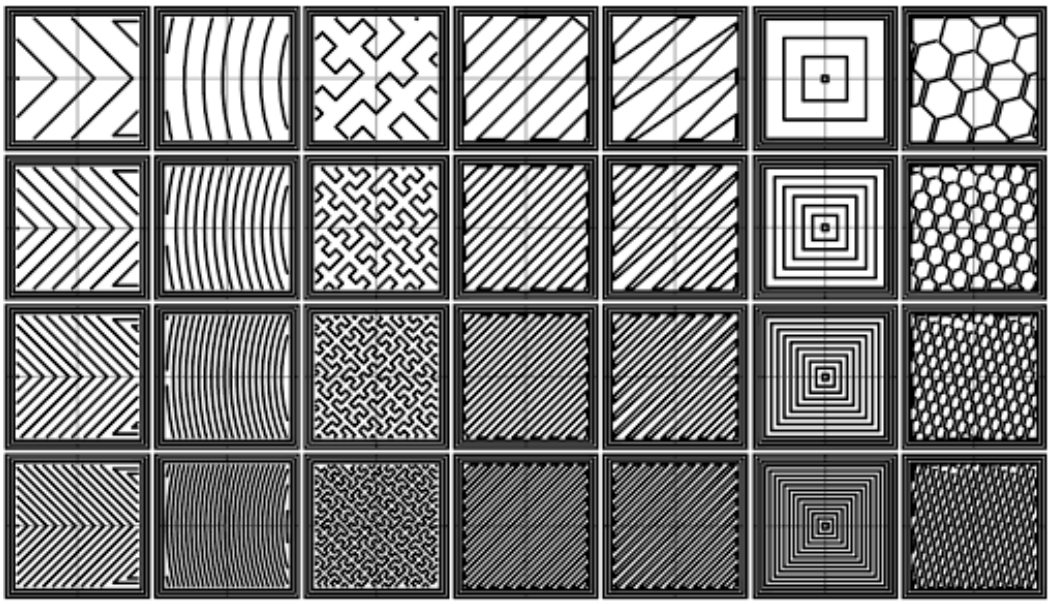

Figure 38. Printing geometries available on Slic3r [53].

- **Speed:** The movements of the printing plate can be configurated on this section. This configuration is done togheter with the extrusión speed in order to avoid printing problems as described in **section 1.3.2** and obtaing the best moving/extruding speed ratio.
- **Skirt and Brim:** This section is reffered to the first pre-printing extrusión filament which skirts the 3d printng design, in order to prepare the material inside the nozzle, and eliminate air, water or voids on the material inside the siringe. The parameters that can be configurated on this section are the number of skirting filament loops (loops), the distance of these filaments to the 3D design (skirt height). The minimum extrusion length and Brim options have no effect on Syringe extrusion 3D printing.

Table 11 shows a resume of all the values of the printer settings options.

Table 11. Values of all the 3D printer settings adopted.

Layers and perimeters		**Infill**		**Speed**		**Skirt and brim**	
Layer height	1.5 mm	Fill density	100%	External perimeters	100 mm/s or %	Loops	1
First layer height	1.5 mm or %	Fill pattern	rectilinear	Infill	8 mm/s	Dist. from object	6 mm
		Top/bottom fill pattern	rectilinear	Solid infill	10 mm/s or %	Skirt height	1
		Comb. infill every	1 layers	Top solid infill	8 mm/s or %		
		Fill angle	90º	Support material	10 mm/s		
				Sup. mat. interface	100 mm/s or %		
				Travel	20 mm/s		
				First layer speed	100 mm/s or %		

After that, a configuration of the **Filament settings** is required. Inside of this section exists two different options:

- **Filament:** The only parameter that has to be modified is the Diameter that is the syringe diameter on the extruder unit. This parameter controls the extrusion speed and combined with the plate's movement determines the printing result. Despite of being 9.5 the syringe diameter used, the combination of this parameter and the

viscosity of the viscous paste used has shown the optimal response between the range of 8 and 9, being the value adopted 8.6.

All the temperature parameters have to be desactivated, due to the material is extruded at room temperature an there is o necessity to heat the paste.

- **Cooling:** The 3D-printer used does not have cooling fans; then, the cooling process is done at room temperature under ambient humidity.

Finally, the **Printer settings** that have to be configurated are described below:

- **General:** Inside this section there are the bed size of the plate, which is a 110x240 mm (x,y) and the print center, which is a 55x120 mm (x,y). One useful parameter is it is wanted to print on a determinet height in order to print on top of another printed geometry, is the Z offset parameter, modifying the zero position on the *z*-axis. The option Extruders determines the number of extruder units on the 3D-printer, creating a window for every extruder insde Printer settings.
- **Custom G-code:** This section is available for customing the g-code language of any programme.
- **Extruder #:** The only parameter that has to be modified inside this section is the nozzle diameter, which is 1.5 mm.

Once configurated all the 3D printing parameters, the last step is save the STL. Configurated file as a G-CODE and it will be available to be printed. This printing file can be inspected with the online programme G-code Analyser, see **figure 39** which shows all the 3D printing orders that will realize the 3D-printer. With this programme is possible to see all the 3D printing process animation, a 3D view of the final printing with its layers, or the G-code language, among other information.

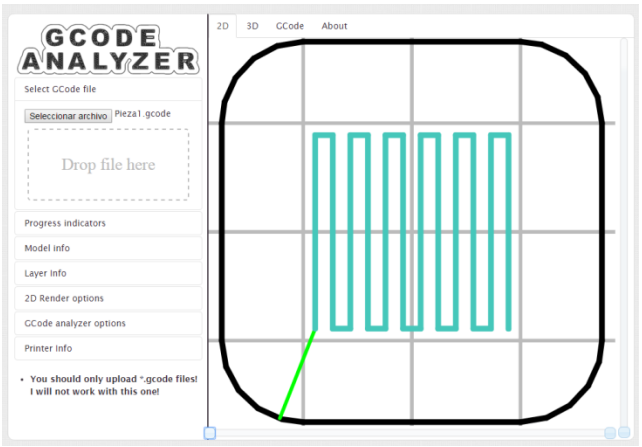

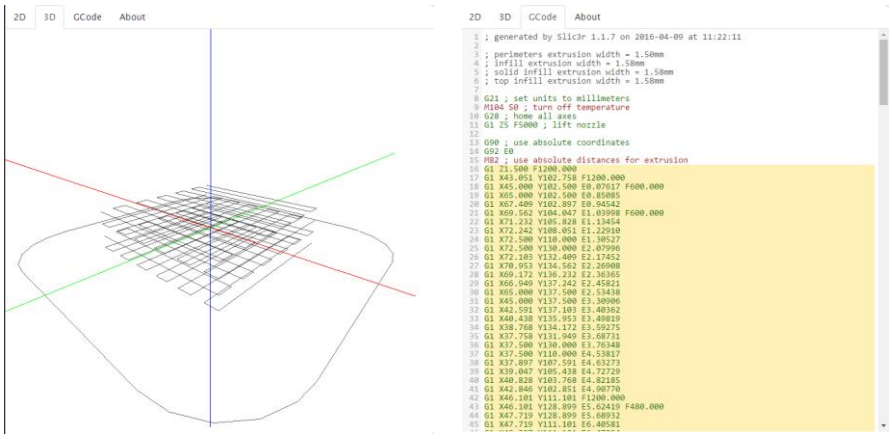

Figure 39. View of the different printing program analisis with G-Code Analyzer.

iv) Printing of the CAD design:

Once prepared the 3D-printer and its parameters, it has to be introduced the printing file on it using a SD card or directly connecting a PC on the 3D-printer.

Before executing the printing programe, there are some steps that are needed to do carefully. There are several steps to take into consideration:

- **Syringe filling**. The best way in order to completely fill the syringe with the viscous ceramic powder paste is put the desired amount inside a plastic bag, and then cut one of the corners and fill the syringe using this gap as a pastry sleeve. It is important to fill the syringe with the nozzle placed on it, due to the volume inside the nozzle has to be filled too.
- **Extrusion preparation**. After filling completely the syringe and the nozzle, the second step is the preparation of this material, which contains air voids, water and discontinuities that may affect the printing process. This preparation part can be separated into two steps:

  The first step is pressing the material on the top of the Syringe with the piston while it is making a partial caping on the nozzle's exit. This allows the evacuation of the possible amount of air and water, and makes the correct compactation of the material inside the extrusion system.

  The second step consists on introducing the preparated syringe inside the extruder's unit and iniciate a pre-extrusion. Once collocated the syringe, it has to be collocated and moved the extruder shift until do pressure on the piston while it is done a partial caping on the nozzle's exit again. This movement is realized selecting /Prepare/Move Axis/Move 10 mm, see **figure 34** and allows the correct interaction between the extruder shift and the syringe, making a first contact. Once made the first contact, it has to be made the first pre-extrusion also selecting the axis movement options but changing the speed at 1

and then at 0.1 mm, valorating the extruded filament and stoping while is has a good extrusion.

- **Height adjustment**. The height adjustment parameter consists on adjustment modification of the z-axis limit switch in order to avoid printing problems related with the nozzle's height, see **section 1.3.2** and summarized in **table 5.**
- **File printing**. Finally, before starting the 3D-printing programme, it has to be put on the printer plate a square of absorbent paper in order to drink the printed sample's water excedent. Then it has to start the printing programme selecting /Print from SD and selects the desired file.

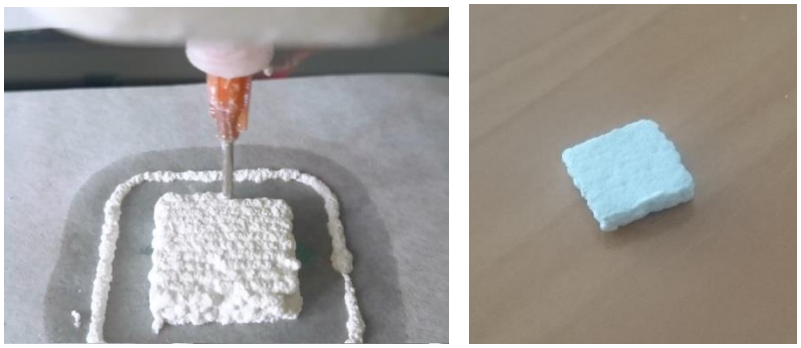

Figure 40. Sample's conforming process using the 3D-printing technique

After printing, the samples need a drying process depending on the ceramic powder material paste used, being the Zirconia/Ceria the fastest to evacuate the water and the Zirconia/Alumina the slowest. The final step needed is a sintering process; see **section 3.3.4.**, on the samples in order to obtain densiy and mechanical properties.

3.3.3. Cold Isostatic Pressing

The obtaining of cold isostatic pressed samples using ceramic powder with a tablet shape of ¾ inches of diameter (19 mm), has been realized using the Cold Isostatic Pressing technique, see **section 1.4.1.**, with the *MTI Corporation* electrical pressing machine, model *YJL-CIP 20TA*. A general view of this electrical pressing machine is shown on **Figure 41**:

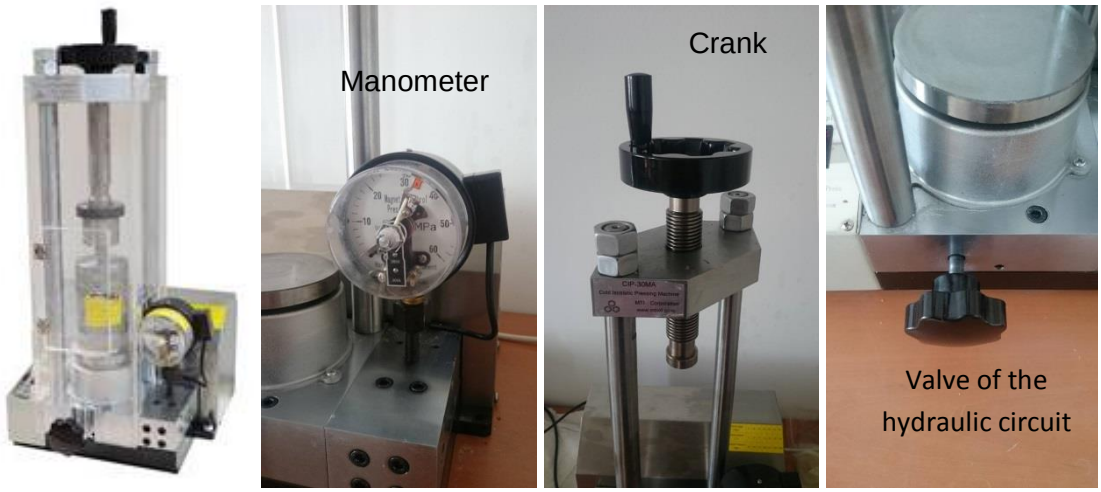

Figure 41. General view of the MTI Corporation electrical pressing machine YJL-CIP 20TA

This equipment has an electric motor with 180W of power and an hydraulic circuit which provides a compression pressure of 278 MPa. The complements of the pressing machine are shown below, see **Figure 42**.

Figure 42. Accessories of the MTI Corporation electrical pressing machine YJL-CIP 20TA

Once presentatd the equipment, it is explained the pressing process of CIP powder pressing technique. During the process, there are a few number of steps that have to be considerated in order to obtain a good compacted product. These steps are listed below:

1. **Creation of a pre-form** of the ceramic powder desired to compact, in order to obtain a compactable and handling product. The production of this preform consists on the realization of the pressing assembly showed on **Figure 43**, compacting the ceramic powder with the CIP machine at an hydraulic circuit pressure of 8 bars during 30 seconds. If the pressing piston does not introduces easy, a bit of magnesium oxide powder can be applied in order to facilitate the inserting. Remove the hydraulit circuit pressure slowly.

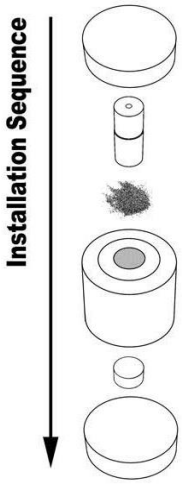

Figure 43. Pressing assembly for the obtaining of the pre-form [53].

2. After the compacting time, the pressure on the assembly is removed and it proceeds to realize the demoulding assembly showed at **figure 44**. With this step is only used the mechanical CIP machine's crank pressure, without using the hydraulic circuit.

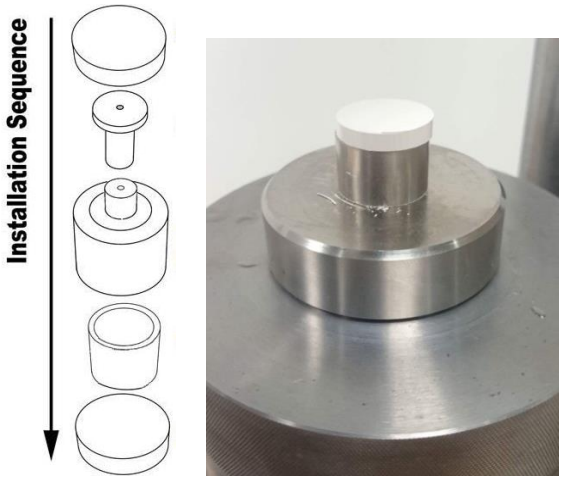

Figure 44. Demoulding assembly for the extraction of the preform [53].

3. Before the Cold Isostatic pressing, the specimen should be protected with a waterproof cover. By doing this, the ceramic compacts do not interact with the fluid used to increase the pressure and improve the densification of the green body. This protection is made using a plastic laboratory glove which it is introduced the pre-form and it is realized the vacuum using the *BUCHI Vacuum Pump V-100* with an *I-100* interface, **figure 45**.

Figure 45. General view of the waterproof protection on the pre-forms

4. Finally, the pre-form is introduced inside the CIP chamber, introduce the piston on it and adjust the piston with its tool. Then, using the hydraulic circuit, apply a pressure of 30 bar during 1 minutes (if the manometer exceeds 34 bar, the hydraulic circuit staps automatically). Afterwards, remove the hydraulic circuit pressure slowly again.

Figure 46. General view of the Cold Isostatic pressing assembly.

5. After pressing, it only rests removing the pressed products inside the CIP chamber, dry them carefully and remove the waterproof cover protection in order to carry the product to sinterize, **figure 47**.

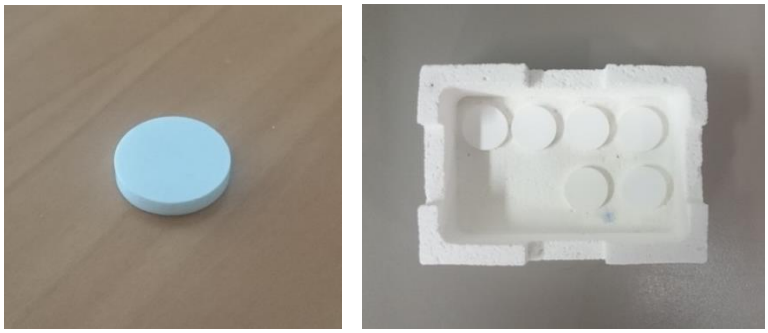

Figure 47. Example of a finished CIP pressed sample ready to be sinterized.

3.3.4. Sinterization

In order to obtain the final product it is necessary to sinterize the green bodies to reache the desired microstructure and mechanical properties. The sintering of all the samples investigated along this Bacheloor's project has been made with a *Nabertherm* furnace with constant cooling and heating rates to 3 ºC/min. **Table 12** shows a resume of the thermical threatment's characteristics realized on all the samples sinterized.

Table 12. Temperatures of all the sintering thermal threatments of the samples

Sample name	Ramp (ºC/min)	Sinterization temperatures (ºC)			Stabilization time (h)
A5 IMP	3	1650	1550	1650	2
A10 IMP	3	1650	1550	1650	2
A15 IMP	3	1650	1550	1650	2
A20 IMP	3	1650	1550	1650	2
A25 IMP	3	1650	1550	1650	2
A5 SG	3	1650	1550	1650	2
A10 SG	3	1450	1550	1650	2
A15 SG	3	1450	1550	1650	2
A20 SG	3	1450	1550	1650	2
A25 SG	3	1450	1550	1650	2
A5 CIP	3	1450	1550	1650	2
A10 CIP	3	1450	1550	1650	2
A15 CIP	3	1450	1550	1650	2
A20 CIP	3	1450	1550	1650	2
A25 CIP	3	1450	1550	1650	2
C15 IMP	3		1450		2
C15 SG	3		1450		2
C15 CIP	3		1450		2
Z100 IMP	3		1450		2
Z100 SG	3		1450		2
Z100 CIP	3		1450		2

Figure. Exterior and interior views of the Nabertherm furnace.

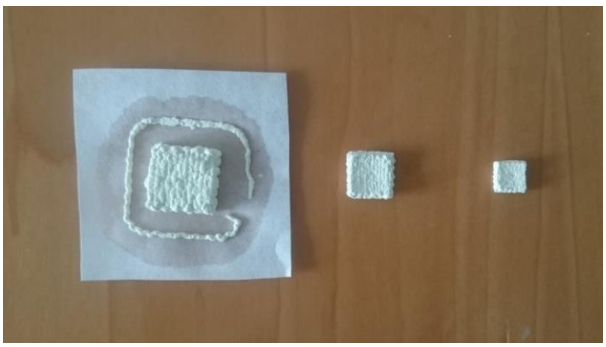

Figure . Size comparison between a 3D printed, dried and sintered samples.

3.4. Sample preparation

In order to allow the application of all the different experimental techniques for the mechanical and microstructural sample characterization, it is necessary to prepare the surface by means of the conventional polishing process. During the sample preparation process it is important that the specimens present a planoparallel surfaces in order to avoid any mistake during the mechanical characterization process. For this reason, the specimens previous the polishing process where embedded in Bakelite..

3.4.1. Cutting process

Along this Bacheloor's project, some specimens have been characterized transversally from the printing direction. In doing so, it is necessary to cut the specimen by using an automatic *Buehler IsoMet 4000 precision cutting saw* and an *IsoMet wafering blade 20LC* with a 7 inches diameter, see **Figures 48 and 49**.

Figure 48. Accessories of the IsoMet 4000.

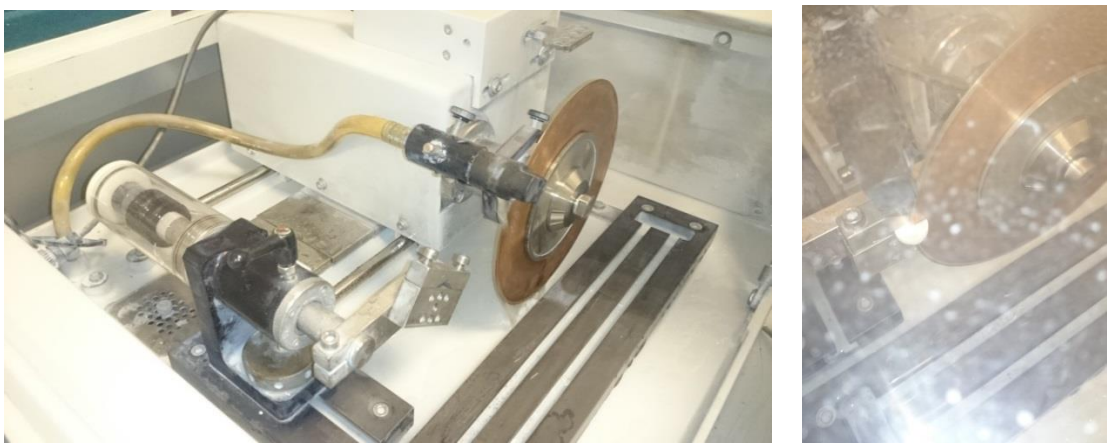

Figure 49. IsoMet 4000 sawing assembly

This equipment allows the automatic control of the blade speed and the feed rate. The wafering blade allows the precision cutting of almost any hard material due to the diamond coating present on the metal blade sheet. The Surface aspect after the precision cut, depending of the cutting parameters selected, is as good as a *MD Piano 600* polish.

3.4.2. Sample mounting

For a better mechanical properties characterization, it is preferable to embed the samples into a baquelite. However, it is necessary to keep in mind that some samples are not recommended to be mounted, due to the presence of high porosity on their material where the baquelite could bury itself, or the need to remove the baquelite tablet in order to extract the sample after the polishing process, in order to realize posterior techniques.

This mounting process has been realized with a Struers automatic hot mounting press machine, model LaboPress-3. The baquelite used to realize the encapsulating tablet has been *Durofast Bakelite* from *Struers*.

Figure 50. General view of the Struers LaboPress-3 mounting machine

This mounting machine allows obtaining planoparallel encapsulating specimens of 15-20 mm height up to 50 mm (depending on the amount of baquelite used), and 30 mm of diameter, allowing their posterior utilization on polishing machines. The planoparalellity obtained is desired for posterior indentation tests sor any procedure which needs planoparalel surfaces.

The *Durofast bakelite* is an epoxy hot mounting resin with mineral and glain which prevents against edge retention, but also insulates the sample. There is available a conductive *bakelite* called *Polyfast* also from *Struers*, which is baquelite mixed with conductive carbon particles, specially used for a posterior FESEM or FIB sample analysis.

Finally, the samples have been marked on the base and sides using an authomatic percutor, in order to not confuse each other.

Figure 51. General view of the Durofast baquelite (left) and a finished mounted sample (right)

3.4.3. Sample polishing

In order to get the most suitable surface for their posterior characterization, it is necessary to realize a sample polishing process to get planoparallel and free of scratches polished sample surfaces.

The sample polishing has been realized with a Buehler *Metaserv 250 polishing machine* with *Vector Power Head*. This polishing machine allows

the control of the rotation speed, the pressure force in the samples, and the rotation direction in order to obtain the best polished samples conserving their planoparalellity, see **Table 13**. The polishing discs used have been *Struers MD Piano 220/ 600/ 1200, and Struers MD Plan/ Dac/ Nap* ceramic polising discs, of 30 mm diameter with *Saint Govain coating solutions* polishin suspensions model *30µm, 6µm, 3µm STB MD,* and Buehler Matermat 2 colloidal Silica suspensión for a final speculating finish.

The methodology for the correct polishing of samples is based on the progressive decresion of the polishing disc and suspension abrasiveness, changing to the following step only when there is no visible scratch of the provious.

Table 13 shows a summary of all the steps and parameters of the polishing process (Rotation direction parameter is refered comparing the direction of the rotary head and base of the polishing machine).

Table 13. Polishing process steps and parameters

Order	Polishing disc	Polishing suspension	Spin speed (rpm)	Pressure force (N)	Rotation direction	Polishing time (min.)
1	MD Piano 220	Tape Water	150	15	Different direction	5
2	MD Piano 600	Tape Water	150	15	Different direction	10
3	MD Piano 1200/ MD-Plan	Tape Water/30 µm	150	15	Different direction	15
4	MD-Plan (white)	6 µm	150	10	Same direction	20
6	MD-Dac (blue)	3 µm	150	10	Same direction	30
6	MD Nap (brown)	Colloidal Silica	150	10	Same direction	40

Depending on the morphology of the sample, it is recommended do a previous roughening process with a P80 silicon carbide sanding disc and abundant water. If the sample morphology is is too irregular, it is recommended to realize a sawing process with a diamonded cutting blade saw.

It is necessary to use abundant water during the starting and ending of the polishing process, due to they are the two stages which present more friction. During the rest of the polishing steps, the use of water, if it is not required, is replaced for the corresponding polishing suspensions.

Finally, it is recommended to chamfer the sample edged in order to avoid scratching problems between the sample and the polishing discs during their rotation on the polishing process.

Figure 52. General view of all the polishing discs used ordered from left to right [54].

Figure 53. General view of the polishing process with the Buheler Metaserv 250 polishing machine

3.5. Microstructural characterization techniques

3.5.1. Porosity

The superficial porosity of the samples has been obtained with microscopical images using a confocal microscope (see **section 3.5.7.**), and afterwards processed using the image processing program ImageJ.

The microscopical images of the samples have been taken at 5X magnifications due to the high size of the sample's pores, and have been taken 10 images per sample, in order to make the most representative surface characterization.

The information processing of the microscopical images has been made using the ImageJ image processing program.

The main steps realized are:

- Firstly, it has been defined a scale on the program in order to realize measures. This scale has been defined analising the size of the image scale given by the confocal microscope, and defining the value on the programme.

- Secondly, the image has been converted into 8-bit type image to differentiate the pores from the solid material, taking advantage of the different colour between them. Once obtained a grey scale image, it has been done an adjustment of the pore size threshold, in order to obtain a representative analisis.
- Finally, it has been done a particle analysis including holes and excluding edges. The information obtained for every 10 images of a same sample has been summarized making an average.

Figure 54 shows an example of the porosity characterization of one sample's surface:

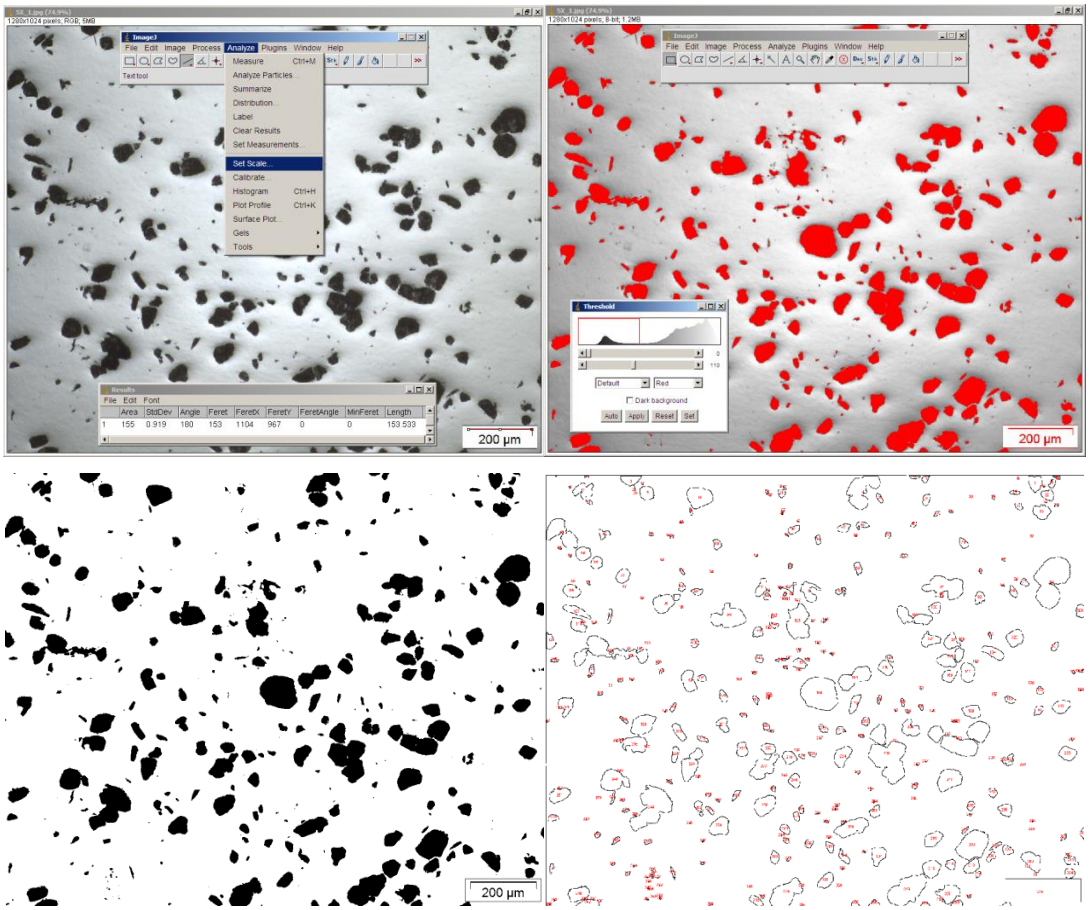

Figure 54. Example of all the steps on the porosity characterization process

3.5.2. Density by using the Archimedes principle

In order to obtain the density values of all the samples it has been used the Archimedes principle technique. Therefore, this method does not contemplates the closed porosity of the samples, see **section 1.2.1.**, but due the elevated superficial porosity, the value obtained has an acceptable error. On the other hand, the density has been also measured using the Helium Picnometry technique in order to compare both results, see **section 3.5.2.**.

The Archimedes method consists on the determination of the sample's density with the determination of its volume and mass. The principle says that the flotation force applied on a sample immersed in a fluid is equal to the weigh of the moved fluid's volume. If the mass of a sample is measured before the immersion and during the immersion, the mass difference is directly the flotation force generated on the sample:

$$F_{flotation} = (m_{dry} - m_{wet})g = \rho_{fluid} g V \quad (11)$$

Where m_{dry} is the sample mass without immersing, m_{wet} the mass during immersion and V the moved fluid's volume which is the same of the sample. Due to the liquid used is water, which has a known density of 1 g/cm^3 at room temperature, is possible to calculate the moved fluid's volume. Finally, the density can be measured dividing the volume and the dry mass of the sample.

The equipment used to measure the density of the samples has been a *Mettler Toledo* precision bascule model *Dual Range XS205*, with the Archimedes principle measurement complement. This bascule also allows the direct measurement of the density with a program routine that realizes the intermediate calculation.

Figure 55. General view of the Mettler Toledo Dual Range XS205 precision bascule equiped with the Archimedes principle's accessory

Appart from the real density, it halso has been calculated the theoretical density of every each sample's material in order to compare the different conforming methods, valorating the densities that can be obtained with them and their performance. These theoretical densities have been calculated using the following expression:

$$\rho_{theoretical} = \frac{\%wt\ M1 + \%wt\ M2}{\frac{\%wt\ M1}{\rho M1} + \frac{\%wt\ M2}{\rho M2}} \quad (12)$$

Where *%wt M1* is the weight percentage of the first material, *%wt M2* the weight percentage of the second material, and $\rho M1$ & $\rho M2$ the theoretical densities of each material.

3.5.3. Desnity by means of Helium Picnometry

Helium picnometry (see **Figure 56**) is a microstructural characterization technique which allows the measurement of the real density (matrix density) for porous materials with closed porosity.

This technique is based on introducing the porous material inside an hermetic chamber with a determined volume. This chamber is filled with a fluid, which has a determined density. The determination of the measured material's volume consists on measuring the volume difference between the hermetic chamber volume and the volume of fluid filled on it.

Once determined the fluid, the density can be obtained measuring the mass of the material with a precision balance, and calculating it afterwards.

The rincipal advantages of this technique compared with others like Arquimedes principle are listed below:

- Measurement of the totall density (open and closed porosity)
- Utilization of a non reactive fluid.

If the sample volume is so small, the picnometer could not make a good measurement. To solve this problem, is possible to introduce calibrated steel spheres to decrease volume on the hermetic measurement chamber.

The measurement of the sample's density has been realized using helium picnometry technique with a *Micromeritics* helium picnometer model *AccuPyc 1330*, which allows the density measurement in a range between 0.01cm^3 and 350 cm^3.

Figure 56. General view of the Micromeritics AccuPyc 1330 helium picnometer.

3.5.4. Profilometry

The determination of the surface roughness of the samples has been determined using a perfilometer *Veeco* model *DEKTAK150* with a stabilising

table Table Manufacturing Corporation. The stylus radius used is 2.5 mm and the force applied, 1.5 mg.

The measurement procedure of this equipement is based on the position searching of a calibrated palpador in contact with the sample surface, which works as a caliper, measuring the length in all the surface profile. The tip of the palpador is a pyramidal diamond, which guarantees a good roughness measurement. The **figure 57** shows a general view of the machine.

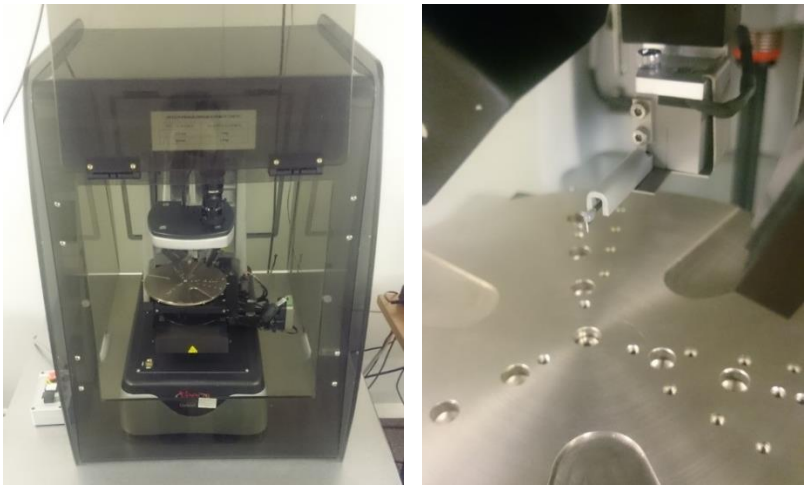

Figure 57. General view of the Veeco DEKTAK150 perfilometer

The surface roughness has also ben measured with the confocal image taking of sample surfaces using an *Olympus LEXT* OLS 3100 confocal laser microscope, and analyzing the roughness with the *LEXT OLS* data caption software, using the roughness measurement anlysis option. The **Figure 58** shows an example of this surface roughness measurement process.

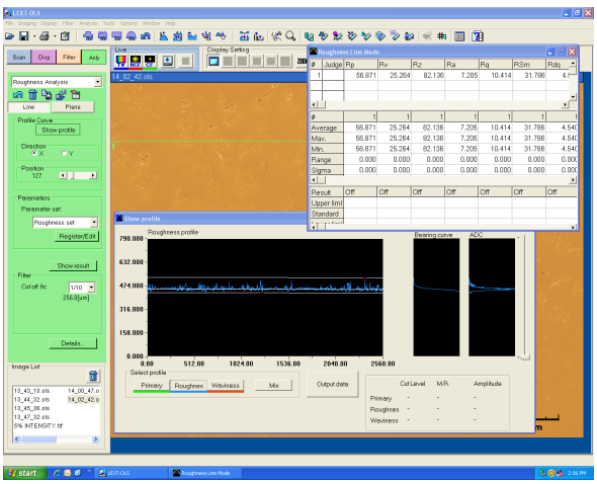

Figure 58. Example of roughness measurement using the Olyumpus LEXT OLS 3100 analysis software

The main difference between the profilomer and the confocal presented above, is that the first is a contact technique where a stylus is in contact with the specimen while the second technique allows the roughness measurement by taking some images. In this Bacheloor's work, both technique has been used to complement the microstructural data get from each one.

3.5.5. Rheology

The viscosity studies of ceramic powder pastes for the conformation of the samples using the 3D-printing technique has been done using a rheometer *Anton Paar Rheolab QC* equipped with a temperature device *C-PTD 180/AIR/QC*, a measuring cub *C-CC39/QC-LTD* and a sensor *CC39* with a diameter of 39.000 mm and a length of 59.996 mm. The data caption has been done using the program Anton Paar RheoCompass software.

The test realized has been a controlled-torque test at a constant temperature of 25°C. This Consists on the measurement of the torque needed to spin on a determined angular velocity a detector immersed on a container with the viscous material tested.º

The ceramic powder paste tested has been 3Y-TZP paste 28 (see **section 3.3.1., Table 10**). After grinding the gel-casting product, the paste has been maintained at 25°C inside a plastic container without cover, to evaporate water excess and make a progressive humidity reduction until the obtaining of the best texture for its 3D-printing extrusion.

Figure 59. General view of the Anton Paar Rheolab QC rheometer

3.5.6. Optical Microscopy

The optical microscopy has been used to obtain sample images, principally to take care of the sample's condition, but also to obtain images with high magnification of the surface just before and after the polishing process. With this technique it is possible to take images of the printing gooves as well as the pre-existing superficial porosity revealed after the polishing process

The optical microscopy equipments used has been two; an *Olympus SZX16* loupe, and an *Olympus BX51* optical microscope.

Figure 60. General view of the optic microscope (left) and the loupe (right)

3.5.7. Confocal laser microscopy

The confocal miscroscopy allows the obtaining of high focus depth images but with low magnification. The confocal microscopy has been used to take all the sample images that have to be posteriorly analyzed in order to obtain mechanical or microstructural properties, if the image scale is enough for this technique, reserving lower scales for more powerful techniques as FESEM or FIB.

The confocal microscopy technique consists on the taking of different image along the focal planes, for a posterior height reconstruction, creating a 3D image. This wide focus height is due to the use of a powerful laser instead of light, in order to increase the focalizing range, before delimited for the light's wave length.

The wide amount of height information also offers the obtaining of different parameters as roughness, height or 3D images. The programme analysis available also makes the confocal microscope powerful equipment, being possible to realize tilt corrections on the surface, smoothings and a lot of improving actions on the images taken.

For the confocal microscopy technique has been used an *Olympus LEXT OLS 3100 confocal laser microscope* with a *Table Stable Ltd.TS-150* stabilishing table.

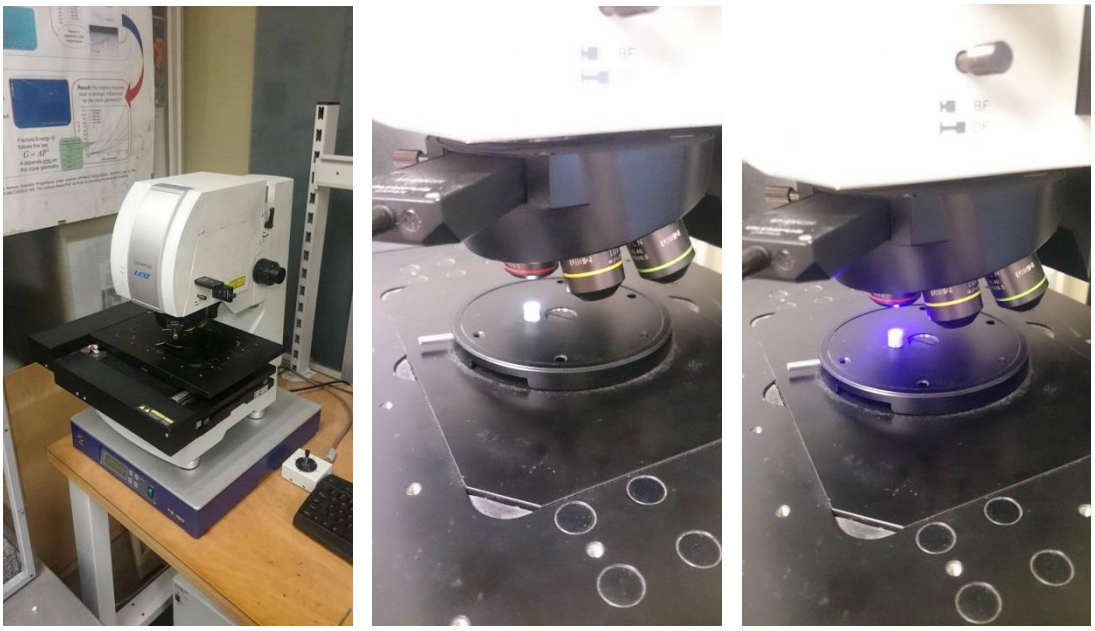

Figure 61. General view of the Olympus LEXT OLS 3100 Confocal laser microscope

3.5.8. *X-ray Diffraction (XRD)*

X-ray Diffraction technique is used to obtain microstructural information of the samples with the spectrum analysis, as if it has an amorphous or crystalline structure, an which crystal phases presented in the specimen (tetragonal, monoclininc and/or cubic) .

This technique is based on the analysis of the dispersed X rays spectra after sample colliding. When the X rays collide on the crystal surface of one material, a percentage of the ray is dispersed and another continues penetrating on the interior of the material, continuing this process successively during the penetration. The resulting effect on this x-ray dispersation during the penetration and colliding with the material generates a spectrum of all the dispersed rays. Every crystal surface has its own type of X-ray diffraction, being possible to identificate the different crystalline structures present on a material [ref].

The measurement of sample's powder spectra for the determination and cuantification of crystalline and amorphous phases, has been obtained with the X-ray diffraction technique using *Bruker D8 Advance* diffractometers equipped with three different configurations:

System 1: Vertical goniometer, Bragg-Brentano \–\ configuration, scintillation (NaI), Cu anode without monochromator for filtering the K‹2 line, Ni filter for the Cu K® line.

System 2: Vertical goniometer, Bragg-Brentano \–\ configuration, Cu anode, Sol-X detector with discriminator for Kβ line.

System 3: Vertical goniometer, Bragg-Brentano \–2\configuration, Cu anode with a monochromator for filtering the K‹2 line, PSD LynxEye

detector, 9-position rotary sample changer, goniometer head with rotating capillary for powder diffraction measurements.

The samples measurement has been realized on a range of 0 to 100º for the angle spectra.

Figure 62. General view of *Bruker D8 Advance* diffractometers for DRX technique.

3.5.9. Field Emission Scaning Electron Microscopy (FESEM)

The Field Emission Scanning Electron Microscopy (FESEM) allows the obtaining of high magnification and focusing depth, combining the advantages of optical and confocal microscopy. This technique also allows the obtaining of microstructural informationl, in quantitative and qualitative composition analysis.

The FESEM technique has the same working as the confocal technique, but with the difference on the image capturing system, which is an electron beam. This electron beam allows the obtaining of images on a smaller scale, conserving a high magnification and focusing depth due to the higher energy of the electrons.

The samples used on FESEM normally have to be conductibe, in order to avoid the overcharging on the surface due to the electron colliding. For non conductive samples, it is possible to avoid this problem too, realizing a thin carbon coating in order to make conductive only the surface of the sample.

The microstructural information is given by the secondary electrons, which depending on the energy that their have after the surface collision with the sample's atoms that determines the composition. These electrons also affect on the image taken, being the darker colors on the sample image more heavy elements.

The microscopical image obtaining and microstructural informationof the samples has been obtained using FESEM technique with a *JEOL microscope* model *JSM-7001F*, which has a maximum magnification resolution of around 600000X.

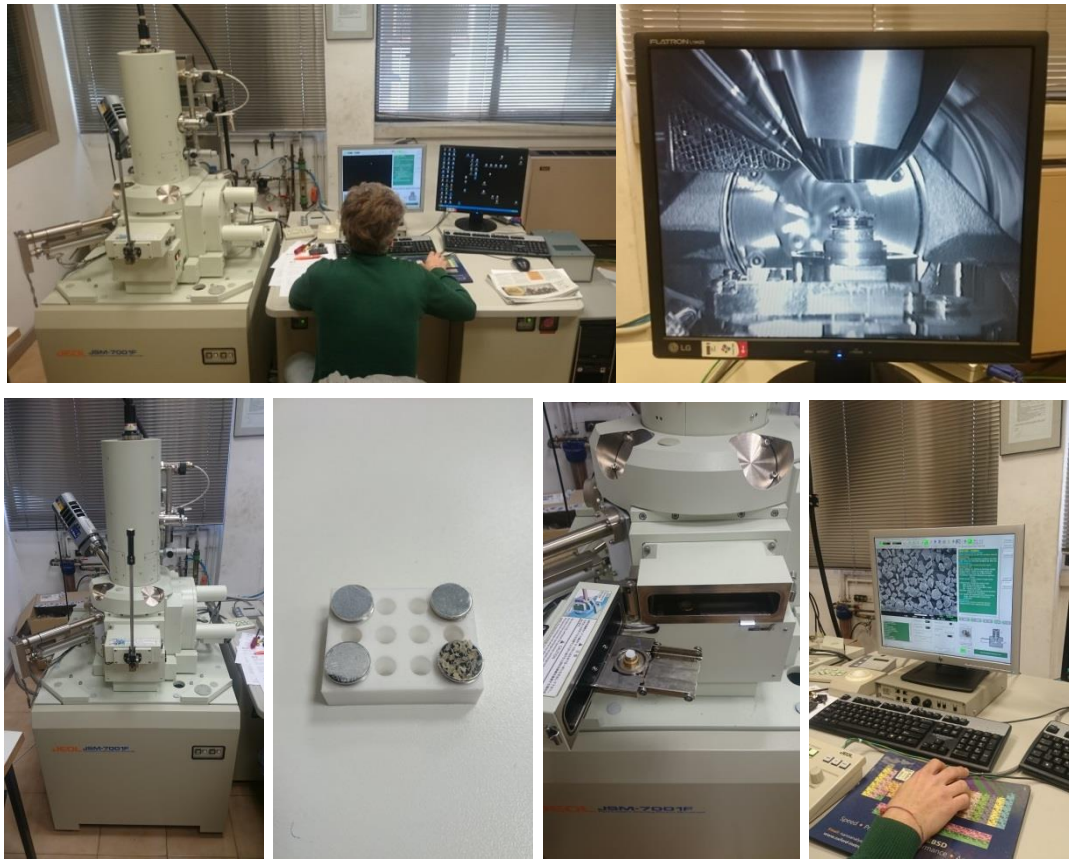

Figure 63. General view of the JEOL JSM-7001F FESEM microscope.

3.5.10. Focused Ion Beam (FIB)

The Focused Ion Beam technique allows the nanometric machinability of the materials using a powerful ion beam, in addition to sample observation, 3D tomography, TEM lamella preparation, and elemental analysis. The FIB technique can be considerated as a complement of Scaning Electron Microscopy equipment, due to it also uses an electron beam in order to obtain the images of the samples.

The machining on the sample surface is usually made as transversal cuttings. The obtaining of a surface perpendicular cut is obtained protecting the cutting zone with a platinum coating with a determined shape. This coating protects the gallium ions machining on the material.

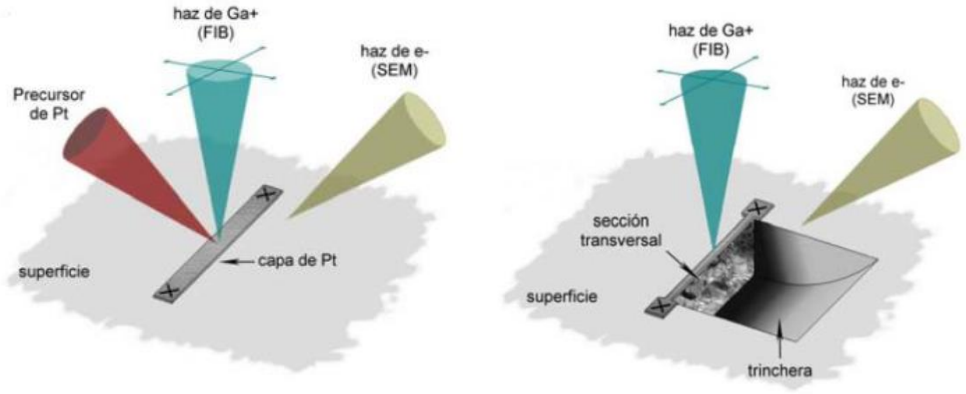

Figure 64. FIB's working for the cutting obtaining

The equipment used to realize the Focused Ion Beam is a cross-beam workstation *Zeiss Neon 40* with FIB/SEM beams, equipped with the following parts:

- CANION31 Gallium FIB column: 1pA-50nA, 3-30kV, 7nmresolution
- GEMINI SEM column with (Shottky-FE) gun: 4pA-20nA, 0.1-30kV, 1.1nm resolution at 20kV
- BSE, SE, SE in-lens & STEM detectors
- Gas Injection System (Pt, I2, SiO2, H2O, XeF6) for deposition and selective milling
- Supereucentric 6-axes sample stage
- In-chamber micromanipulator for TEM lamella extraction
- EDS (INCAPentaFETx3 detector, 30mm2, ATW2 window) for elemental analysis

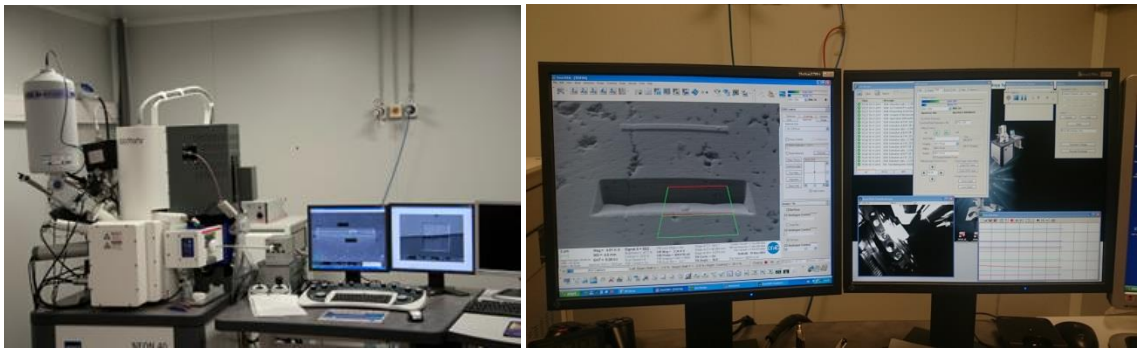

Figure 65. General view of the Zeiss Neon 40 FIB/SEM microscope.

3.6. Mechanical characterization techniques

3.6.1. Vickers Hardness

Vickers micro-hardness test allows the obtaining of the hardness value of the material in a micrometric length scale. This test allows the testing of thin samples due the low indentation height and volume of material tested, and not homogeneous samples with different materials or full of imperfections as porosity due to the small surface indentation, being a more located test in general.

This test was developed in 1921 by Robert L. Smith and George E. Sandland at Vickers Ltd as an alternative to the Brinell hardness test. The test consists on an indentation on the material using a diamond square-based pyramid indenter with an angle of 136º between faces, in order to observe the material's ability to resist plastic deformation from a determinded charge. Once done the indentation, a measurement of the diagonals of the square print are done to measure the hardness of the material with a determined equation, being the test regulated by rule ASTM E 92-82. The Vickers test can be used for all metals and has one of the widest scales among hardness tests.

The realization of the Vickers micro-indentaion test has been done using a Akashi micro-durometer, model MVK-HO.

It has been realized 10 indentations per sample at a charge of 1 kgf. It has been adopted one charge value for all the samples in order to obtain comparative results and valorate the materials resistance. The value of the charge has been adopted being 1 kgf a representative value due to the materials hardnees of the samples. Finally, is has realized 10 indentations per sample due to the high porosity content in order to obtain the most materials representative characterization of the hardness, assuming that some indentations may be realized on pores, being necessary to make an average on the results.

The steps on the Vickers micro-indentation hardness test are listed below:

1. Firstly, put a planoparallel and surface polished sample on the base of the Vickers micro-hardness testing machine, and subject it correctly
2. Using the lens, facalize and positionate the sample moving calibrated calipers of the machine.
3. Configure the parameters of the test. The indentation time adopted has been 20 seconds, and the charge has been 1 kgf. Change the lens for the indenter and realize the indentation.
4. Remove the sample and analize the imprint. All the images of the indentation prints have been taken with the Olympus LEXT OLS 3100 confocal laser microscope, and then analyzed with ImageJ image analysing programme.
5. Once measured the diameters of the suare imprints, determine the material's hardness. The equation used to calculate the hardness of the materials indented has been the following expression:

$$HV = \frac{F}{A} = \frac{F*2\sin(136º/2)}{d^2} = \frac{1.8544F}{d^2} \quad (13)$$

,

where *F* is the indentation charge, and d the average of the two diameters of the imprint. **Figure 66** shows the equipment and the main steps during the indentation process described above.

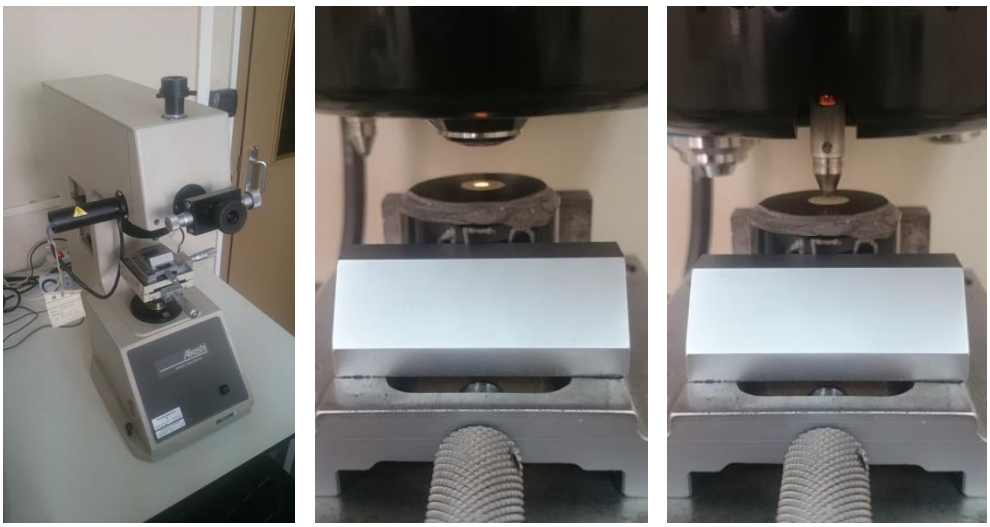

Figure 66. General view of the Akashi HVK-H0 Micro-durometer

3.6.2. Fracture toughness

Due to the nature of the specimens investigated here (ceramic materials), during the indentation process it is possible to generate several cracks from the corner of the residual imprint. The appropriate inspection of the imprints by knowing their main properties (i.e. Young's modulus and Hardness) it is

possible to determine or at least stimate the indentation fracture toughness by using the following expression [55]:

$$K_{IC} = \varepsilon_R \left(\frac{E}{H}\right)^{1/2} \frac{P}{c^{3/2}} \tag{14}$$

where *E* is the Young modulus, *H* is the Hardness, *P* is the indentation load and *2c* is the total crack length (i.e. 2c=2l+2a, where l is the length of the crack from the indentation corner, and 2a is the indentation diagonal). The term is a material constant containing elements related to the geometry of the indenter and the morphology of the cracks system, adopting a value of 0.016 [56].

CHAPTER 4: RESULTS AND DISCUSSION

In this section, the main and relevant data get from this Bacheelor's degree will be presented trying to correlate their microstructural properties with their mechanical response. Also, along this section representative and relevant information observed during the experimental procedure will be presented.

4.1. Base material characterization

The sample conforming techniques used in this bachelor's degree have been three: Gel-casting, 3D-printing and Cold Isostatic Pressing. The material used to build the sample needs to be on a determined state (in terms of particle shape and grain size) depending on which of these techniques is used, being a ceramic powder state if the sample is conformed using CIP, an almost liquid state in the Gel-casting technique, or a viscous paste state in the 3D-printing technique.

Previously to start the chemical route to produce the different ceramic pastes, it is necessary to characterize the ceramic particles by using FESEM

as it is presented in **Figures 67** to **69**. These images present several micrographs showing the particle size and shape:

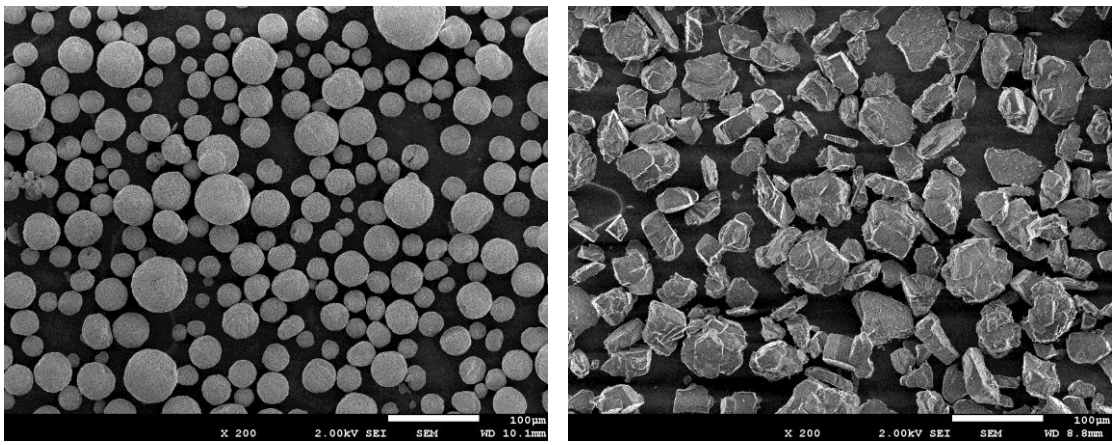

Figure 67. Powder particles of 3Y-TZP Zirconia (left) and Alpha Alumina (right)

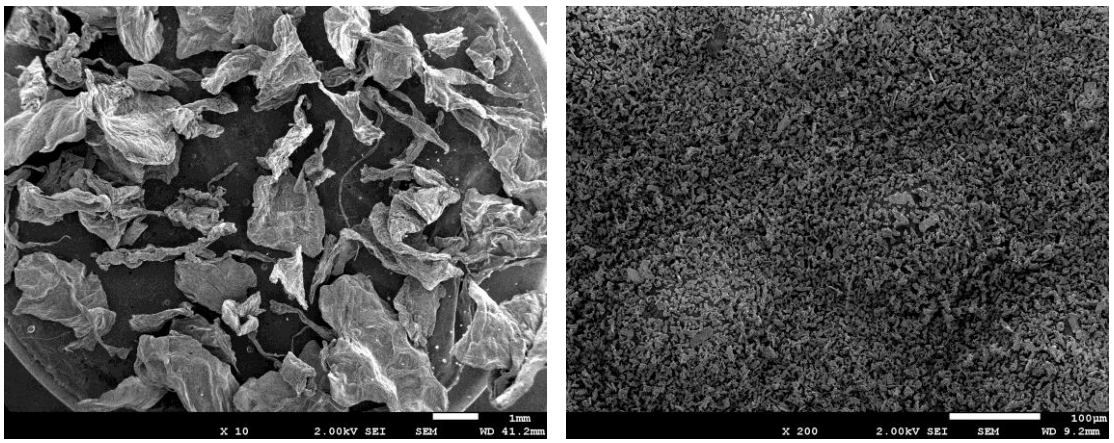

Figure 68. Powder particles of Agar-Agar (left), and Ceria III (right)

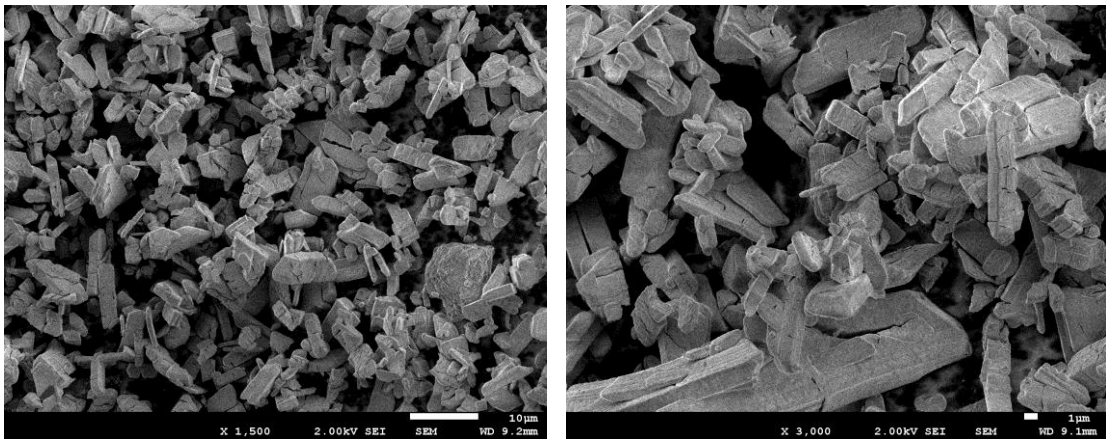

Figure 69. Powder particles of Ceria III at higher magnifications

From the micrographies observation of all the powder particles of the sample's materials, it is possible to suggest different manufacturing skills. These suggestions are listed below:

- The first interpretation is that, compared with the ceramic powder materials, the Agar Agar powder particles are big enough to generate problems of extrusion or compactation itself if it is not well melted, or structural problems as porosity on the conformed and sintered samples. For that reason, it is important to control the melting range temperature of this raw material to avoid this effect previously commented and/or possible problems of polymer degradation (when the temperature is around 1.25 higher than the melting temperature and the polymeric molecules can be degraded).
- All the ceramic powder particles are small enough to not present blocking problems on the nozzle, being these problems only generated for the Agar-Agar size if they happen.
- Comparing the powder particles sizes between 3Y-TZP Zirconia, Alpha Alumina and Ceria III it can be suggested an estimation of the mixing between them, and the behavior of the viscous pastes obtained with these composite ceramic powders during the extrusion. The 3Y-TZP Zirconia powder particles should have a good extrusion behavior due their spherical shape. Therefore, the composite powder ceramics of Zirconia/Alumina probably should present some mixing problems due to the high difference of shapes with a similar size. On the other hand, the composites of Zirconia/Ceria should have a good mixing due to the good shape of the Zirconia and the high difference between particles, facilitating the mixing of Ceria between the Zirconia powder particles.
- Finally, the Ceria powder particles should have a good extrusion due their small size, and a faster water evaporation to obtain the optimal viscosity, compared with Alumina and Zirconia, which probably will need more time.

For the obtaining of the Gel-casting's liquid state material and the 3D-printing's viscous paste, it has been used the Gel-casting technique explained in **section 3.3.1.**. Once obtained and realized a printing test with all the Gel-casting compositions showed on **table 10**, the 3Y-TZP Zirconia powder based viscous paste that shows the best printing properties is the following:

Table 14. Composition of the optimal Gel-casting's ceramic powder based viscous paste.

Test	Water (g)	Ceramic powder (g)	Agar-Agar (g)	Ceramic powder (%)	Agar-Agar (%)
28	55	15	0.71	21.2	1.0

The viscous paste obtained with these proportions allows a continuous filament and extrusion. All the viscous pastes made of Zirconia, Alumina/Zirconia and Ceria/Zirconia ceramic powders have been obtained using the same Gel-casting's solution proportions, in order to not introduce a new parameter on the porosity created by the Agar-agar proportion, and adjusting the paste's viscosity with the water content evaporation during a certain resting time.

After being grinded and put inside a glass, the resting times needed for the different ceramic material's printing pastes in order to evaporate a certain amount of water and obtain the best viscosity to achieve an optimal extrusion on 3D-printing conformation technique are resumed on the following table:

Table 15. Resting time for the different ceramic powder based viscous pastes

Viscous paste's material	Resting time
Zirconia	4 days
Zirconia/Alumina	3-4 days
Zirconia/Ceria	1-2 days

Once obtained the solution's proportions and the resting time in order to obtain an optimal 3D printing process, it is needed to determine the proportions of the ceramic composite materials on the ceramic powder proportion.

These proportions have been found verifying the interaction between the ceramic composite materials and 3Y-TZP Zirconia. This checking has been done obtaining Gel-casting technique's product of both materials, cutting a certain portion of both and assembling one over the other like a sandwich configuration. Then the configuration has been sinterized in order to observe if was possible to obtain a solid product or if the tensions and different constrictions of both materials where excessive.

These experiments have started with a first sweep of 100%, 75%, 50% and 25% of Alumina on Zirconia. The results were only acceptable for 50% and 25%, thus another sweep of 50%, 40%, 30%, 20%, and 10% was done. Valorating the results, the Alumina on Zirconia final proportions for their study were 25%, 20%, 15%, 10% and 5%.

It has been observed some problems after the sintering for the Zirconia/Alumina, being those the following:

- It has been observed a precipitation problem on the Gel-casting's conformed samples of all the proportions of Zirconia/Alumina composite materials. This problem is due to the fact that Alumina does not present an emulsionated state during the sonification as Zirconia or Ceria, and the high particle's mobility for the high temperature during the gellying process, allows the Alumina particle's

to dipositate on the bottom of the sample due to differences on density. The next image shows this phenomenon on the most critical sample, the A25 SG 1650:

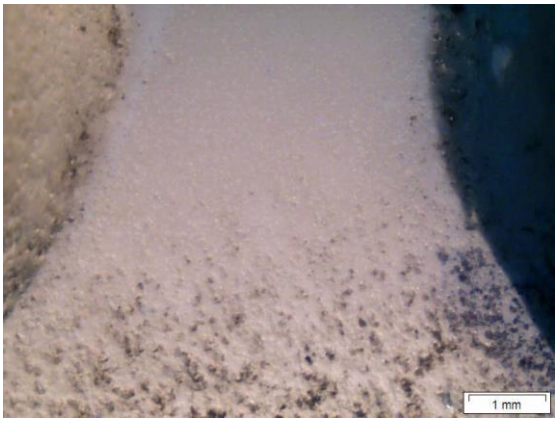

Figure 70. Example of the precipitation phenomenon observed on Zirconia/Alumina Gel-casting samples

This problem present on Gel-casting samples of Alumina/Zirconia is not present on 3D printed samples of the same chemical composition. This fact could be due to the grinding after the gellying process of the Gel-casting solution, which helps to mix the precipitated materials during the gellying. After the grinding and obtaining of the viscous pastes, the composite ceramic materials have not enough mobility to precipitate again due to the high viscosity of the paste.

- The Zirconia/Alumina CIP and 3D-printed specimens have shown sintering problems during the sample polishing. The initial sintering temperature of 1450ºC was enough in order to obtain a solid material, showing a behavior similar to gypsum while polishing. In order to solve this problem, a second sintering temperature of 1550ºC was applied to those samples. That temperature was also enough, being to apply one more sintering threatment with a temperature of 1660ºC. This last sintering temperature allows the obtaining of solid samples made of Zirconia/Alumina composite materials. However, as it can be observed, in order to get a material with convenient mechanical properties it is necessary to do the sintering process at high temperature, higher than 1600ºC. Thus temperature can induce the generation of cubic zirconia grains, being these grains harder but at the same time more brittle than the tetragonal grains. Furthermore, by doing sintering temperatures at high temperature, the grain size also increases, reaching dimensions of around several micrometers. This phenomena may produce a reduction of their mechanical properties due to the grain boundary is not able to block the deformation induce during the micromechanical characterization as well as fine grains of 300-340 nm.

Finally, the last step previous to the starting on the final samples of study conforming has been the measuring of the amount of solid waste of Agar-Agar that remains after a sintering process, being a non desearable fact for the samples. This experiment has been realized putting a certain amount of

Agar-Agar (12.12g) on a previously weighted crucible (72.88g) and applying on it a temperature high enough to burn the al the material, simulating a sintering threatment for a sample (600ºC) .After burning all the Agar-Agar, the crucible with the solid waste has been weighted (73.49g).

The Agar-Agar's percentage of solid waste that remains after the sinterization is 5.05%, a value that has to be kept in mind if the final samples must not contain solid organic wastes.

Figure 71. Solid organic waste of Agar-Agar after burning

4.2. Microstructural characterization

4.2.1. Porosity

The superficial porosity measurement has been realized taking ten different images of the polished surface per each sample. It has ben done an average on the ten images of every sample in order to obtain a single representative value for every sample. **Figure 72** shows an image of the surface of each specimen investigated here.

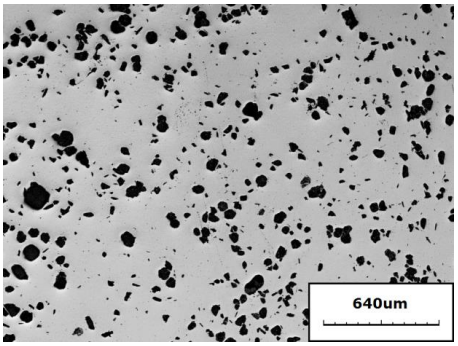

A5 IMP 1650

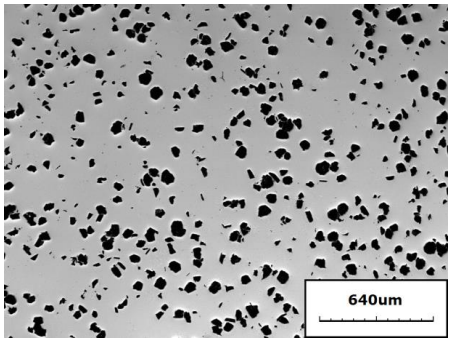

A5 CIP 1450

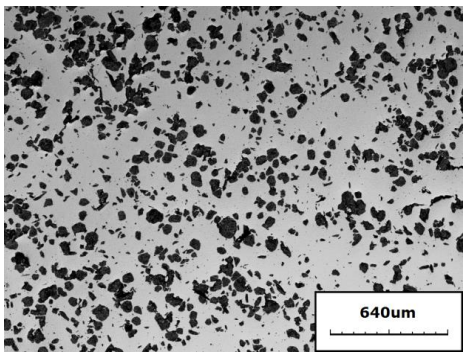

A10 IMP 1650

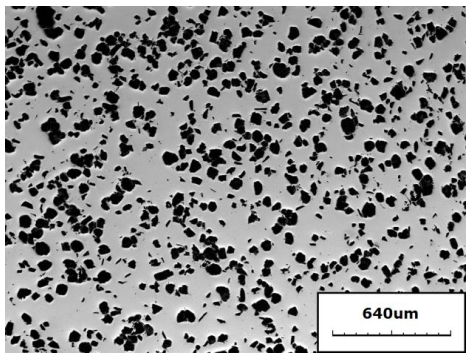

A10 CIP 1450

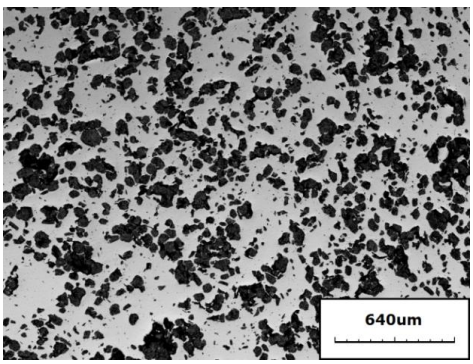

A15 IMP 1650

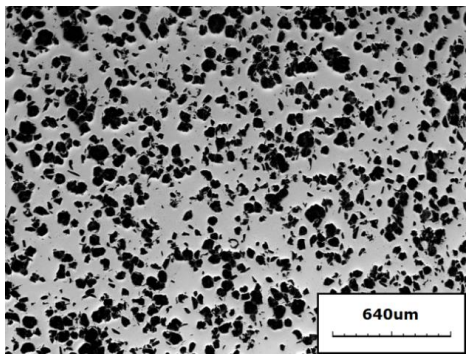

A15 CIP 1450

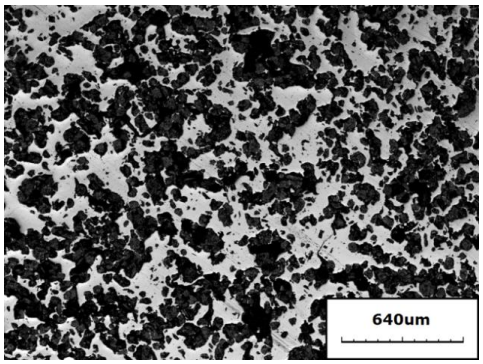

A20 IMP 1450

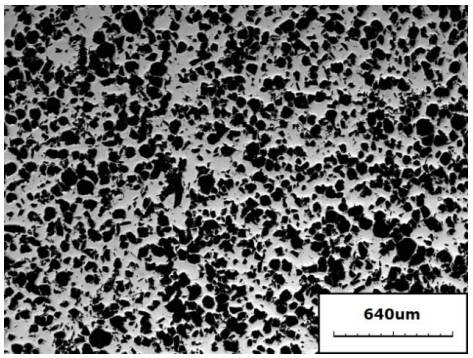

A20 CIP 1450

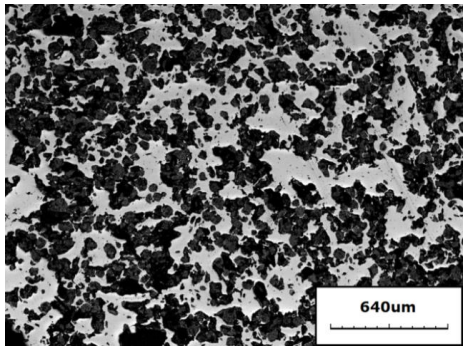

A25 IMP 1650

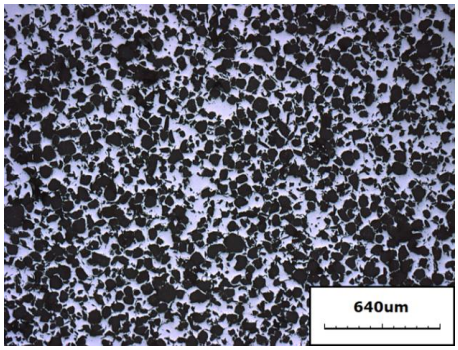

A25 CIP 1450

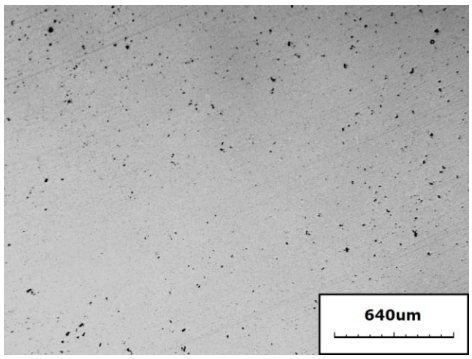

Z100 CIP 1450

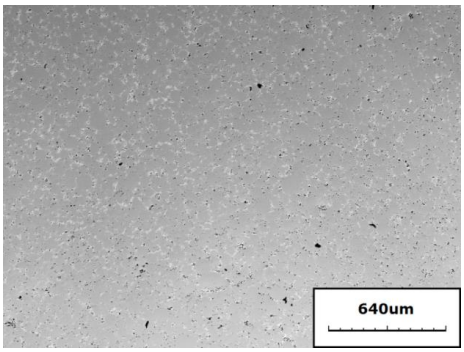

C15 CIP 1450

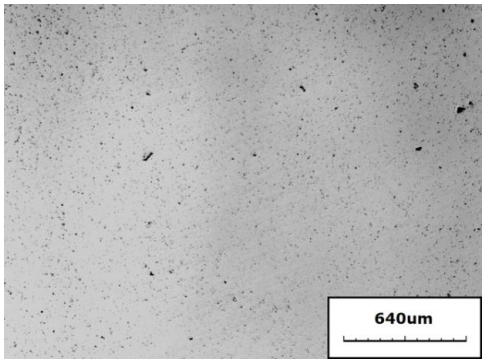

Z100 SG 1450

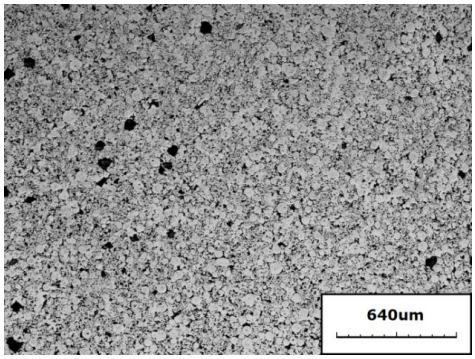

C15 SG 1450

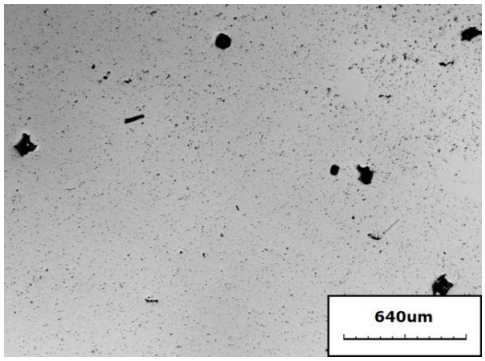

Z100 IMP 1450

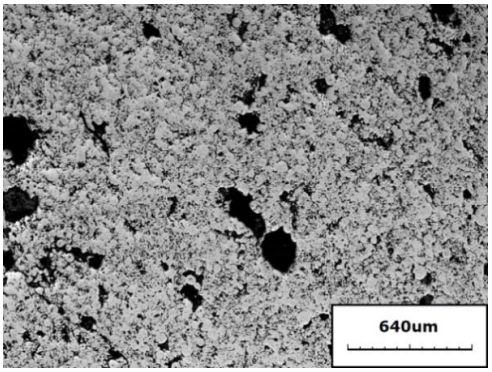

C15 IMP 1450

Figure 72. General view of the surface of all the samples of study

The resulting porosity value obtained from the average of the ten image measurements per sample is summarized in **Figures 73** and **74**.

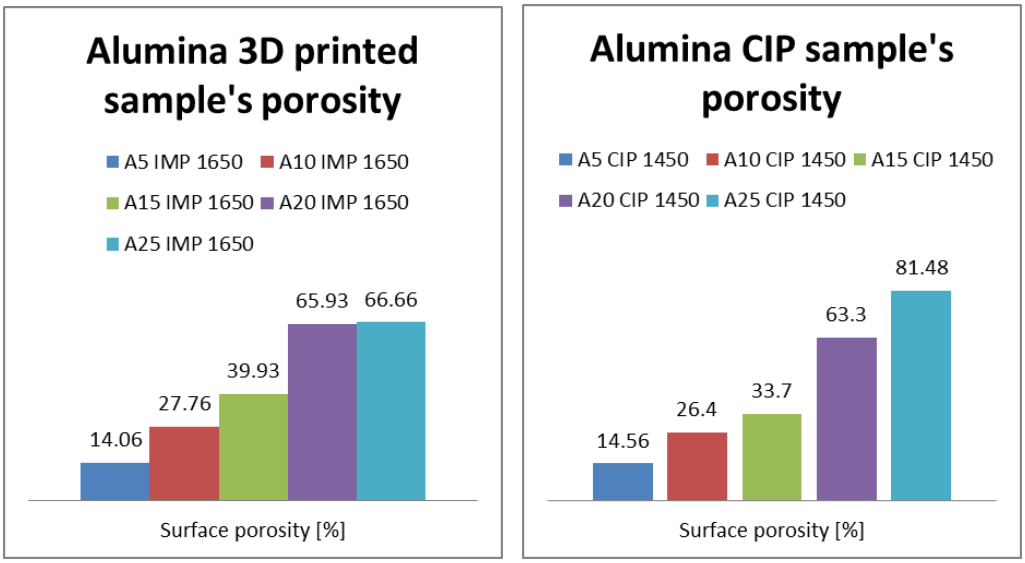

Figure 73. Representaion of the Alumina 3D printed and Cold Isostatic Pressed sample's porosity.

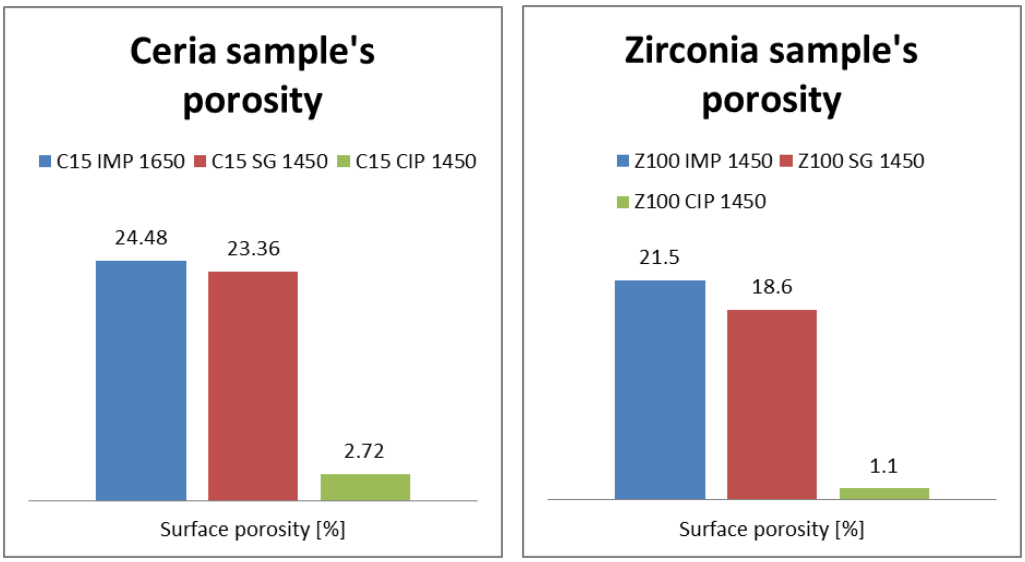

Figure 74. Representaion of the Ceria and Zirconia sample's porosity.

Due to the anormally high porosity values obtained, a comprobation of the sample's surface was made using the height option on the confocal laser microscope, observing the expected height differences of the pores. The result was an almost flat surface without no evident height differences. This fact exhibits that the black zones considered as pores are not actually pores on their totality.

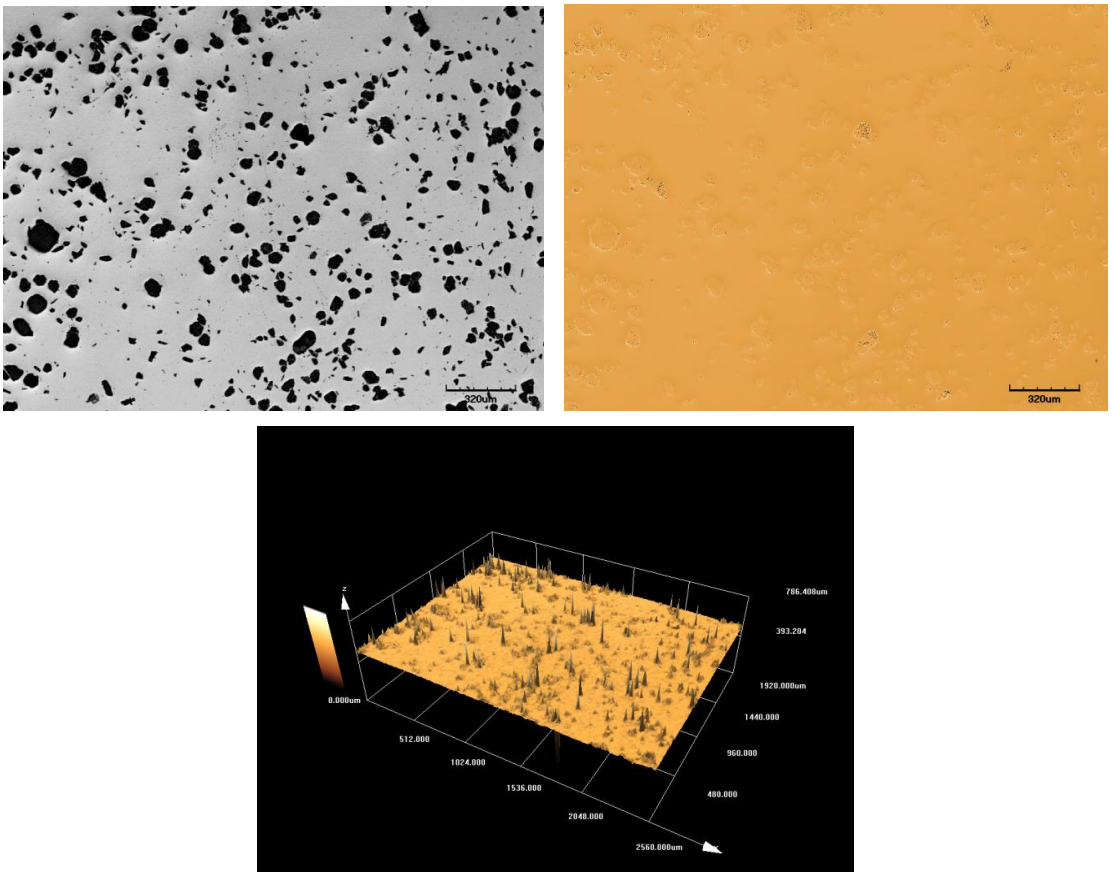

Figure 75. Observation of the height differences on a sample's surface

As it shows **Figure 75**, for all the specimen it is difficult to determine if the black regions (considered as porosity) are pores and by optical or electronical techniques we are able to observe the texture of the ceramic material coming from the printin line or they are filled with the polished slurries used. In order to solve this problema, a FESEM elemental analysis was made on the matrix and in the pores of the samples, determining if the pore was the segregation of the composite material, porosity or dust coming from the polishing process. This analysis has been realized on the C15 IMP 1450, C15 SG 1450, C15 CIP 1450, and for the A25 IMP 1650 and A25 CIP 1450, being the most critical samples for the Zirconia/Alumina and Zirconia/Ceria composites, see **Figures 76** to **85.**

A25 IMP 1650

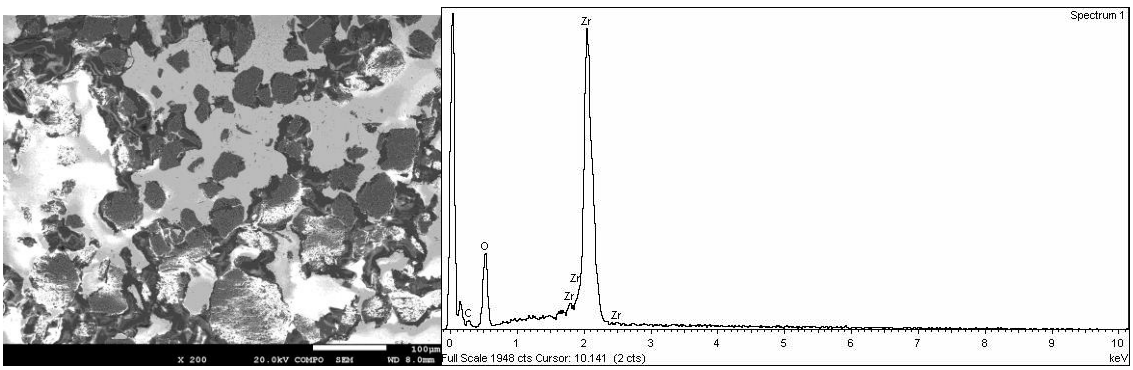

Figure 76.SEM's elemental analysis realized on the matrix of A25 IMP 1650 sample

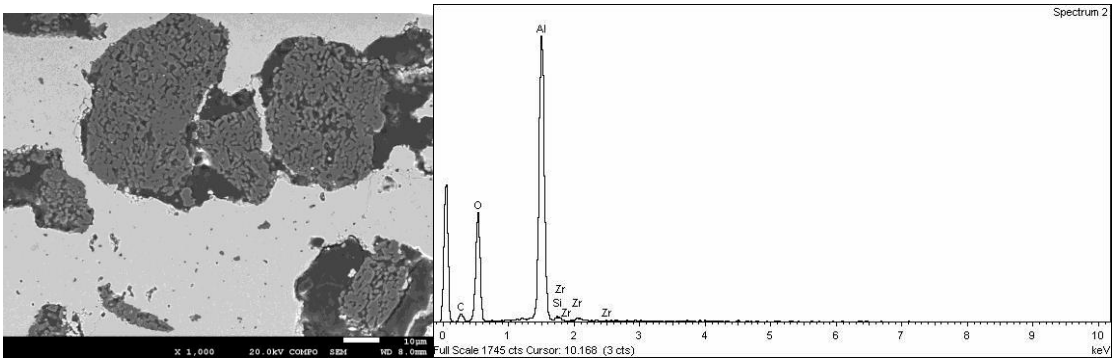

Figure 77. SEM's elemental analysis realized on the pores of A25 IMP 1650 sample

A25 CIP 1650

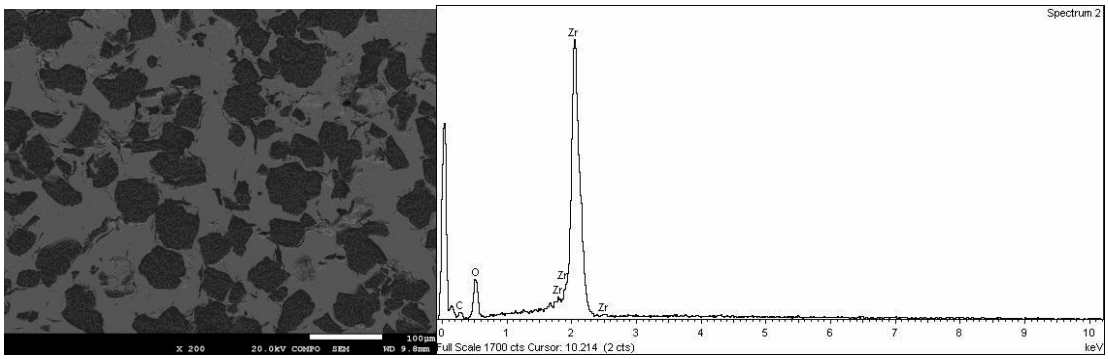

Figure 78. SEM's elemental analysis realized on the matrix of A25 CIP 1450 sample

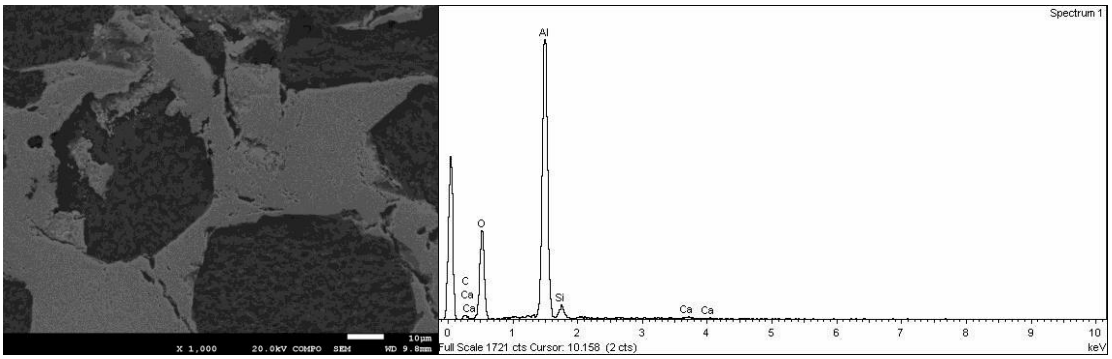

Figure 79. SEM's elemental analysis realized on the pores of A25 CIP 1450 sample

C15 IMP 1450

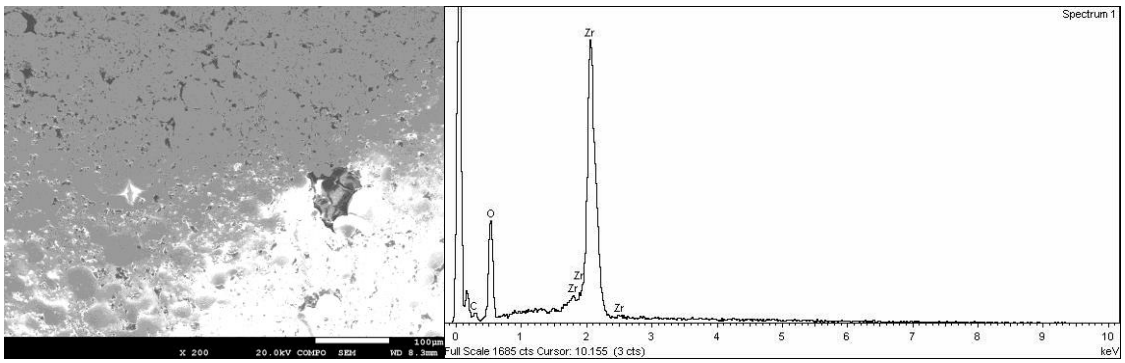

Figure 80. SEM's elemental analysis realized on the matrix of C15 IMP 1450 sample

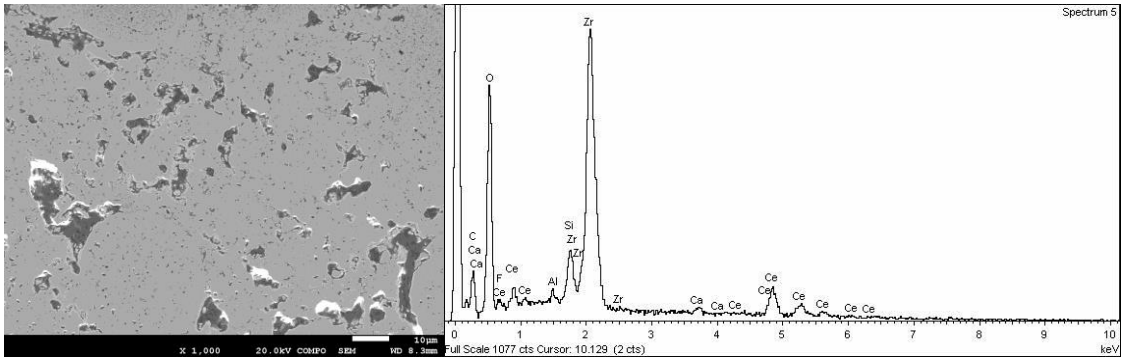

Figure 81. SEM's elemental analysis realized on the pores of C15 IMP 1450 sample

C15 CIP 1450

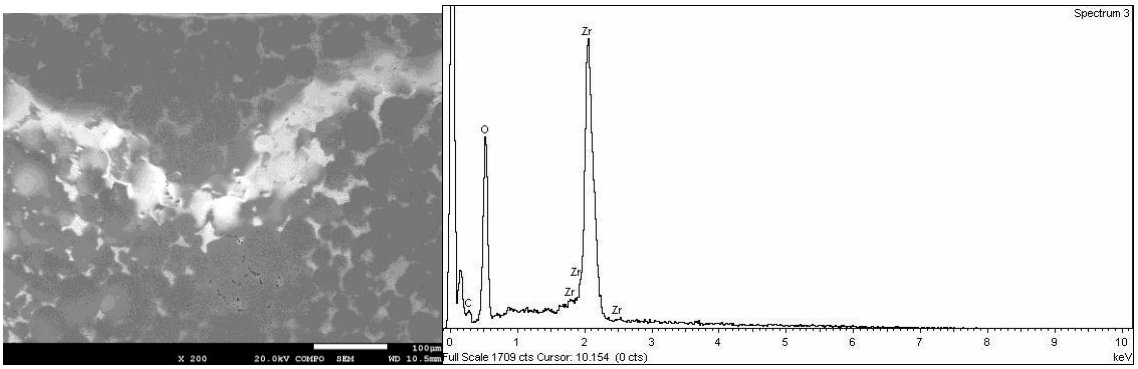

Figure 82. SEM's elemental analysis realized on the matrix of C15 CIP 1450 sample

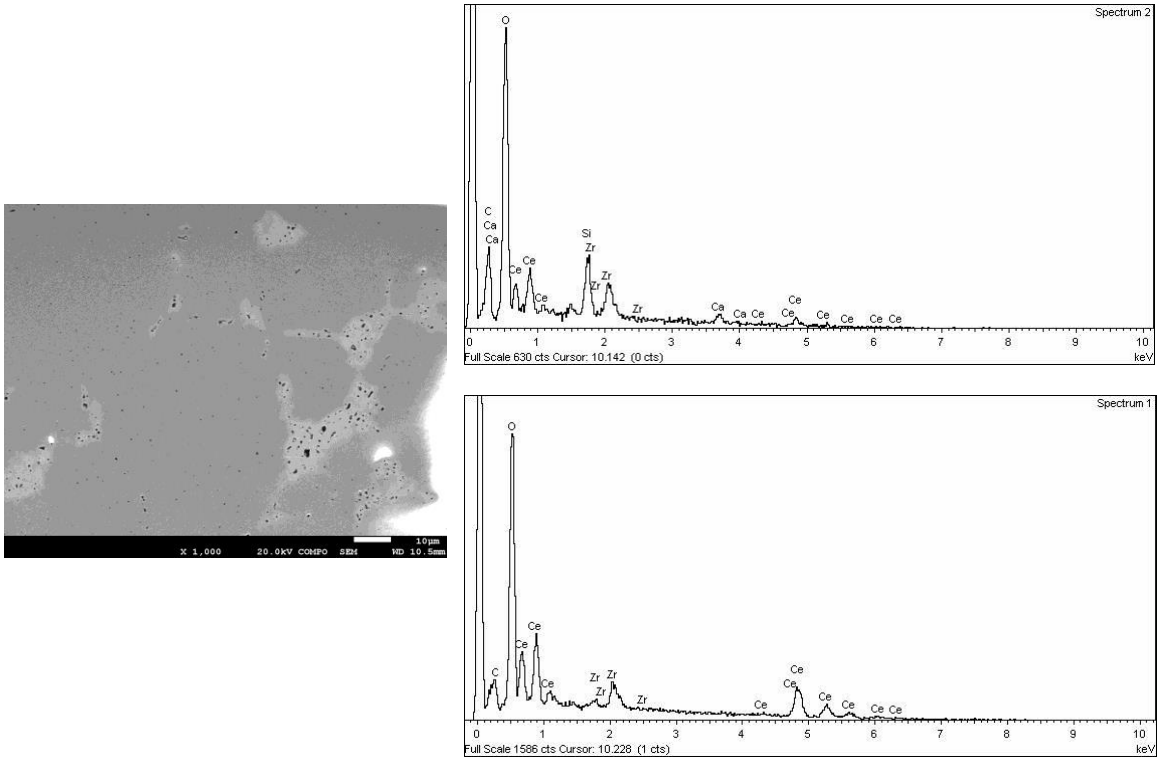

Figure 83. SEM's elemental analysis realized on the clear zone (over) and pores (under) of C15 CIP 1450 sample

C15 SG 1450

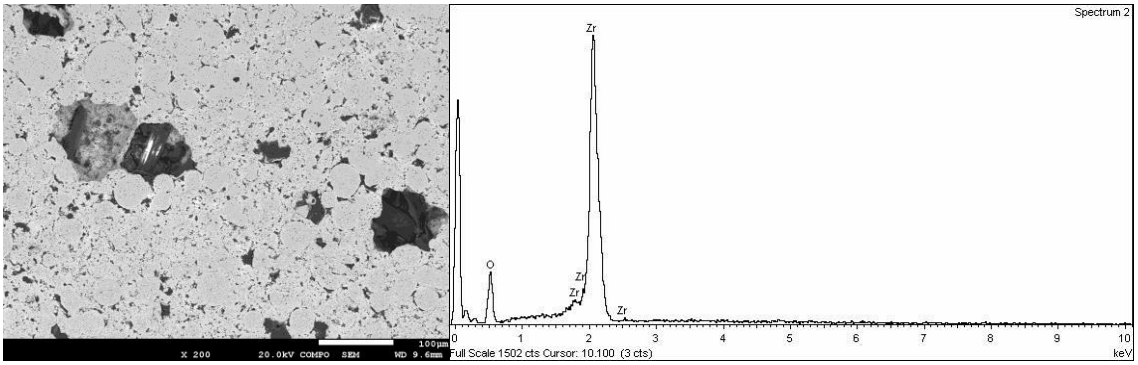

Figure 84. SEM's elemental analysis realized on the matrix of C15 SG 1450 sample

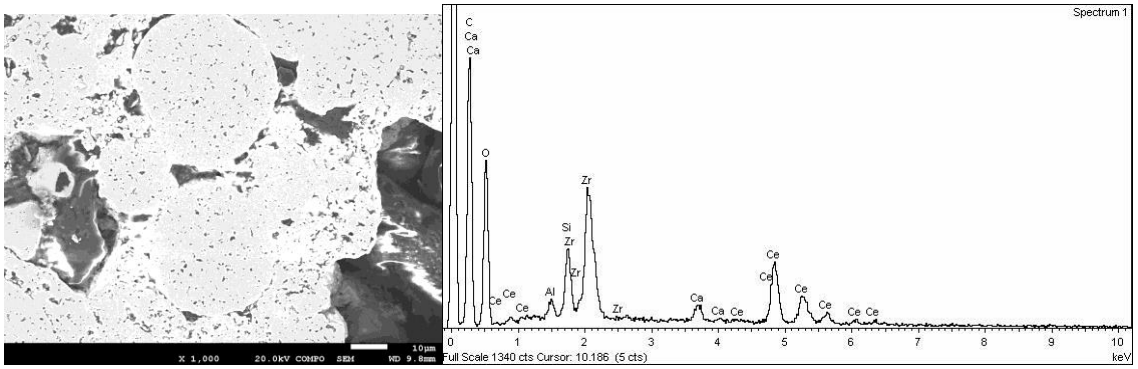

Figure 85. SEM's elemental analysis realized on the pores of C15 SG 1450 sample

FESEM's elemental analysis has shown that the sample's matrix only contains Zirconia, and the secondary elements (Alumina and/or Ceria composite materials) are accumulated in those pores. This finding highlights the complexity to mixt two dissimilar ceramic materials, and it is necessary to develop a new research line in order to better understand how they interact in order to get an homogeneous mixture suitable to print complex ceramic materials. This fact shows a bad mixing of the composite material samples, accumulating the minoritary material on the pores of the structure, creating a high anisotropic sample.

So, in order to avoid this artifact coming from the segregation process of alumina and ceria particles, a new measurement of the porosity was realized, adjusting the threshols of the porosity analysis software on the next hill showed, see **Figure 86**.

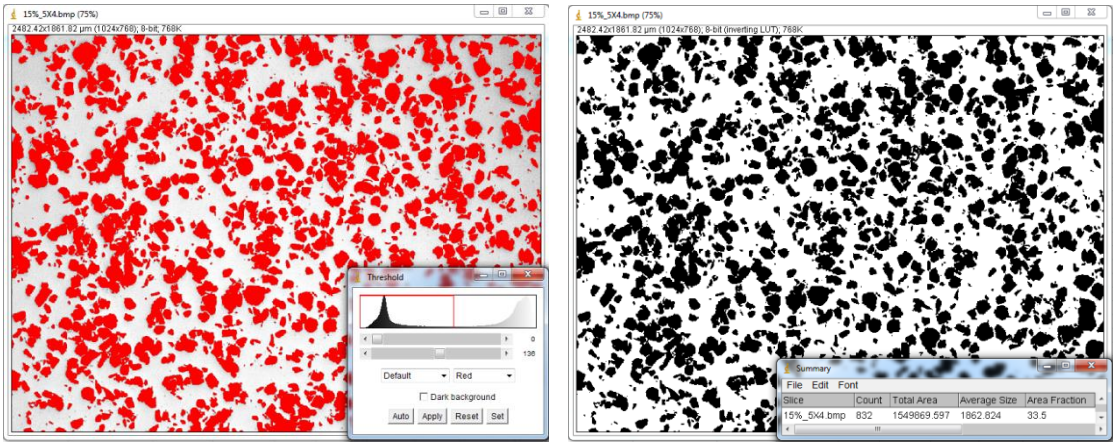

Area fraction= 33.5

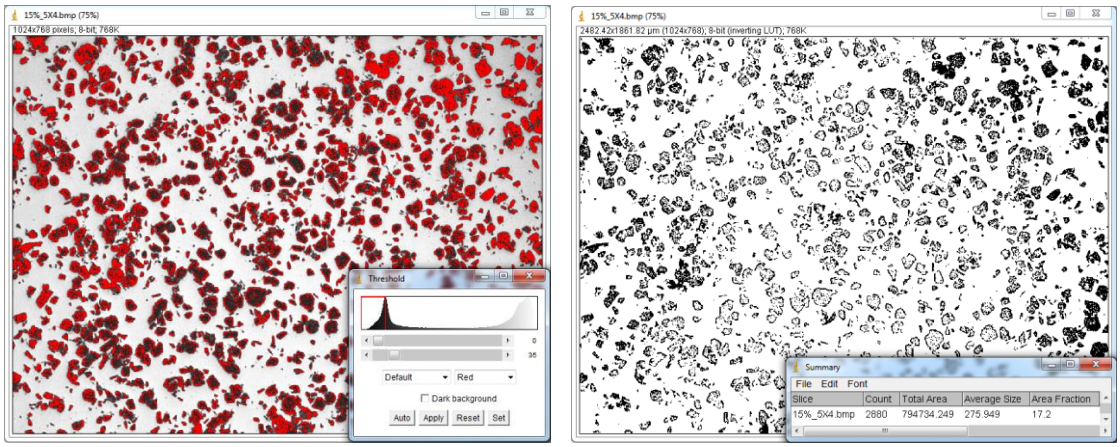

Area fraction= 17.2

Figure 86. Difference on porosity values depending on the threshold adjustment.

This adjustment allows the representation of the porosity without taking into account the segregated material on the pores, representing only the porosity. Comparing the first porosity measurement and the new, the difference obtained is 16.3% less porosity for the example shown. The results obtained are summareized on the following graphics, see **Figures 87** and **Figure 88**.

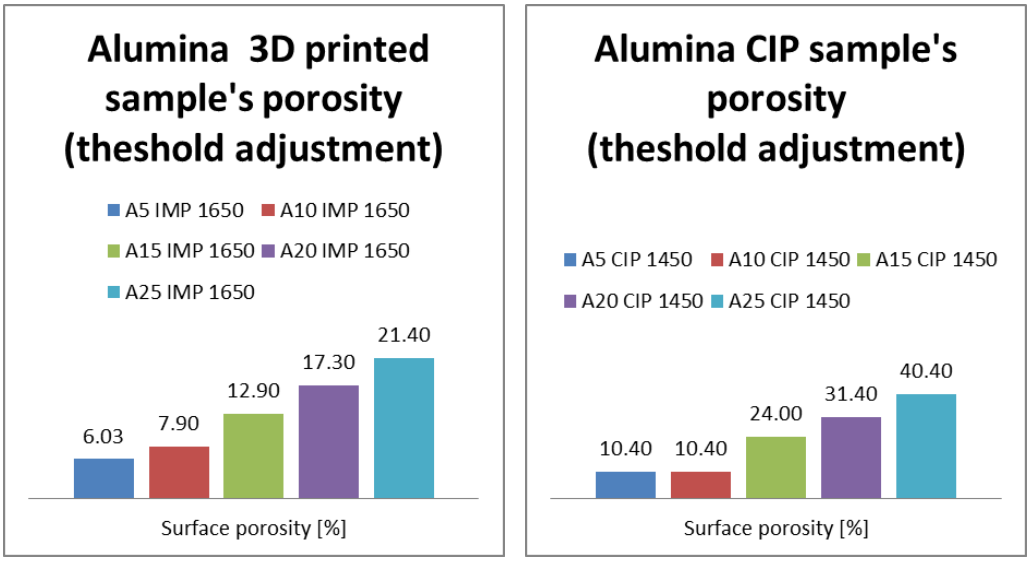

Figure 87. Representation of the pososity values for Alumina 3D printed and Cold Isostatic Pressed samples after the threshold adjustment.

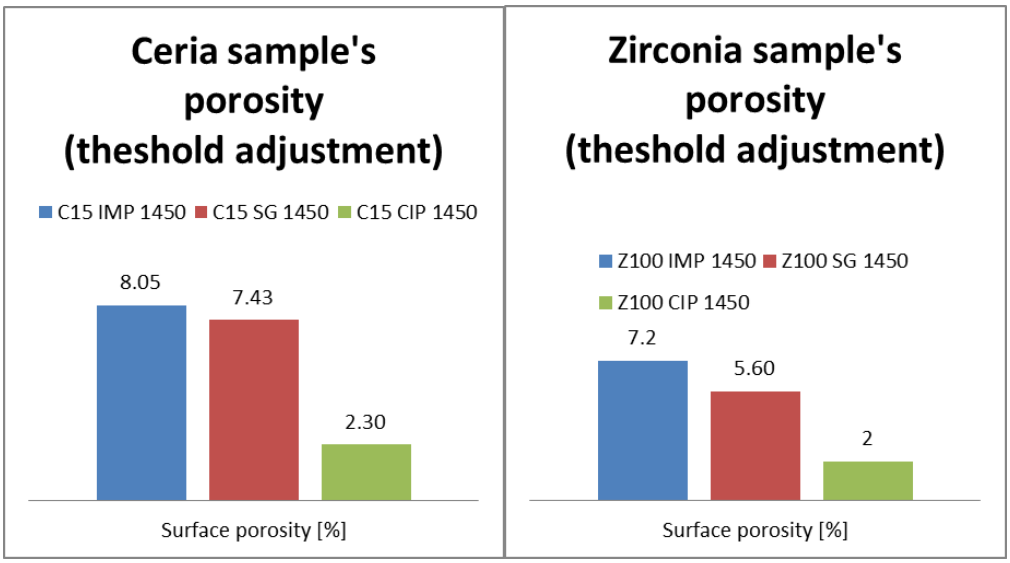

Figure 88. Representation of the pososity values for Ceria and Zirconia samples after the threshold adjustment.

Comparing both measurements (taking into account segregation and no segregation elements) we can conclude that the general trend is similar.

If it is observed the Zirconia/Alumina composite graphics it will be seen that the porosity of the samples is higher in the 3D printed samples in comparision with the CIP samples, opposite to the logical tendence of a higher porosity on the 3D printed samples as the Zirconia and Ceria samples accomplish.

4.2.2. Density

The density of the samples has been measured using the Archimedes and the Helium picnometry methods in order to compare the obtained values and valorate the characteristics of both techniques, see **Table 16**.

Table 16. Density values for all the samples of study.

Density [g/cm^3]				
Sample	Archimedes principle	Helium picnometry	Theoretical	HP density regarding to theoretical density [%]
A5 IMP 1650	5.358	5.631	5.842	96.4
A10 IMP 1650	5.152	5.562	5.691	97.7
A15 IMP 1650	4.682	5.488	5.549	98.9
A20 IMP 1650	4.210	5.380	5.413	99.4
A25 IMP 1650	4.083	5.249	5.284	99.3
A5 CIP 1450	5.540	5.503	5.842	94.2
A10 CIP 1450	5.111	5.393	5.691	94.8
A15 CIP 1450	4.670	5.138	5.549	92.6
A20 CIP 1450	4.167	4.399	5.413	81.3
A25 CIP 1450	4.699	4.135	5.284	78.3
C15 IMP 1450	4.555	5.953	6.201	96.0
C15 SG 1450	4.573	5.982	6.201	96.5
C15 CIP 1450	5.904	5.993	6.201	96.6
Z100 IMP 1450	5.554	5.895	6.000	98.3
Z100 SG 1450	5.738	5.898	6.000	98.3
Z100 CIP 1450	5.895	5.940	6.000	99.0

In order to observe the tendence of the density values depending on the sample's conforming technique employed or the material refered, a graphic representation of all of them is shown on **Figures 91** and **92**:

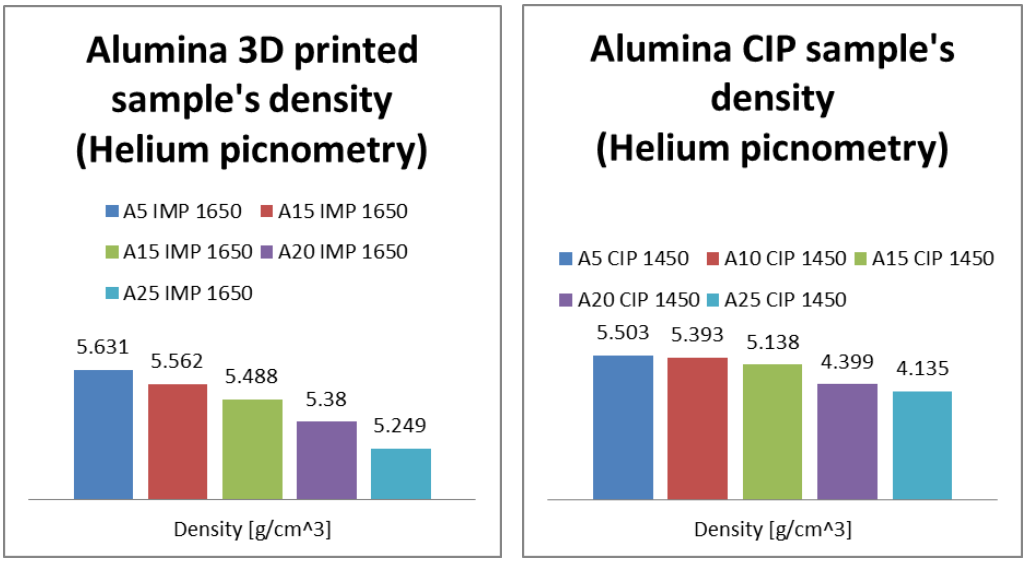

Figure 89. Representation of the density values for Alumina 3D printed and CIP samples

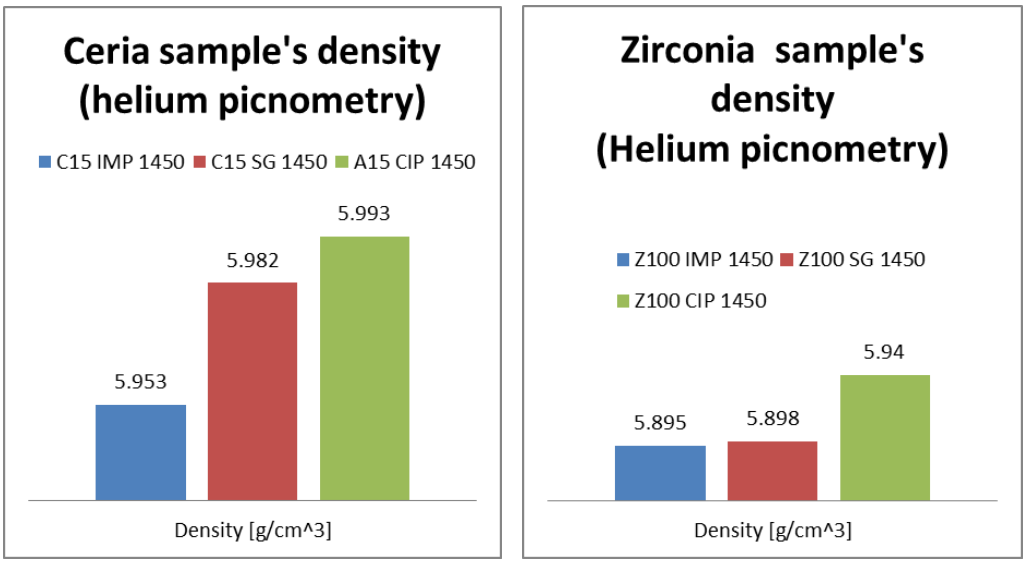

Figure 90. Representation of the density values for Ceria and Zirconia samples.

Observing the results obtained, there is some information that can be extracted relative to the two different measuring techniques, the sample's density obtained depending on the conformation and the reasonability of the results:

- Starting for the reasonability of the results, due to all of them are lower than the theoretical porosity, they could be possible. Moreover all the composite material's densitiy values follow the theoretical tendence, being a higher density on Ceria composites and lower on Alumina composites respect to Zirconia samples.
- Comparing the different densities obtained for Archimedes principle and for Helium picnometry method, the first results are lower. This fact is due to considering only the open porosity on the Archimedes

principle technique, computing as sample's volume the empty volume of the closed pores inside the sample. This comparison shows that helium picnometry allows the obtaining of more precise density values, computing the open and closed porosity of the sample.

- Finally, observing the tendencies of the graphics, can be deduced that for Zirconia and Ceria samples, 3D- printing technique have the lower density, being Gel-casting technique the next with very similar values, and the CIP technique as the last, obtaining the higher denisties, as it was thinked. For the Alumina samples this rule is not complished, being the 3D printed sample's densities higher than CIP. This fact is due to the sintering temperature of both, being the 3D printed a 1650ºC temperature and a 1450ºC temperature for CIP.

4.2.3. Perfilometry

The sample roughness has been measured with a perfilometer and a confocal laser microscope. The following tables summarize the values of roughness obtained determined by using two different techniques, one of contact (profilometer) and non-contact techniques (confocal laser microscope).As it can be depicted, the Ra is lower than the Rq. However, it is necessary to mention, that the values extracted from the profilometer measurements are higher than the obtained by using confocal laser microscope. This difference is attributed to the fact that the perfilometer allows to measure larger regions in comparition than the non-contact techniques, yielding the perfilometer more realistic values than the other technique employed.

Table 17. Roughness values for all the 3D printed samples

3D-printing samples				
	Profilometer		Confocal laser microscope	
Samples	Ra [nm]	Rq [nm]	Ra [nm]	Rq [nm]
A5 IMP 1650	369	461	6.62	10.01
A10 IMP 1650	487	596	9.09	18.72
A15 IMP 1650	659	826	9.84	23.22
A20 IMP 1650	694	1089	27.95	72.04
A25 IMP 1650	884	1202	29.09	74.63
C15 IMP 1450	315	363	16.80	41.91
Z100 IMP 1450	326	380	20.47	43.64

Table 18. Roughness values for all the Cold Isostatic Pressed samples.

Cold Isostatic Pressing samples				
	Perfilometer		Confocal laser microscope	
Sample	Ra	Rq	Ra	Rq
A5 CIP 1450	706,79	771,49	8.39	14.80
A10 CIP 1450	498,28	675,30	13.06	24.40
A15 CIP 1450	321,53	461,25	13.87	41.06
A20 CIP 1450	636,05	790,39	23.17	50.37
A25 CIP 1450	816,43	1133,53	31.04	68.60
C15 CIP 1450	203,04	251,20	1.57	2.53
Z100 CIP 1450	215,09	270,21	2.08	3.53

Table 19. Roughness values for all the Gel-casted samples.

Gel-casting samples				
	Perfilometer		Confocal laser microscope	
Sample	Ra	Rq	Ra	Rq
C15 SG 1450	226,54	330,08	7.85	11.86
Z100 SG 1450	233,88	336,26	10.67	18.30

The results show that Alumina samples have a higher Surface roughness compared with the Zirconia samples, increasing their value with the increasing of Alumina's proportion. This phenomenon is attributed to the heterogeneously distributed agglomeration of alumina clusters inside the zirconia matrix, while for the ceria specimens this difference is practically not observed due to these specimens present a better mixing in spite of presenting agglomeration too.

4.2.4. Rheometry

As we commented in **section 1.3**, one of the main parameters to take into consideration during the 3D-printing process is the ceramic viscosity. For this reason, this property has been measured for the Z100 ceramic paste due to is the main constituent for all the specimens investigated in this Bachelor's degre. in **Figure 93**, shows the average for the three measurements done for the specimen of interest.

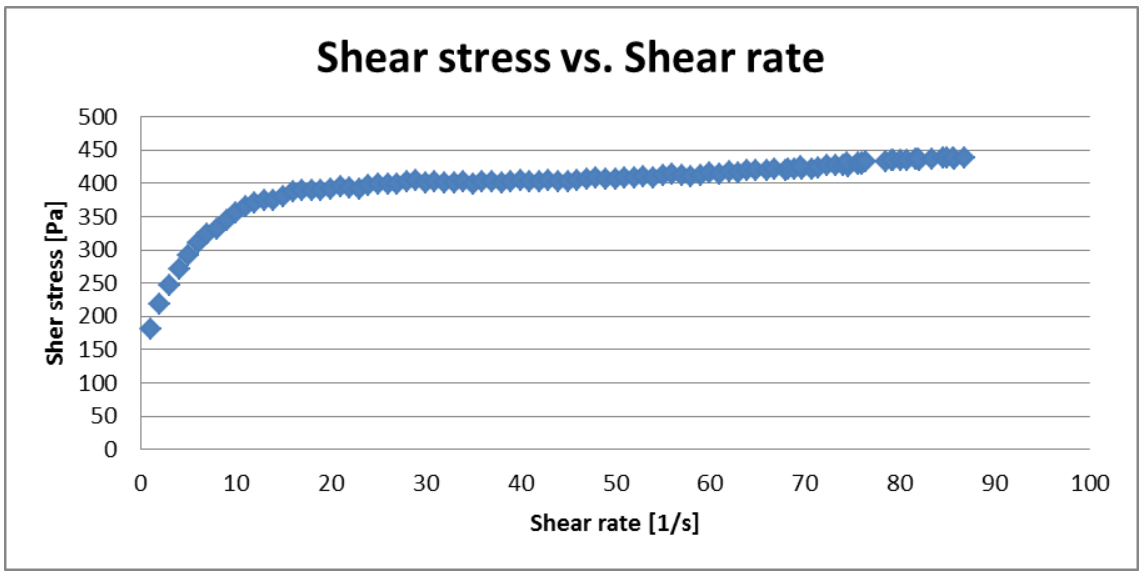

Figure 91. Representation of the Shear stress versus shear rate of the Zirconia ceramic powder based viscous paste.

As it can be depicted in the previous figure, the Zirconia viscosity presents a shear thinning or pseudoplastic behavior, yielding a reduction of its apparent viscosity when the stress increases. On the other hand, the viscosity variation along time is not considered to be evaluated due to the time required to print the specimens of interest is practically negligible and .

Representing **Figure 93** in a ln scale, it is possible to observe that the material under investigation follows a power law. Mainly, the experimental points can be fitted with two different power law, for a low and high shearing rates. In the case of study here, it is only interesting the first power law, due to the maximum shearing stresses takes place during the extrusion process which takes place in the nozzle of the 3D-printer. The values extracted from both power law fittings are summarized in **Table 21:**

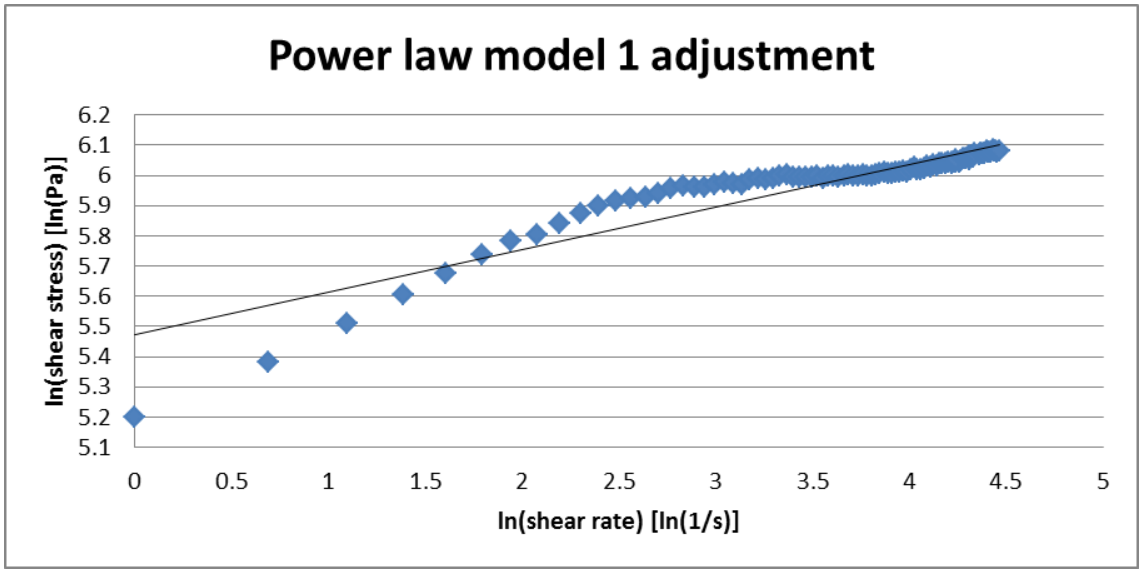

Figure 92. First power law adjusted model for the viscosity of Zirconia viscous paste.

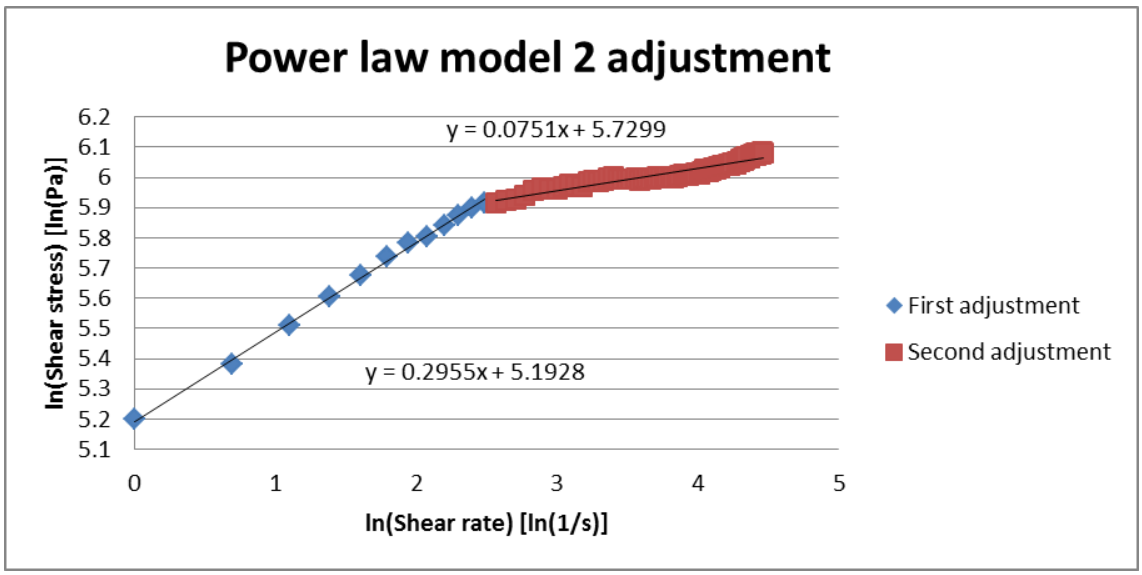

Figure 93. Second power law adjusted model for the viscosity of Zirocnia viscous paste.

Finally, the characteristic power law model values are resumed below:

Table 20. Power law model characteristic parameters.

Power law model 1 parameters			
	ln(k)	k	n
Model 1	5.4726	238.078	0.1412
Model 2 (first adjustment)	5.7299	307.939	0.0751
Model 2 (second adjustment)	5.1928	179.972	0.2955

In doing this investigation, the power law parameters obtained from this experimental data; allows to adjust the the extrusion pressure in order to obtain a certain volume flow rate depending of the ceramic viscosity and/or the shear rate which is maximum in the nozzle region. By doing this experiments, the main goal is to better understand how this material will behaves under this particular processing conditions.

4.2.5. Microstructure

In order to obtain microstructural information with the sample it has been realized XRD test son them to observe if they present an amorphous or crystalline state as well as if the sintering temperatures produces some phase transformation. This analysis also has been used in order to compare samples with same material but different conforming techniques, observing if there are some microstructural changes. It has been applied a normalization on the intensity values for every sample's spectra.

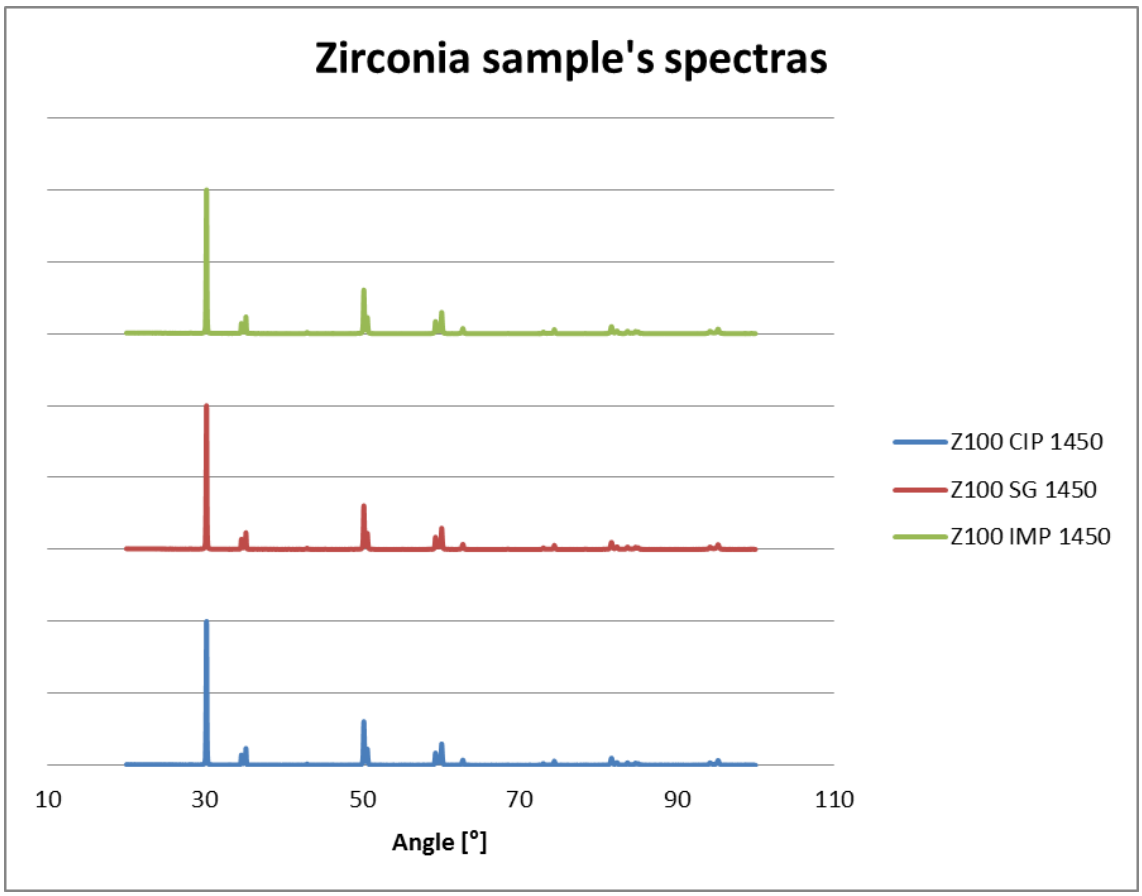

Figure 94. XRD spectra of all the Zirconia samples.

On this first graphic can be observed that the microstructure of the material remains constant independently of the conforming technique used. This fact means that there is no restriction for the conformation techniques used in order to obtain a specific microstructure, being the resultant samples of them only different in structural terms of porosity and thus density.

It also can be appreciated the different peaks of the Zirconia's tetragonal phase, beig present on the positions of 30º for the (111), 35º for (200) and (002), 50º for (220) and (200), 60º for (311) and (222). Finally, a cubic peak can be observed on 80º.

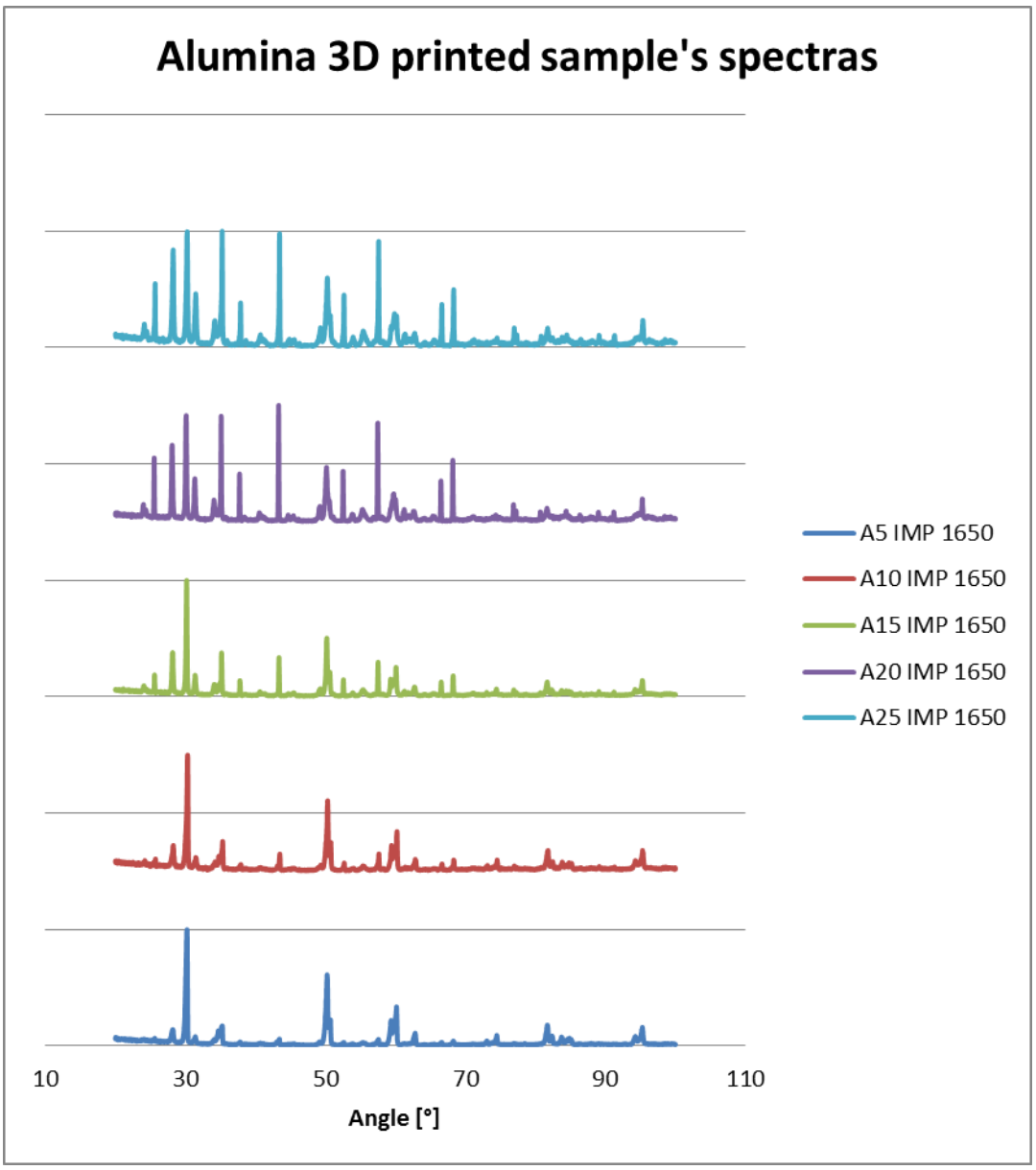

The XRD related to the specimens with different content of alumina shows the spectra evolution during the Alumina's percentage increasing from 5% to 25% wt on Zirconia. At samples of lower Alumina's percentage, the specta obtained is almost equal compared with the Zirconia samples. Therefore, with the increasing of the Alumina's percentage, a new group of peaks on 35º, 45º and 60º increase between the tetragonal Zirconia peaks observed on the first graphic. Finally there are another pair of peaks that also increase with the Alumina's percentage increase, being situated at rounds of 70º and 95º.

Finally, a summarizing graphic with the spectras of the most critical 3D printed samples and another graphic of the Agar-Agar ashes are presented:

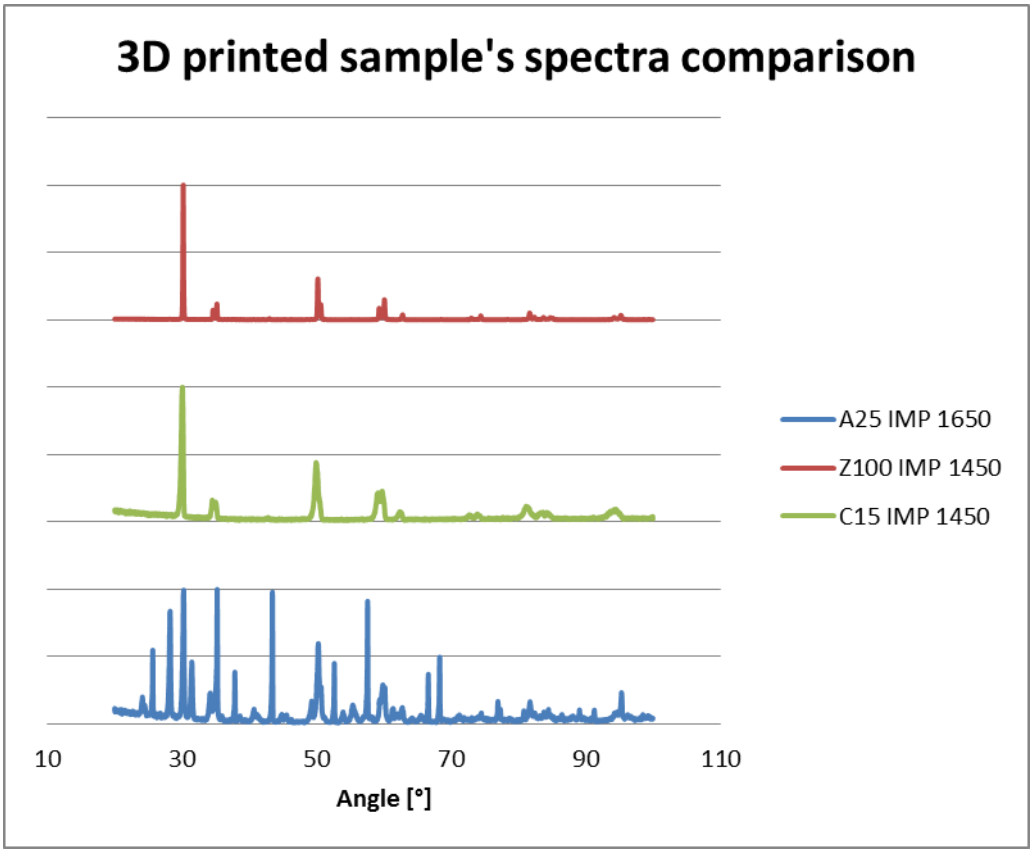

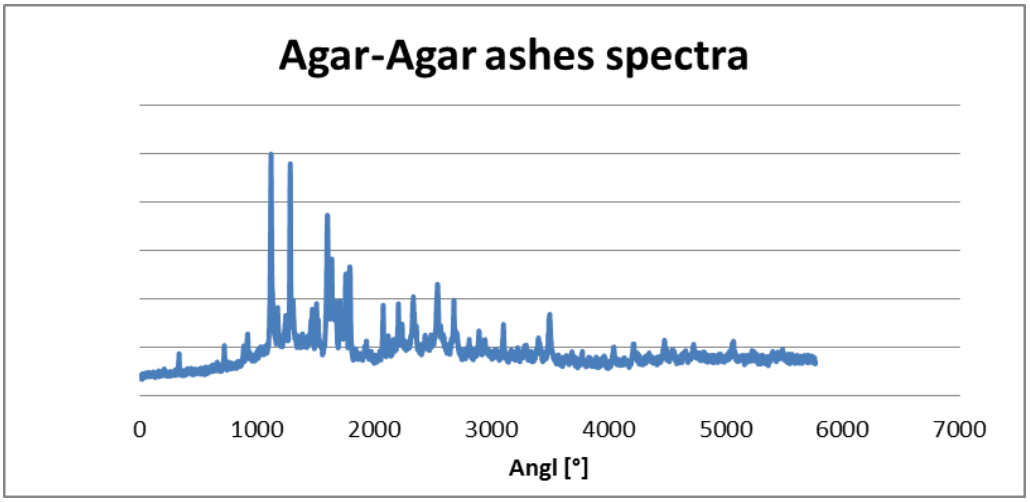

4.3. Mechanical characterization

4.3.1. Hardness

Figures 95, 96, 100 **and 101** represents the Vickers hardness averaged get from ten imprints performed at 1 kgf for each specimen of investigation. As it can be observed for **Figure 98**, when the content of Al_2O_3 increses inside the 3Y-ZrO2 matrix, the hardness decreases. This finding is a bit

surprising due to the addition of this component may improve the mechanical properties in terms of hardness. Furthermore, when the amount of Al_2O_3 increases the variability in the measurements also increases, pointing out that the specimens of interest presents some heterogeneities; mainly attributed to the Al_2O_3 clusters observed and analyzed by EDX, see **Figures from 76 to 79**. Furthermore, this anormal behavior can be attributed to several factors: i) the sintering temperature for the Al_2O_3 reinforcement is not enough to get a dense material, ii) at those temperatures some tetragonal grains for the 3Y-ZrO_2 phase transforms into cubic phase, which is harder than the tetragonal one and iii) indentations done in some regions where porosity exist being this phenomena the main responsible for the hardness dropping (see **Figure 97**).

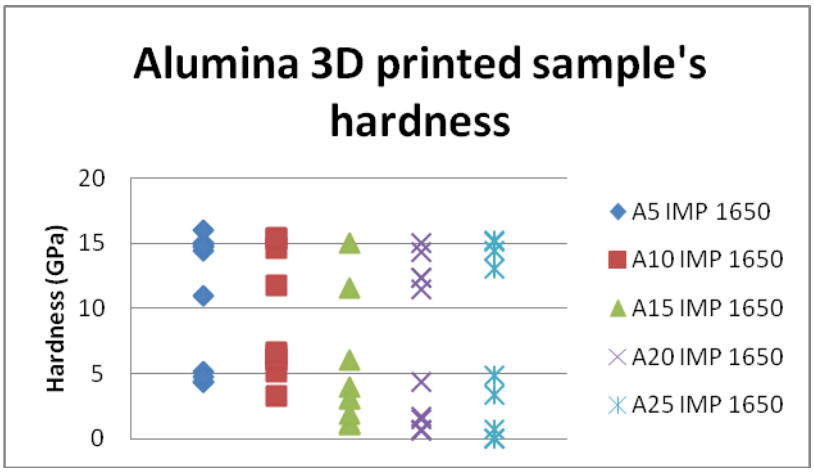

Figure 95. Representation of the hardness values for Alumina 3D printed samples.

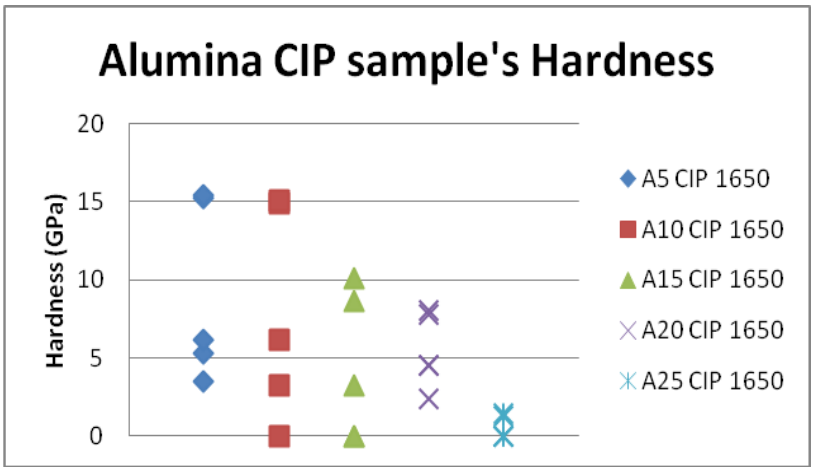

Figure 96. Representation of the hardness values for Alumina Col Isostatic Pressed samples.

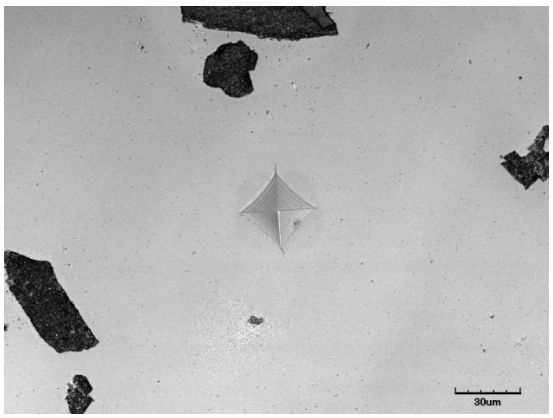

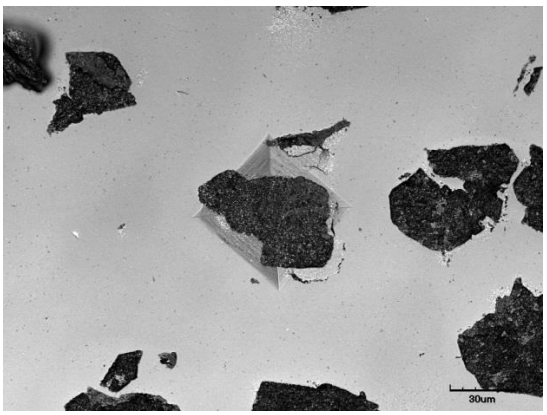

HV = 15.40 GPa	HV = 6.18 GPa

Figure 97. Example of the hardness variability for the same material

As it can be observed in **Figure 97**, the residual imprint for the dense material (left hand side) is smaller than the indent confined in the interface (material/porosity) where clearly can be appreciated that for the same load, the shape of the imprint bigger than for the dense material. This finding, plays an interesting role, due to without the need to observe the surface after polishing in order to characterize their microstructure, it is possible to perform several residual imprints and predict the pre-existing porosity after the 3D-printing process. Then, in **Figure 98**, the hardness is presented only taking into account the residual imprints which are not affected by the pre-existing porosity. However, the trend presented here is the same as we presented before. In other words, excluse the imprints performed in the interface between the material and the pre-existing pores does not help to improve the micromechanical properties in terms of hardness. Then, the main problem related to the hardness dropping may be attributed to the presence of heterogeneities inside the composite material.

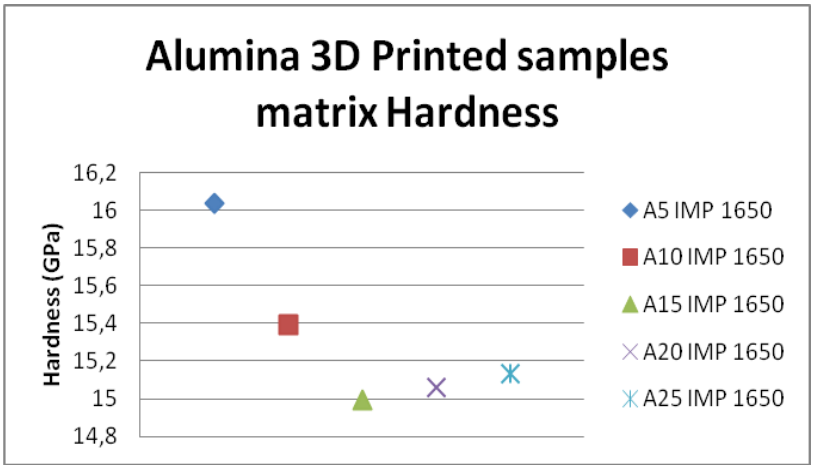

Figure 98. Representation of the Alumina 3d printed sample's matrix hardness values.

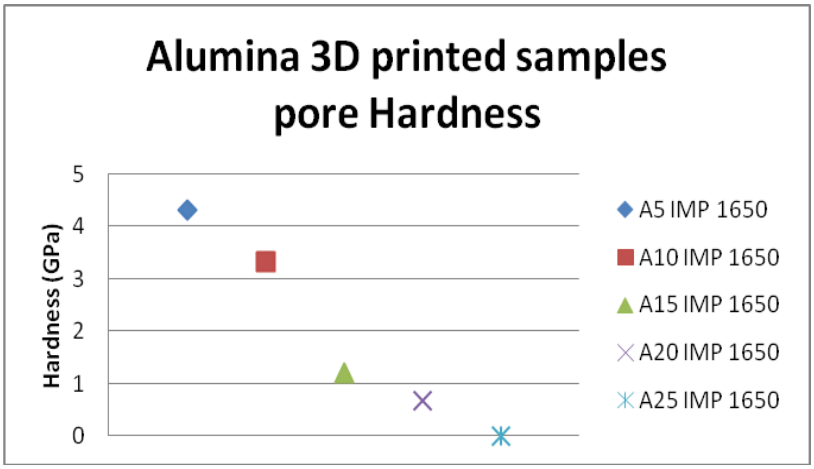

Figure 99. Representation of the Alumina 3d printed sample's pore hardness values.

Finally, the two following graphics show the hardness for Ceria and Zirconia samples. The Ceria samples show a hardness decreasing among the conforming techniques. This behavior may be attributed to the same effect as we mention above The difference between both is that Zirconia ceramics present more focused values with better hardness values in general.

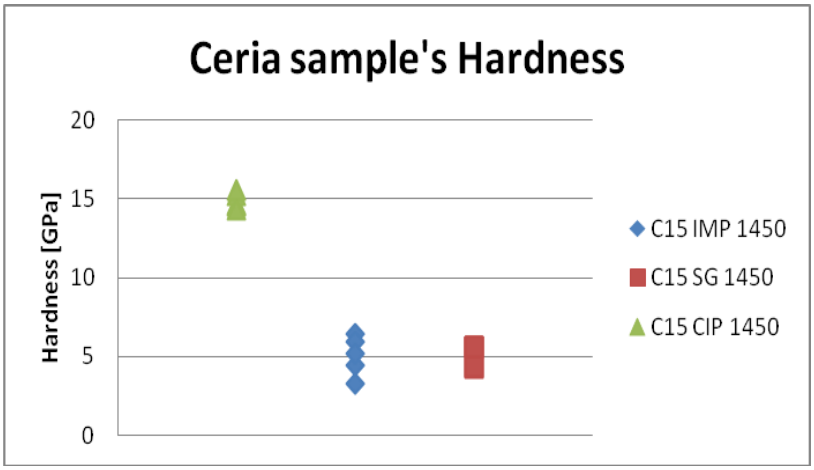

Figure 100. Representation of the hardness values for Ceria samples.

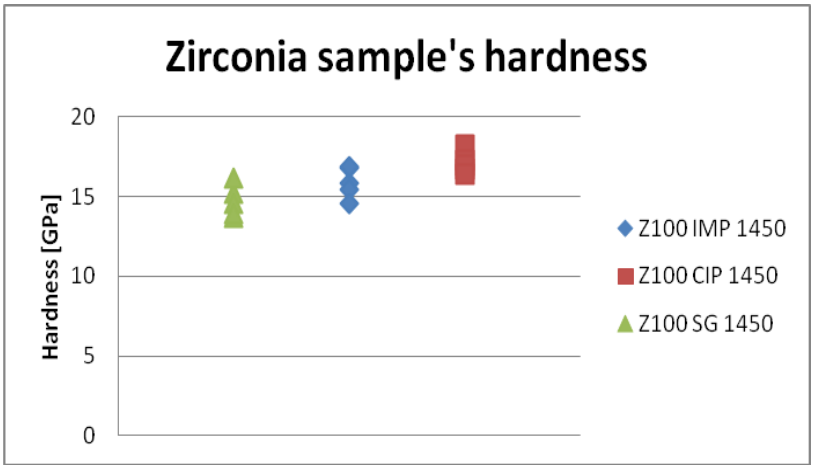

Figure 101. Representation of the hardness values for Zirconia samples.

4.3.2. Fracture toughness

The indentation fracture toughness has been measured by a direct inspection of the residual Vickers imprints and measuring the crack length, see **Figure 102**.

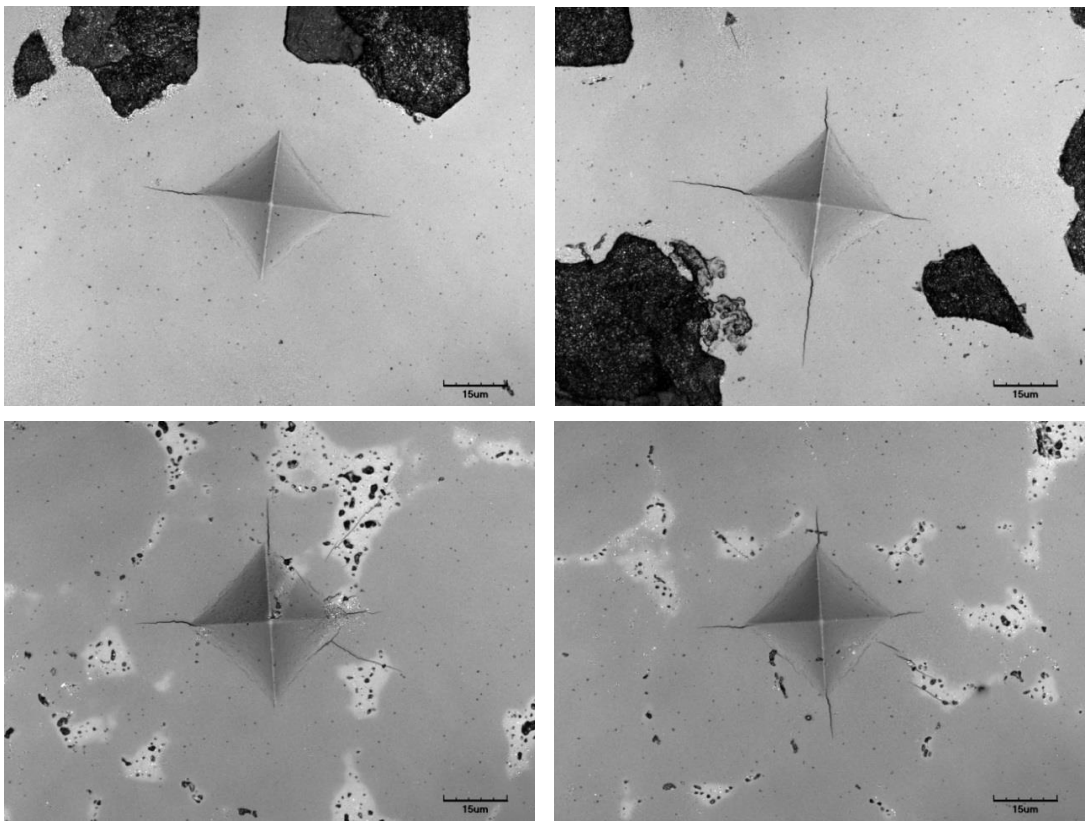

Figure 102. Crack generation on the corners of the micro-indentation imprints

As it can be appreciated in the previous figure, several cracks propagate from the corner of the residual imprint. For these particular cases, the indentation fracture toughness is possible to determine by using the expression shown on **section 3.6.2.,** while for other particular cases, apart of the radial crack's activation also exist other mechanism that takes places at the same time, like chipping effect (see **figure 103**).

The indentation fracture toughness determined from all the specimens investigated here are summarized in **Table 22**.

Table 21. Sample values for the fracture toughness

Sample	Kic ,Mpa·m$^{1/2}$
A5 IMP 1650	5.770
A10 IMP 1650	6.620
A15 IMP 1650	6.431
A20 IMP 1650	6.109
A25 IMP 1650	6.332
A5 CIP 1450	5.147
A10 CIP 1450	2.993
C15 CIP 1450	1.443

Z100 CIP 1450	5.818

As it can be appreciated for the specimens printed, the indentation fracture toughness increases if we compare with the value for the pure 3Y-ZrO_2, which is around 4.5 MPa√m. Furthermore, it is possible to get a partial conclusion from this data, as it can be observed when the amount of Al_2O_3 is equals or higher than 10%, the indentation fracture toughness remains quite stable, being that the maximum content that is possible to add inside the 3Y-ZrO_2 matrix. Due to the addicion of more content Al_2O_3 homogeneous does not help to improve this property. On the other side, for the CIP specimens are possible to observe that this property is in the best case around 20-40% lower than the value reported for the 3D-printed specimens. This trend can be attributed to the fact that for the CIP specimens the powder mixture between 3Y-ZrO_2 and Al_2O_3 or CeO_2 was mechanically mixed allowing the presence of several heterogeneities into the specimen, while for the 3D-printed specimens the mixture was done in solution.

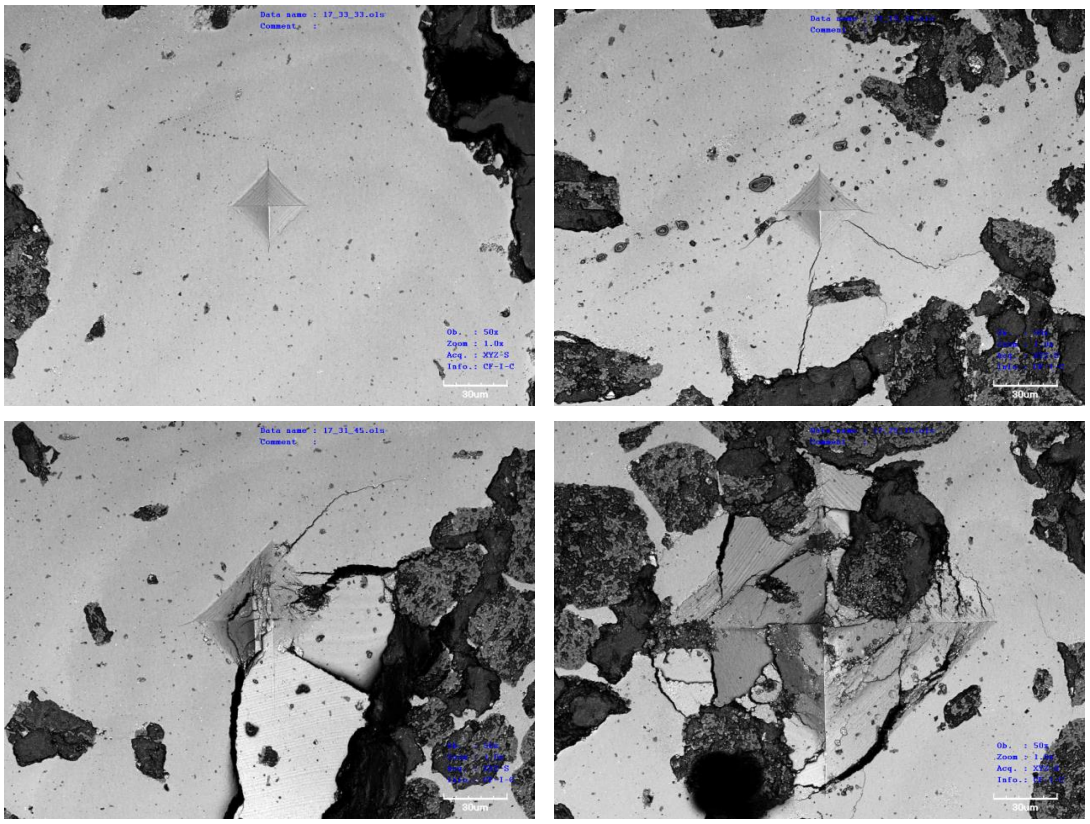

Figure 103. High variability of the imprint cracks on a same sample.

CHAPTER 5: CONCLUSIONS

Sintered samples of zirconia obtained using the syringe extrusion 3D printing technique have been successfully achieved by applying an intermediate step in order to transform powders into printable materials with gel-casting technique.

- Printed zirconia samples have shown similar mechanical properties compared with the same material obtained via cold isostatic pressing.

Printable materials made by mixing alumina/zirconia and ceria/zirconia were succeeded however:

- It was required to increase temperature up to 1650 ºC in order to sintered alumina and ceria. As a consequence, cubic phase was present in zirconia instead of tetragonal phase which cause a reduction of mechanical properties compared to zirconia samples.
- After sinterization process developed at different temperatures, it was no possible to achieve a homogeneous microstructure.

CHAPTER 6: FUTURE WORKS

In order to optimize the 3D-printing process is necessary to:

- Redesign the screws or/and the gear transmission to improve continuos extraction of the syringe without extracting the extruder head.
- Design a pressurized extruding system with the main goal to get more control of the process which hardly affect the microstructure and mechanical properties of sintered samples.

On the other hand, during the development of this bachelor's degree, it has been observed some aspects related to components used to obtain the printable material that may be improved:

- The possibility to change the gellying agent of the gel-casting technique to another with a lower powder size. It has ben observed that the Agar-Agar used as the solution binder for the obtaining of the viscous ceramic powder pastes for 3d printing, presents some problems of nozzle bloquing during the extrusion due to its big powder size. The possibility to change it for another with a smaller powder size would solve this problem but it would need to maintain the rheological properties obtained with Agar-Agar on the viscous pastes.

The water proportion on the viscous paste is a critical factor that determines the viscosity and thus the extrusion process quality and the 3d printind sample result. It would be interesting to control this water loss of the viscous pastes with a humidity controlled chamber, measuring the amount of loss during the time, being possible to optimize it obtaining good

extrudable pastes in a less time or conserving it better for their posterior printing.

CHAPTER 7: ENVIORNMENTAL ANALYSIS

The enviornmental impact of the realization of this bachelor's degree is due to the use of energy and water for the building, syntering, and preparing processes of the samples studied.

All the materials studied are not dangerous or contaminating. The discarded tests during the building of the samples have been putted on specific trash cans in order to be recycled or treated.

The most significant use of energy has been on the sintering process using the Nabertherm furnace, which spends a big amount of electric energy. The rest of the energy has been used to work on the installations and use the rest of the equipments needed to prepare and characterize the samples. All the electrical energy spend has been supplied for an electrical company which uses a little percentage of removable energies in order to obtain it, being the principal source the non removable energies as fossil combustibles or nuclear energy.

CHAPTER 8: BIBLIOGRAPHY

The bibliography is divided into two parts. First are the "References", which are those that correspond to the dates appeared in the text. The "bibliography of query" corresponds to those works not cited explicitly in the text, but which have served as a basis and/or consultation.

8.1. References

[1] Evans A.G., "Perspective on the development of high-toughness ceramics", Journal of the American Ceramic Society 73 [2], 187-206, 1990.

[2] Boutz, M. M. R., Winnubst, a. J. a., Van Langerak, B., Olde Scholtenhuis, R. J. M., Kreuwel, K., & Burggraaf, a. J. (1995). "The effect of ceria co-doping on chemical stability and fracture toughness of Y-TZP". Journal of Materials Science, 30(7), 1854–1862.

[3] Green D.J., Hannink R.H., Swain M.V. "Transformation Toughening of Ceramics". Boca Ratón (FL) CRC Press Inc., 1989.

[4] J. Capdevila, "Síntesis de cerámicos tecnológicos mediante métodos de combustion de geles de acrilamida", Tesisi doctoral, Universitat de Barcelona, facultat de química, 2007.

[5] Materials design, "Temperature-Dependent Phase Transitions of ZrO2", Application note, 1.

[6] W. Danng, G. Yongquan, L. Kaiming, T. Kun, "Crystal structure of Zirconia by Reitveld refinement", Department of Materials Science and Engineering, Tsinghua University, Beijing 100084, China, 1998.

[7] Garvie R.C., Hannink R.H., Pascoe R.T., "Ceramic steel?". Nature 258, 703-704, 1975.

[8] Dissemination of IT for the Promotion of Materials Science, Phase diagram of partially stabilized zirconia (PSZ), Teaching & Learning packages

[9] Yhosimura M., "Phase stability of zirconia". American Ceramic Society Bulletin 67, 1950-1955, 1988.

[10] Collet, M. "Degradación hidrotérmica de la circona 3Y-TZP indentada y desbasta", proyecto fin de carrera, Universidad Politècnica de Catalunya (España), 2011

[11] Chevalier, J.; Gremillard, L. "Zirconia as a biomaterial". In Comprehensive Biomaterials; Ducheyne, P., Ed.; Elsevier: Amsterdam, The Netherlands, 2011; volume 1, pp. 95–108

[12] Lange F.F. "Transformation toughening Part 2: Contribution to fracture toughness". Journal of Materials Science 17, 235-239, 1982.

[13] Kobayashi K., Kuwajima H., Masaki T., "Phase change and mechanical properties of ZrO2-Y2O3 solid electrolyte after ageing", Solid State Ion 3 [3], 489-493, 1980.

[14] Chevalier J., "What future for zirconia as a biomaterial?", Biomaterials 27, 535–543, 2006.

[15] Z. de Armas, F. G. Marro, E. Jiménez-Piqué, M. Anglada, "Estudio por nanoindentación de 3Y-TZP envejecida por degradación Hidrotèrmica".

[16] Lawson S. Enviromental Degradation of zirconia ceramics. Journal of the European Ceramic Society 15, 485-502, 1995

[17] Ian Birkby, "Fabrication and Wear of Yttria Tetragonal Polycrystals", University of Leeds Ph.D. Thesis, 1994

[18] Nitin P. Padture, Maurice Gell, Eric H. Jordan, et. Al., "Thermal Barrier Coatings for Gas-Turbine Engine Applications", 12 Apr. 2002, Science, , Vol. 296, Issue 5566, pp. 280-284, DOI: 10.1126/science.1068609

[19] Masonis J.L., Bourne R.B., Ries M.D., Mccalden R.W., Salehi A., KelmaN D.C. "Zirconia femoral head fractures: A clinical and retrieval analysis". The Journal of Arthroplasty 19, 898-905, 2004

[20] http://periodictable.com/Elements/040/

[21] Nielsen, L. Fuglsang, "Strength and Stiffness of Porous Materials", Journ. Am. Ceramic Soc., 73 (1990), 2684-89.

[22] Chintapalli , "Influence of sandblasting on zirconia in restorative dentistry". Phd Thesis at the Department of Materials Science and Metallurgy Engineering. Universitat Politècnica de Catalunya. Barcelona, Spain, 2012.

[23] Torralba, J.M., Campos, M. (2014). "Toward high performance in Powder Metallurgy". Rev. Metal. 50(2): e017

[24] Tropea, Cameron; Yarin, Alexander L.; Foss, John F. (2007). "Springer handbook of experimental fluid mechanics". Springer. pp. 661, 676. ISBN 978-3-540-25141-5.

[25] Larson, C. M., Choi, J. J., Gallardo, P. A., Henderson, S. W., Niemack, M. D., Rajagopalan, G. and Shepherd, R. F. (2016), "Direct Ink Writing of Silicon Carbide for Microwave Optics". Adv. Eng. Mater., 18: 39–45. doi: 10.1002/adem.201500298

[26] Datar, Anuj, "Micro-extrusion process parameter modeling" (2012). Thesis. Rochester Institute of Technology

[27] M Koizumi, M Nishihara, "Isostatic pressing: Technology and applications", book, 17, ELSEVIER APPLIED SCIENCE, 1991.

[28] Turner, C.D. and Ashby M.F., "The Cold Isostatic Pressing of Composite Powders-I. Experimental Investigations Using Model Powders", Acta Mater, Vol. 44. Nº 11, 4521-4530, 1996.

[29] http://www.designinsite.dk/htmsider/pb1007.htm

[30] C. Krause, "ORNL`s gelcasting: Molding the future of ceramic forming?", Oak Ridge National Laboratory Review; Journal Volume: 28; Journal Issue: 4; Other Information: PBD: 1995.

[31] L. Gibson, B. Stucker, and D. Rosen, "Additive Manufacturing Technologies: Rapid Prototyping to Direct Digital Manufacturing" Springer Verlag, 2009

[32] D. T. Pham and R. S. Gault, "A comparison of rapid prototyping technologies," International Journal of Machine Tools and Manufacture, vol. 38, pp. 1257-1287, 1998.

[33] J. P. Kruth, M. Leu, and T. Nakagawa, "Progress in additive manufacturing and rapid prototyping," CIRP Annals-Manufacturing Technology, vol. 47, pp. 525-540, 1998.

[34] http://www.custompartnet.com/

[35] K. G. Cooper, "Rapid prototyping technology: selection and application" CRC, 2001

[36] http://www.3ders.org/articles/20141002-italian-studio-lab-unveils-open-source-syringe-extruder-for-fdm-3d-printers.html

[37] http://www.olo3d.net/

[38] Michael P. Snyder, Jason J. Dunn, and Eddie G. Gonzalez, "Effects of Microgravity on Extrusion based Additive Manufacturing", Made In Space AIAA SPACE 2013 Conference and Exposition San Diego, CA

[39] Vladimir Mironov, Dr. Nuno Reis, and Brian Derby. "Tissue Engineering". May 2006, 12(4): 631-634. doi:10.1089/ten.2006.12.631

[40] Ben Utela, Duane Storti, Rhonda Andersonb, Mark Ganter, "A review of process development steps for new material Systems in three dimensional Printing (3DP)", University of Washington, Seattle, WA, USA.

[41] J. Ebert, E. Ozkol, A. Zeichner, K. Uibel, O. Weiss, U. Koops, R- Telle, and H. Fisher, "Direct inkjet Printing of dental prostheses made of zirconia", J Dent Res 88(7):673-676, 2009.

[42] Jens Bauera, Stefan Hengsbachb, Iwiza Tesaria, Ruth Schwaigera, and Oliver Krafta, "High-strength cellular ceramic composites with 3D microarchitecture", January 9, 2014.

[43] Enrique Escobar de Obaldia, Chanhue Jeong, Lessa Kay Grunenfelder, David Kisailus, Pablo Zavattieri, "Analysis of the mechanical response of biomimètic materials with highly oriented microestructures through 3D Printing, mechanical testing and modeling"

[44] Ogbemi 0. Omatete, Mark A. Janney & Stephen D. Nunn, "Gelcasting: From laboratory Development Toward Industrial Production", Oak Ridge National Laboratory, PO Box 2008, Oak Ridge, TN 37831-6087, USA.

[45] Erik Adolfsson, "Gelcasting of Zirconia Using Agarose" Swedish Ceramic Institute, IVF, 43153 Molndal, Sweden.

[46] M. Faes, H. Valkenaers, F. Vogeler, J. Vleugels, E. Ferraris, "Extrusion-based 3D Printing of ceràmic components"

[47] Ming-Tsung Weng, Wen-Cheng J. Wei, and Chi-Yuen Huang, "Influence of 3Y-TZP on Microstructure and Mechanical Properties of Al2O3-based Composites".

[48] S. Maleksaeedi et al., "Property enhancement of 3D-printed alumina ceramics using vacuum infiltration"

[49] Dongxu Yao et al., "Near zero shrinkage porous Al2O3 prepared via 3D-printing and reaction bonding"

[50] M. Turón-Vinas, J. J. Roa, F. G. MarroM. Anglada, "Mechanical propertiesof12Ce–ZrO2/3Y–ZrO2 composites", 2015, Ceramics International

[51] http://www.tosoh.com/our-products/advanced-materials/zirconia-powders

[52] BCN3D+ Dual Paste V 1.0, Guia de usuario, Fundació CIM, Barcelona TECH, UPC, 2015.

[53] http://manual.slic3r.org/expert-mode/infill

[54] http://www.mtixtl.com/20T-cold-isostatic-press.aspx

[55] https://e-shop.struers.com/UK/EN/

[56] N. Cuadrado, D. Casellas, M. Anglada, E. Jimenez-Piqué, "Evaluation of fracture toughness of small volumes by means of cube-corner nanoindentation",

[57] G.R. Anstis, P. Chantikul, B.R. Lawn, D.B. Marshall, J. Am. Ceram. Soc. 64 (1981) 533

8.2. Query bibliography

J. Muñoz Tabares, 2010, "Cambios microestructurales en 3Y-TZP desbastada y su influencia en la degradación hidrotérmica"

F. Grannec, 2009, "Caracterización de la transformación de fase del material Y-TZP mediante ensayo de rayado
"Degradación hidrotérmica de la circona 3Y-TZP indentada y desbastada"

A.Joly, 2015, "Desarrollo y caracterización de circona dopada con itria y ceria"

J.J. Roa, "Mechanical properties of HTSC at micro/nanometric scale", Thesis, Universitat de Barcelona (2010).

Escola Universitària d'Enginyeria
Tècnica Industrial de Barcelona
Consorci Escola Industrial de Barcelona
UNIVERSITAT POLITÈCNICA DE CATALUNYA

Pressupost

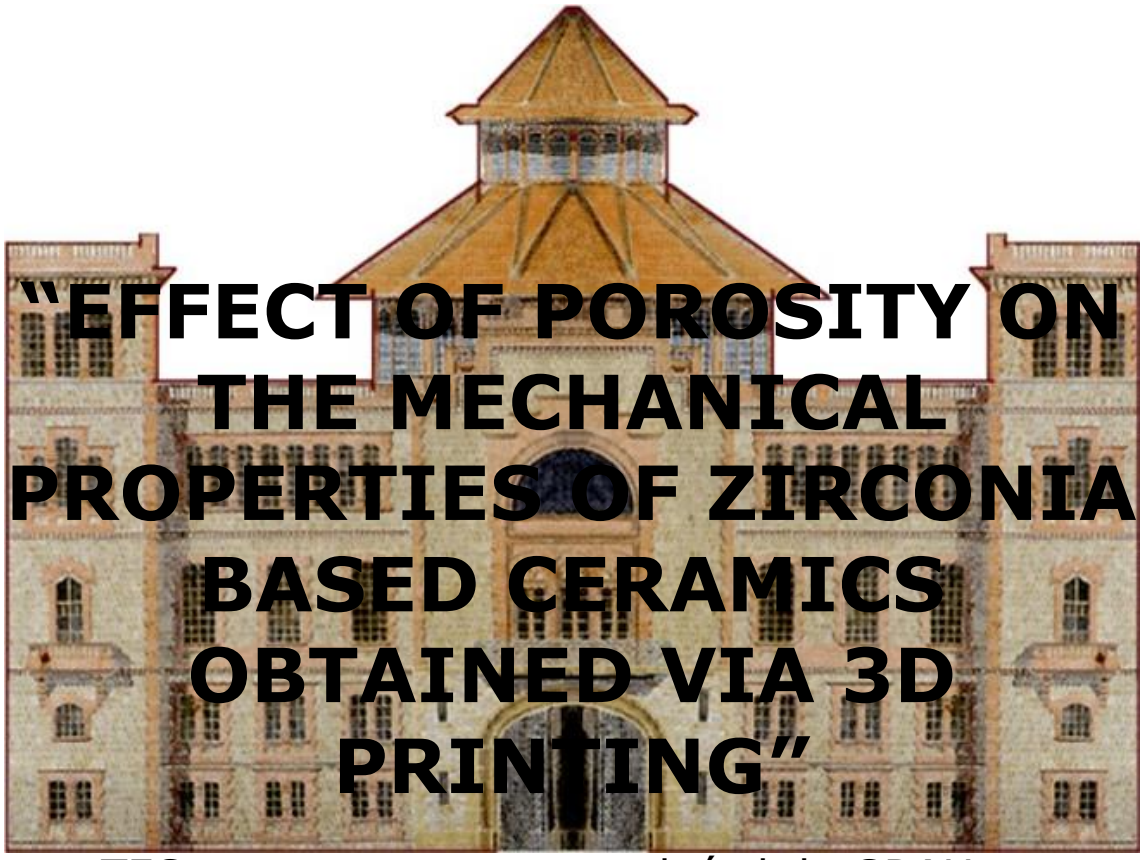

"EFFECT OF POROSITY ON THE MECHANICAL PROPERTIES OF ZIRCONIA BASED CERAMICS OBTAINED VIA 3D PRINTING"

TFG presentat per optar al títol de GRAU en
ENGINYERIA MECÀNICA
per **Ferran Crespo Petit**

Barcelona, 26 de Juny de 2016

Director: Joan Josep Roa Rovira
Codirectora: Gemma Fargas Ribas
Departament de Ciència i Enginyeria de Materials i Enginyeria Metal·lúrgica (CMEM)
Universitat Politècnica de Catalunya (UPC)

BUDGET

In this chapter is exposed an economical analysis of the bachelor's degree.

All the perishable material's prices have been taken directly from the manufacturer's web, or in the absence of them, from a supplier's web as an orientative value, considering always the cheapest option:

PERISHABLE MATERIAL			
Product	**Quantity**	**Cost per unit**	**Cost**
3Y-TZP	900 g	151€/Kg	135,90€
Alumina	230 g	38,4€/Kg	8,83€
Ceria	50 g	183,5€/Kg	9,18€
Agar-Agar	40 g	0,025€/Kg	0,001€
Water	12 m3	0,6188€/m3*	7,43€
Saint Govain 30µm polishing suspension	0,3 l	110€/Kg	33,00€
Saint Govain 6µm polishing suspension	0,25 l	90€/Kg	22,50€
Saint Govain 3µm polishing suspension	0,25l	90€/Kg	22,50€
Buehler Mastermet 2 colloidal Silica (1 µm) suspension	0,1 l	180€/Kg	18,00€
Struers MD-Piano 220 polising disc	1 u.	100€/u.	100,00€
Struers MD-Piano 600 polising disc	1 u.	100€/u.	100,00€
Struers MD-Piano 1200 polising disc	1 u.	100€/u.	100,00€
Struers MD-Plan	1 u.	65€/u.	65,00€
Struers MD-Dac	1 u.	65€/u.	65,00€

Struers MD-Nap	1 u.	90€/u.	90,00€
Nitrogen	0,9 l	42€/l	37,80€
Durofast baquelite	400 g	8€/Kg	3,20€
Acetone	0,20 l	10€/l	2,00€
Laboratory paper	1 u.	0,5€/u.	0,50€
SUBTOTAL		780,83€	

*Considering a 12 m3 supplying quote from Aigües de Barcelona

SAMPLE'S CHARACTERIZATION			
Service	**Quantity**	**Cost per unit**	**Cost**
3D printer	70h	15€/h	1.050,00€
Sonicator	1,5h	5€/h	7,50€
Heating magnetic stirrer	10h	5€/h	50,00€
Carbon coater	1u.	3€/u	3,00€
FIB/SEM with technician	7h	50€/h	350,00€
Archimedes test	1h	5€/h	5,00€
Helium picnometry with technician	2h	15€/h	30,00€
DRX with technician	6h	60€/h	360,00€
Vickers micro testing machine	8h	15€/h	120,00€
Polishing machine	40h	15€/h	600,00€
Linear semiautomatic precision saw with diamond wafering blade	8h	10€/h	80,00€
Mounting machine	7h	5€/h	35,00€
Nabertherm furnace	80h	15€/h	1.200,00€
Confocal laser microscope	40h	50€/h	2.000,00€
Optical microscope	3h	20€/h	60,00€
Loupe	1h	20€/h	20,00€
SUBTOTAL		5.970,50€	
OTHER COSTS			
Cost			
Laboratory material		200,00€	
Laboratory use		1.600,00€	
Office material		30,00€	
SUBTOTAL		1.830,00€	
PROJECTIST'S ENGINEERING COST			
Concept	**Quantity**	**Cost per unit**	**Cost**
Sample preparation	160h	10€/h	1600
Sample characerization	110h	10€/h	1100
Results analysis	85h	10€/h	850
Memory developement	200h	10€/h	2000

SUBTOTAL		5.550,00€	
SUPPORT ENGINEERING COST			
Concepte	**Quantitat**	**Cost per unitat**	**Cost**
Bachelor's degree tutor	240h	40€/h	9.600,00€
Bachelor's degree coordinator	50h	40€/h	2.000,00€
SUBTOTAL		11.600,00€	
TOTAL COST OF THE PROJECT			
Concept		**Cost**	
Asociated cost to perishable material		780,83€	
Asociated cost to sample's characterization		5.970,50€	
Asociated cost to other costs		1.830,00€	
Asociated cost to projectist's engineering cost		5.550,00€	
Asociated cost to support engineering cost		11.600,00€	
TOTAL		25.736,33€	